Crashworthiness Modelling of SMC Composite Materials

Vinodhan Selvarajalu

Submitted in fulfilment of the academic requirements for the degree of Master of Science in Engineering in the School of Mechanical Engineering

All work for this dissertation was completed at the former University of Natal

Durban, South Africa

December 2003

Abstract

The purpose of this research is to make an investigation into the crashworthiness modelling of Sheet Moulding Compound (SMC) composite materials, and to study the response of SMC composite structures under dynamic loading. The primary research objectives are thus to review classical and advanced material failure models, and to perform numerical simulation of the crash of composite structures using already available material models. Additionally, a new material model is to be developed for implementation into a commercially available finite element package.

In parallel with the numerical simulation of the crashing of an SMC composite structure, experimentation is performed which is used as a source of validation and comparison with the simulation. For this purpose a testing regime is introduced, which may be mirrored in simulation. As any material model requires initial experimental inputs, the purpose of experimentation is two-fold, with testing required both for the quantification of the required model inputs and the basic material characterisation before simulation may begin, as well as for the proposed validation and comparison after the simulation has been carried out.

Thus the design of the testing methodology, as well as the design, selection and fabrication of the testing equipment and the composite specimens and demonstrators, as well the actual testing itself, are necessary secondary requirements of the project.

Once the testing regime has been facilitated and carried out, numerical simulation validation using already available composite material models may then be carried out at various levels. The results are then analysed and validated with the resultant justification of a new model being developed.

The critical viewpoint to be delivered throughout is the need for theoretical formulations for material modelling to be extensively researched and validated in terms of their implementabilty and practicality, a key analysis seemingly missing in most technical write-ups. Such analyses are performed and discussed here, highlighting the volume of additional work that is encompassed by such a study.

Preface

The author declares this dissertation to be his own unaided work except where due acknowledgement is made to others. This dissertation is being submitted for the degree of Master of Science in Engineering to the University of Natal, Durban, and has not been submitted previously for any other degree or examination.

To Zaheera, for inspiring my dreams *and* my reality.

Acknowledgements

The author wishes first and foremost to thank Professor Evgeny Morozov for his guidance and advice, and also the fellow members of the MODYMIS research team at the former University of Natal, especially Konstantin Morozov and Michael Hoarau, for their contribution to the output of this research study.

I also wish to thank my parents, as well as the rest of my family, for their unwavering support of my studies, and their constant caring.

The author gratefully acknowledges the sponsorship of Renault (France), and the THRIP foundation of South Africa, as well as the National Research Foundation (NRF), for the scholarships awarded him for this study.

List of Figures

List of Tables

Contents

Chapter One

Introduction

1.1 Design, Analysis and Applications of SMC Composite Materials

Composite materials are increasingly being used in as diverse applications as the automotive and sports industries due to their multitude of advantages over metallic counterparts. However it is the nature of these advantages that usually also provides designers with challenging problems in accurately representing the materials. Unlike isotropic materials, anisotropic materials such as composites exhibit complicated mechanical behaviour that needs to be accurately accounted for in constitutive models. This presents a problem in that composites essentially act very differently in different loading situations. Most composite models rely on modelling the material under certain assumptions so that computationally the problem is simplified. However any such assumptions also add to the inaccuracy of the solution, and must be considered carefully before being applied.

Composite materials are generally considered to be at the forefront of future development in a wide variety of disciplines, most notably the aerospace and automotive fields, due chiefly to their remarkable strength to weight ratios and their flexibility to be tailor-designed for specific applications. However the implementation of this family of materials into the general automotive industry has remained relatively limited, due primarily to a lack of knowledge regarding the crash response of these materials bringing about uncertainty regarding their safety and predictability. Thus, unsurprisingly, composite material modelling has been a source of extensive research and at present a variety of different models have been devised which are found to adequately simulate the response of these materials. Some of these models are also found to be ready-implemented in commercially available analysis tools. However, an examination of the most commonly used software packages in the field of automotive crashworthiness shows that although composite material models have indeed been implemented, these models are almost entirely limited to the family of continuously

reinforced composite materials, with the modelling of discontinuous (short-fibre) composites almost completely lacking. At present finite element analysis software generally approaches the modelling of short fibre composites as isotropic media, incorporating some form of damage law to take into account the progressive failure nature of the material.

Due to the complexity of the material structure (matrix reinforced by fibres) and its specific mechanical properties, the nature of transforming collision kinetic energy into material deformation energy for composite materials differs fundamentally from that of conventional structural materials, such as metal alloys. The energy absorption mechanics are also significantly different for advanced composites and depend on both the material structure (type of reinforcement) and the structural design of the component. The primary method of energy dissipation in composite materials is the progressive crushing of both the materials themselves and the structural components (beams, tubes, plates) made of such materials.

The nature of composites as a class of material lends itself to describing what is in essence an infinitely large family. Definitions sometimes vary, and slight nuances in wording sometimes have a major effect on the materials that are encompassed. In modern terms we tend to readily envision composites as the family of glass and carbon fibre reinforced plastics (GFRP and CFRP respectively), even though on further contemplation, it is common knowledge that this class of material is in no way limited to only these. It is these materials however, becoming exponentially more prevalent in every conceivable industry and application, which dominate current research and use, and have come to serve as the 'poster-children' for composite technology.

Thus as a matter of course, the bulk of research is geared towards these two (relatively specific) classes of composite materials, especially as they are the most widely available as a direct result of their popularity, while interest in materials such as fabric reinforced composites, and other composites comprising reinforcements of various other shapes and materials are relegated to specialist application research. It is fair to say therefore that general studies into, for example, as is being looked at in this work, composite modelling, as a whole, will usually begin with application, development and verification pertaining to these materials, and then move on to further classifications.

A branch of the composite family tree has therefore been identified for the modelling research that is to be undertaken, but this still remains too broad a classification.

Considering the application of this study, namely crashworthiness modelling for automotive applications, Sheet Moulding Compound composites, or SMC composites are the specific branch of these materials that probably have most relevance, at least in so far as structural panelling and formed sections of the vehicle are concerned. These materials are especially suited for this use; combining high strength-to-weight ratios, relatively good formability and fairly simple and efficient manufacturability, not to mention relatively low cost. Add to this its inherent composite nature, which brings to the table the somewhat marvellous ability to 'tailor-make' required properties, and we have a material that is almost ideally suited to its purpose. Almost, that is, except for a few other notable inherent properties of the composites family, namely brittle failure (certainly in the case of the glass fibre plastics to be used here), repeatability issues, and complicated, difficult to model, material responses under dynamic loading. The latter of course is the very reason for this study; the need to adequately model these materials so that their response may be predicted in crash situations.

Now, the nature of the mechanical properties of fibre-reinforced SMC composites, like any fibre-reinforced composites, is to a large degree dependent on four key factors, namely fibre material, fibre percentage, fibre orientation and lastly of course, matrix material. In this study glass fibres are exclusively used; it has already been mentioned that GFRP and CFRP represent the bulk of composite research and utilisation, and, limited by budget and

availability, glass fibres are the practical choice between the two of these. Also, even more prescriptively, it is a glass fibre composite that was produced by the industrial partner involved in the project of which this study represents a portion, as a sample of the material that was looked at being analysed and employed.

A survey of related publications gave some indication to the scope of the work being researched. The closest thing to existing material models for the chosen SMC materials yielded by this search proved to be those models designed for the general modelling of the family of short-fibre reinforced composites, of which the specific SMC material being investigated here is certainly a member, but which may not necessarily incorporate the specific nature of the actual material in question. For example, SMC composites are definitively moulded into thin-walled components, which results in the reinforcing fibres aligning themselves in a two-dimensional orientation with so called 'through-the-thickness' fibres, lying across the thickness of the composite, for the most part not in evidence. Of course, the thicker the component, and the shorter the constituent fibre strands, the greater the chance that complete three-dimensional orientation of the fibre phase might exist. Thus, wall thickness and fibre length are introduced as very necessary conditions to be considered.

The idea of fibre orientation is sometimes catered for by a 'fibre-orientation distribution', or FOD. For short fibres composites this usually incorporates some sort of statistical modelling of the fairly random orientations each fibre may take up. Zak et.al. (2001) used a so-called 'Two-Section Method' for this statistical characterisation. This method builds on the previously presented (single) section method, conceived, developed and discussed by, amongst others, Fischer and Eyerer (1988), Bay and Tucker (1992) and Hine et al. (1993), who all measured short-fibre orientations by examining polished cross sections using an optical microscope. Zhu et. al (1997) suggested a similar method. This 'single section' method analyses the ellipse-shaped intersection of a cylindrical fibre and a plane, and from this calculates the misalignment angle between the plane's normal and the cylinder's longitudinal axis, thus defining the fibre orientation using this single angle. Problems associated with this original method were that inaccuracies occur when the misalignment angle is close to zero and secondly that twin solutions for fibre orientation existed for each elliptical cross section (orientation duality), in which the azimuth angles of the fibre differ by 180°. Various solutions were proposed to deal with the former, mostly involving sectioning at a non-zero angle to the 'preferential' fibre direction, thus making this not very practical in the case of widely three dimensionally distributed fibre orientations. To deal with the latter, Zhu et al. (1997) proposed a solution incorporating the use of two orthogonal plane sections, while Bay and Tucker (1992) claimed that only three planes are sufficient. Practically, these approaches may be difficult to implement, even if they are theoretically possible, and also, the results remain valid only if the FOD remains unchanged between section locations, which we know in fact to be not necessarily true; in fact usually necessarily untrue. Zak et al.'s (2001) method addresses each of these shortcomings, by making use of two consecutive sections through the material.

Such an FOD matrix is the cornerstone of the 'Interpolative Aggregate Model' presented by Toll (1992) (discussed in further detail in the next chapter). In this model short fibre composites are modelled as an isotropic matrix reinforced with transversely isotropic unit cells. Each cell has an identical stiffness matrix assigned to it, whose components are found by interpolation from measurable macroscopic stiffnesses. Each cell has an orientation defined by two (for the 3D case), or one (for the 2D case) orientation angles

One manner in which to eliminate the need for the rather cumbersome procedure of describing a complex and large FOD is to rather consider the composite on a more global scale, by analysing the multi-phase material as a single 'homogenised' medium. Homogenisation entails the theoretical 'summing' of the properties of the constituent phases of the short fibre composite, such that the end result is a single, usually isotropic, material,

which displays the overall response of the original composite. This method of short fibre composite analysis is probably the most popular manner in which these materials have come to be traditionally been modelled, and various different homogenisation schemes abound.

One such method, possibly the most popular, the Mori-Tanaka homogenisation scheme (Mori and Tanaka, 1973), is employed in a model presented by Desrumaux, Meraghni and Benzeggagh (1995), after continuous work laid down by the latter two authors. According to this scheme, the overall stiffness of two phases, in this case the matrix and another inclusion phase, either a void at the first level of homogenisation, or a fibre at the second level, is estimated by an expression written in terms of the stiffness tensors of the matrix and the other phases, and the localisation tensors of those other phases. The model is presented in detail in Chapter 1.3 following, and it is clearly seen from even initial glances, that it presents a strongly theoretical-based approach to material modelling, which brings up a rather crucial point of contention when it comes to this area of research.

Any synopsis of modelling trend will immediately show a distinct division between those models that are theoretically based, using mathematical formulations to relate the material properties of the overall composite to those of more simply characterised constituents, and those that are based strongly on experimental testing and data of the composite as a material. Though each method sometimes makes use of techniques that are characteristic to the other, it is the *basis* of the formulation, the foundation upon which the material characterisation stands, that is made reference to here. It is the need to balance the sometimes impractical and expensive experimental testing with the necessarily approximative theory of one or other method that results in continuing research.

Another model, in which use is again made of the Mori-Tanaka homogenisation scheme to express the overall properties of a randomly reinforced short fibre composite in terms of the properties of its constituents, was proposed by Chen et al. (1992). Unlike the model presented by Desrumaux and his colleagues, however, the presentation of the homogenisation is much simpler, and is completely defined in terms of the material properties of the constituent phases (fibres and matrix). The composite material is modelled as an isotropic medium, with properties derived from the homogenisation of the properties of the isotropic matrix phase and the transversally isotropic fibre phases. Of course, the simpler presentation comes with a penalty; that being the greater inflexibility of the model as compared to the Desrumaux model's relative 'first principles' approach. Both these are presented in greater depth later, suggesting the Mori-Tanaka method has thus been chosen as the homogenisation scheme of choice in this particular work, but it should be noted that numerous other formulations do exist. However these are generally considered to be fairly similar in concept at least. For example, Chen himself showed in a later works (Chen (1994) and Chen (1996)) that homogenisation using the Mori-Tanaka method and results derived for fibrous (and platelet) reinforced composites by Walpole (1969) and then Laws (1974), from the earlier, equally popular 'self-consistent' scheme (originally devised by Hershey, 1954)), although different in nature, yield exactly the same results, at least for the moduli that were being investigated. It should also be noted that a series of researchers; Norris (1989), Ferrari (1991), Benveniste et al. (1991), Christensen et al. (1992); all worked on showing the validity of the Mori-Tanaka method, as did earlier researchers like Hill (1965) and Budiansky (1965) for the self consistent method.

Other homogenisation schemes have been developed by Kalamkarov and Liu (1998) and Liang et al. (1995) (who used a statistical averaging process), for example. The concept of 'reiterated homogenisation', discussed, for example, by Bylund et al. (2001) with automotive modelling specifically in mind, in which the homogenisation process is repeated at several different material scales, should also be mentioned and noted.

Other homogenisation theories, the 'displacement' and 'force' methods, were derived by Lukkassen et al. (1995), considering different types of representative volume elements, the 'building-blocks' of a micro-level averaging or homogenisation scheme.

A distinction should thus also be noted here between some of these concepts, which lies in the chronological order of the homogenisation and damage evolution processes being carried out. In the 'macromechanical' approach, homogenisation is performed first and damage is then introduced to this new medium. In the 'micromechanical' approach, damage is applied to each phase, followed by homogenisation.

Thus it is evident that work in this particular aspect of composites modelling has been fairly extensive, with most authors showing correlation with either experimental data or previously derived results. However these correlations should be noted and assessed along with the proverbial 'pinch of salt', since the nature of homogenisation is so rooted in mathematical formulation that control of error estimates and convergence is usually strongly governed by input to the model, which in some cases may lead to only example-specific solutions which may have little predictive capability for other situations.

After the undamaged material characterisation is complete, it is required to move on to probably an even more crucial component of the material modelling process, especially considering the materials being studied, namely damage initiation and progression. Composite material failure physically incorporates the phenomenon known as 'progressive degradation', which refers to the fact that composite materials may continue to bear loads even after initial and even subsequent 'failures'. Each point of failure corresponds to a relatively severe degradation of the material's load-bearing capacity, due to a mode of failure linked with either the constituents themselves or the bonding between them. In present day composite failure models the composite material properties are degraded either according to the specific mode of failure that has been induced or by the general application of a damage factor to the material properties. The delineation of these failure modes as well as the form of the degradation, coupled with the material constitutive equations in fact define the premise of composite modelling along with the initial constitution. To fully take advantage of the benefits of these materials, it is necessary for the modeller to include this ability in any representation for it to be an accurate reflection of the materials response.

As an additional complication, the nature of each and every failure is also variable, with a multitude of failure mechanisms being exhibited, dependant upon factors including, but by no means limited to, the exact nature of the constituent materials, and the specifics of the manufacturing process being employed. This variability of course makes pertinent representation of these materials highly dependent on the accurate modelling of the failure mechanisms in play and highlights the fact that as a classification, the term 'composite material' is itself much too broad for modelling purposes, and highlights the need for more specific modelling options within this theoretically infinite family.

Even limited, as we are here, to the study of just one branch of the composite materials family tree, it is immediately evident that the various forms of failure that may take place are indeed multitude, and that these different failure possibilities initiate very different material responses. It is thus of obvious significance to further investigate these modes of failure and those models that have already been used to replicate them.

In a study pertaining specifically to SMC composites, as is to be focused on in this study, Derrien et al. (2000) performed in-situ tensile tests on SMC composite (quasi-random oriented short-fibre reinforcement in a polyester matrix, and a Calcium carbonate filler) inside a scanning electron microscope (SEM), and concluded from these that damage evolution in such a material occurs in three phases; a linear stage corresponding to elastic behaviour, a non-linear stage, and a second linear stage until final fracture. Additionally it was observed

that no damage occurs in the first (elastic) stage, the second (non-linear) stage corresponds to the occurrence of interfacial cracks localised on fibres oriented between 50° to 90° relative to the loading direction and less so by quickly stabilised matrix micro-cracking, and the final stage corresponds to the propagation and opening of the interfacial cracks around the fibres, and the initiation of cracks on fibres that are oriented more in line with the direction of loading. At final fracture, the fibres oriented in the tensile loading direction break. Thus, it was concluded that interfacial damage is the dominant failure mode for this type of SMC composite, so much so that it is suggested by the authors that the other damage mechanisms can be neglected. This cracking is initiated by either shear or normal stresses, depending on the orientation of the specific fibre, and was found to be statistically distributed over the entire composite. Derrien et al. then proceeded to apply the Mori-Tanaka model (similarly to Desrumaux et al. (1995)) to model the material and a statistical Weibull law (again, similar to that used by Desrumaux et al. (1995)) to model the damage process (corresponding to interfacial failure only). The various statistical parameters necessary for this model were identified by finding a 'best fit' of experimental results. Results presented show that such a model is able to fairly accurately predict the tensile response of the SMC material tested, and additionally, to take into account a variation of the interface resistance, by applying it to two SMC composites with similar compositions but different fibre coatings which yield different interfacial strengths.

The Weibull law used in the above study, as well as by Desrumaux et al. will be further delved into in later chapters. The principle behind this statistical failure scheme is that the failure pattern of a structure may be predicted by extrapolating the failure pattern of a certain number of tested representative samples by employing certain shape and scale parameters.

If a micromechanical approach to modelling is taken, damage is usually introduced into the composite by the introduction of voids or cracks into the REV (representative volume element) which defines the 'unit cell' of the composite. These voids occupy volume but do not contribute to stiffness or strength, and thus serve to weaken the material at an elementary level. The size, orientation, shape and propagation of these introduced cracks are themselves a source of exhaustive studies; Cowley and Beaumont (1995) and Tohgo et al. (1997) are just two examples of studies delving into this extensive area. The very strong dependence on micromechanics (which realistically encompasses its very own sphere of research) and the associated mathematically-based nature of this method of modelling, along with what is considered here to be still very difficult to implement or validate models for general situations, meant that this is not delved into any further here. As has been mentioned already, theoretical models tend to lend themselves to being highly dependent on user calibration, which is in turn usually governed by specific test scenarios rather than general cases.

General implementation and validation being the keywords of this study then, those modelling techniques that were considered most practical, after being researched and further analysed, are given preference. Two damage models that adopt a more macromechanical approach and are dependent on experimentally derived results rather than overly complex mathematical formulations are the statistical damaging process discussed above (in this case using the Weibull distribution) and the implementation and use of a damage factor to degrade the properties of the material in question.

The latter method is physically sensible when the material is considered in the macromechanical or global, sense. What this entails is the application of a degradation factor to the (usually) stiffness properties of a material when it is considered 'damaged'. Thus, the material undergoes a reduction in stiffness, but continues to bear load until another 'failure point' is reached, is degraded again, and so on, until ultimate failure is attained and the material can no longer carry any load. An example model executing such a law is discussed in detail later, and validation analysis of this law also appears later in this work. The application of the damage variable may not be restricted to a 'global' response though. Models also exist

in which the damage variable is dependent on the mode of failure that is initiated. As has already been discussed, failure may arise in any of the constituent phases, and it is considered advantageous to be able to reflect this phenomenon in the degradation of the material. Thus, failure in any of the phases being identified by whatever means, each may be assigned a respective damage variable so that each phase degrades at different rates, until ultimately one of these phases results in the catastrophic failure of the material.

This 'phase-specific' progressive degradation is not unique to those models that implement a damage variable however. It has already been intimated that the institution of cracks in micromechanically-defined media may be related (through orientation, shape and size) to the mode of failure, and this is generally considered to be the appropriate manner in which to treat the progressive degradation of composites. It is in defining the phase in which damage initiates, and the rate and manner in which this damage propagates that requires careful consideration and application.

Another necessary input into a model, especially in the light of highly dynamic situations, such as crash analysis, is the need to somehow qualify and quantify the strain rate dependency of the material in question. Strain rate effects have been catered for by the application of various models; each relying on experimentally determined calibration factors for the material in question. These models are usually ready-implemented in most finite element analysis solvers and a sample of these are discussed in the next chapter Necessary consideration must be made, depending on the material being analysed, and its relative strain rate sensitivity.

1.2 Vehicle Crashworthiness and Composite Materials

The primary requirement of crashworthiness studies is to ensure that vehicle design is such that the occupants should survive, and in fact, avoid serious injury of any kind, at reasonable impact velocities (that which would be expected in the normal application of the vehicle in question). Automotive safety considerations have been increasingly gaining importance for consumers before a purchase is to be made, due mainly to the spotlight being placed on safety measures in recent times by more stringent international legislation. In the European Union for example, since 1974 until as recently as 1998, single frontal impact tests were the only criteria for assessing the safety of a passenger vehicle. Since 1998 the testing regime has been increased to incorporate frontal, frontal offset, and side impacts as standard. Multiple air bags, side impact beams, ABS braking; these are just a sample of relatively new features, now considered almost standard in new car designs, borne solely out of a need to address the previously adjudged deficiencies in automotive safety. Safety has become such an issue, that vehicles are now able to market themselves purely on the basis of superior safety features; a concept which would surely have been considered unheard of as recently as the 1980's, when automobiles were primarily rated by either their cost, performance or reliability, and the meagre seat-belt was still considered sufficient in its capacity as the sole form of passive restraint. The inclusion of new safety features such as those mentioned, and also the debates that arise regarding the effectiveness of these, has necessarily directed the thoughts of design engineers to new avenues by which they might earn an advantage; and it is the structural crashworthiness of the automobile as a whole that one such avenue leads to.

In modelling of automotive components, the same parameters as directed by relevant safety standards should be applied, and used as analysis constraints. For example, even at the relatively modest travelling velocity of 15 km/h, typical of the lower limit of the classification 'low-velocity' impact speeds as directed by standards, the crash process of the component takes on a dynamic nature, and as such, effects typical of and specific to dynamic loading conditions should be incorporated into the modelling regime.

Components employed in automotive structures have to be considered in light of their crashworthiness; which in turn is dictated primarily by the energy absorption characteristics of both the geometry of the component in question, and the material being utilised. Energy absorption by way of design of component geometry is a concept with decades of crashworthiness studies behind it, primarily dominated, in the case of low velocity automotive crashworthiness applications, by the design of bumper systems. The motor vehicle bumper is designed to provide the first point of contact, especially in typical low-velocity collisions, and as such is used to contain the entire damage of such collisions. Thus the bumper system is considered to be a fairly replaceable component, and should thus be manufactured with a view to not only fit design specifications for crashworthiness standards, but, in a world driven by economics and competition, to ideally minimise the cost of replacement as well.

Energy absorption systems are by no means limited to this area of 'first contact' design though. To guarantee the primary law of crashworthiness, namely the complete safety of the vehicle's passengers, it is necessary for the entire vehicle to act as an energy absorption system, and each and every structural component of the vehicle should ideally be designed and manufactured to optimise its contribution to this.

Since the mechanics of composite materials and composite structural components differs so substantially from the conventional applications, and considering the large scope for the application of composite materials in this field, there is at present a pressing need to develop appropriate methods of modelling and analysis relevant to this problem. Currently there are a large variety of design approaches, test results and research investigations into the problem under consideration, classifiable according to the type of composite material and the design geometry of the parts. It has been found that in general an application of fibre reinforced plastics (FRP) to vehicle compartments can satisfy the structural requirements of the passenger compartment including high strength and light weight. Implementation of the new advanced composite materials provides the opportunity to develop designs of the reliable structural composite parts in high volume for improved automotive fuel economy. Structural optimisation and crashworthiness of the composite components should be incorporated into design calculations to control the mechanical performance.

Development of the specific analysis and design software tools to model the structural behaviour of composite vehicle components should be performed on the basis of establishment of the automotive database containing comparable information on polymer composite materials, existing composite designs in the field concerned, and research results for use in structural analysis. The database would provide the necessary knowledge about material responses to automotive environments, which in turn create the basis for the development of crash models and structural design. This enables the design methodology for implementation of new materials to be created. The corresponding software system could be developed on the basis of the models and methodology taken from the database (dynamic stress analysis, buckling and post-buckling modelling, structural optimisation, crash modelling, and so forth.). This approach could be combined with the analysis and design of composite materials and structures made on the basis of existing industrial software.

Verification of the design and analysis methodology and software would be performed for the specimens of composite structural components (tubes, beams, etc.) by comparison of the predicted analytical data on crushing behaviour with the experimental results (dynamic tests under quasi-static and impact conditions).

Computerised dynamic modelling of automotive components offers the capability of investigating the design parameters without building the actual physical prototypes. In this approach, the dynamic behaviour of the structure is simulated for specified external inputs, and from the corresponding response data the designer is able to determine its dynamic response characteristics, estimate the crashworthiness of structure.

1.3 Existing Approaches to SMC Composite Modelling

SMC-type composites, generally represented as isotropic materials for the purposes of most current models, are in fact just as anisotropic as any laminated composite when considered locally, rather than globally. This presents a problem in that composites essentially act very differently in different loading situations, and exhibit various types of loading and failure modes. Most composite models rely on modelling the material under certain assumptions so that computationally the problem is simplified. However any such assumptions also add to the inaccuracy of the solution, and must be considered carefully in the context of the specific problem before being applied.

Composite material failure is generally modelled using the concept of progressive failure due to the fact that composite materials may continue to bear loads even after initial failure. Typically, one material constituent will fail, degrading the overall properties of the composite, but the remaining constituent or constituents will continue to carry loading. In such models the composite material properties are degraded according to the mode of failure that has been induced. The delineation of these failure modes as well as the form of the degradation, coupled with the material constitutive equations define the nature of the model.

Thus variation in any of the parameters produces a new model that requires analysis in order to ascertain its applicability to a given situation.

A recent model (which we will refer to as the 'Mori-Tanaka Homogenisation model with Statistical Failure Criteria'), mentioned earlier, makes use of the Mori-Tanaka homogenisation scheme (Mori and Tanaka, 1973), as discussed above, to super-impose the properties of the different phases present in a damaged short fibre composite material, and thus obtain a single homogenised material with the overall mechanical properties. Homogenisation is performed as a two-step process, proposed by Desrumaux, Meraghni and Benzeggagh (1995). As a first step, the matrix material is homogenised with voids introduced into the material as a result of damage, to obtain an effective 'damaged matrix', and then this damaged matrix is homogenised with the fibre phases (grouped together in families, defined by orientation) present in the material to obtain the overall damaged composite (see Fig.1.1).

Stresses in the respective phases (matrix and each fibre family) are then computed, and these stresses are used to evaluate the probability of damage in each phase.

Damage is introduced by way of Weibull distribution statistical failure criteria into the matrix, fibres and fibre-matrix interface. This probability distribution is used to define the strength of each fibre in the elementary representative volume of the matrix, and fibres are failed by comparison with this strength. The matrix and interfacial damage is expressed as a probability of failure, and is applied to the respective phases by the introduction of voids in place of the failed portion of the material, oriented according to the mode of failure.
Failed fibres are replaced by voids of similar shape and size with no material stiffness, matrix failure is introduced as cracks oriented transversely to the direction of loading, and interfacial failure is modelled as the introduction of cracks transversely oriented to the fibre phase responsible for the failure (see Fig. 1.1).

The second part of the Mori-Tanaka model (after the homogenisation as described earlier) is the evaluation of the microscopic state of stress in the matrix ($\sigma^{(0)}$), and in the oriented family ($\sigma^{(i)}$), respectively, due to an applied macroscopic stress σ:

$$\sigma^{(0)} = B^{(0)}\sigma \tag{1.1}$$

where

$$B^{(0)} = C^{(0)}\left[I + \sum_{i=1}^{n} f_i (S^{(i)} - I) L^{(i)} \right]^{-1} \left(C^{(0)}\right)^{-1} \tag{1.2}$$

$$\sigma^{(i)} = B^{(i)} \sigma \tag{1.3}$$

where

$$B^{(i)} = C^{(0)}\left[(I + (S^{(i)} - I) L^{(i)}) \left(I + \sum_{i=1}^{n} f_i (S^{(i)} - I) L^{(i)} \right) \right] \left(C^{(0)}\right)^{-1} \tag{1.4}$$

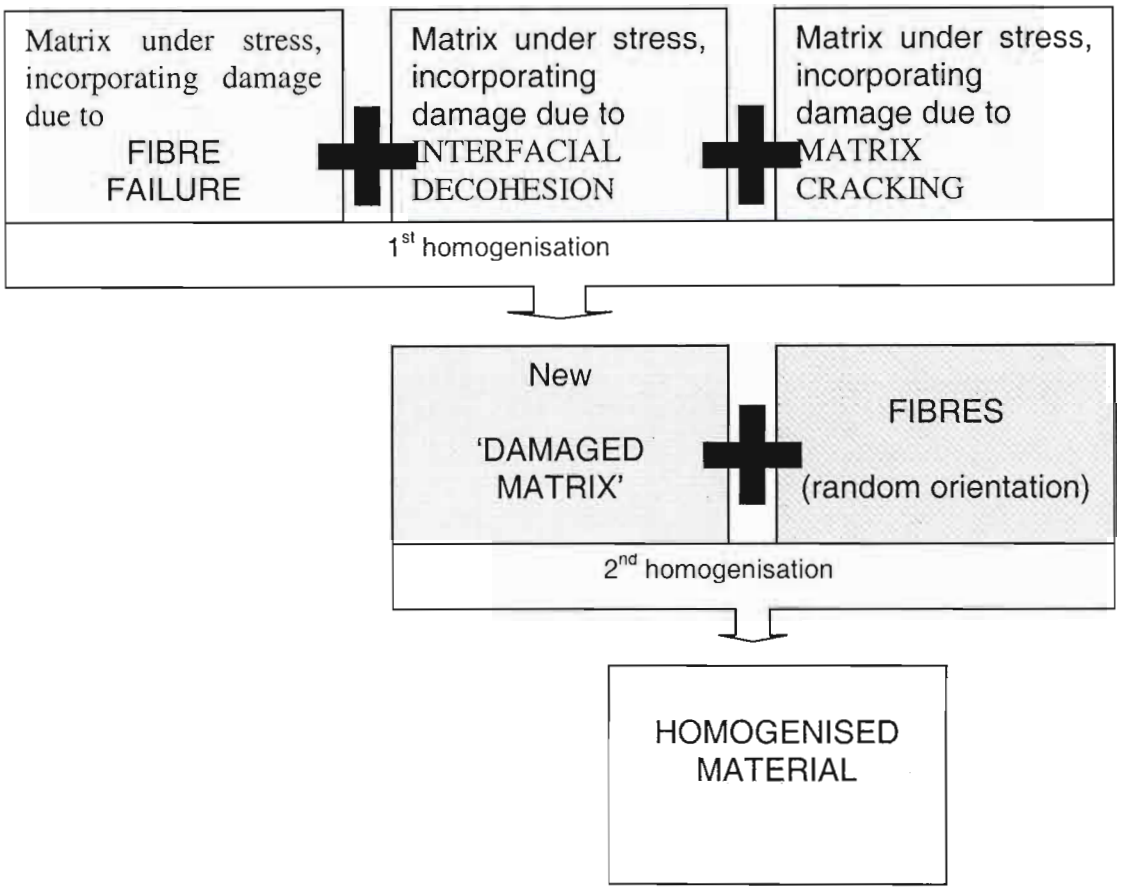

Fig. 1.1 Two-step homogenisation scheme

Failure in each phase i.e. fibre, matrix, and fibre-matrix interface, is determined using statistical criteria based on the Weibull distribution. The stresses within each phase, as computed above, are statistically compared to the respective strengths of the phases through the use of the following set of relations:

For the fibre failure:

$$P_{fibre}(\sigma) = 1 - \exp\left[-\frac{L}{L_0} \left(\frac{\sigma_f}{X_{fibre}} \right)^{m_f} \right] \tag{1.5}$$

where

L_0	is the original gauge length of the fibre filament used in testing
L	is the actual fibre length in the material
m_f	is the Weibull shape parameter
X_{fibre}	is the Weibull scale parameter
σ_f	is the actual tensile stress in the fibre

Using the inverse function, the strength of the j^{th} fibre in the representative volume is determined

$$\sigma_j^{break} = X_{fibre}\left[\frac{L_0}{L}\ln\left(\frac{1}{1-z}\right)\right]^{1/m_f} \tag{1.6}$$

where

z	is a random number taken from the uniform distribution on the interval [0,1]
j	is taken on the interval [1,2,…,M] where M is the total number of fibres in the Elementary Representative Volume (ERV), which has dimensions large enough to be characteristic of the composite material considered and is conditioned by the Mori-Tanaka model.

Thus, to evaluate fibre failure, the stress in each fibre is compared to its corresponding strength as defined by σ_j^{break}.

For the matrix failure:

$$P_{matrix} = 1-[1-F_X(\sigma_{11})][1-F_Y(\sigma_{22})][1-F_S(\tau_{12})] \tag{1.7}$$

where F_X, F_Y, F_S are probability functions expressed in the form of Weibull distributions:

$$\begin{aligned} F_X(x) &= 1-\exp\left[-\frac{V}{V_0}\left(\frac{x}{X_{matrix}}\right)^{m_X}\right] \\ F_Y(y) &= 1-\exp\left[-\frac{V}{V_0}\left(\frac{y}{Y_{matrix}}\right)^{m_Y}\right] \\ F_S(s) &= 1-\exp\left[-\frac{V}{V_0}\left(\frac{s}{S_{matrix}}\right)^{m_S}\right] \end{aligned} \tag{1.8}$$

where

	σ_{11} and σ_{22}	are the maximum global stresses,
	τ_{12}	is the maximum shearing stress,
	V_0	is the original gauge volume of the matrix,
	V	is the actual volume
	x, y, s	are the stresses in the matrix in the two global directions and in shear respectively,
	X, Y, S_{matrix}	are the corresponding Weibull scale parameters,
and	$m_{X,Y,S}$	are the Weibull shape parameters.

Damage in the matrix may then be introduced as a fraction of the volume, where P_{matrix} indicates what fraction of the matrix is to be failed by the introduction of microcracks transversely oriented to the direction of loading.

Finally, for the interfacial decohesion between fibre and matrix:

$$P_{interface}(R) = 1 - \exp\left[-\left(\frac{R}{R_0} \right)^{m_i} \right] \tag{1.9}$$

where R is a linear combination of the normal and tangential stress components of the fibre stress, σ_i, measured experimentally

$$R = \sigma_N + \beta\tau$$

R_0 is the Weibull scale parameter

m_i is the Weibull shape parameter

Interfacial damage is introduced as a microcracks transverse to the fibre in question.

Each probabilistic function above governs the progressive introduction of discontinuities and microcracks into the composite material, which are then homogenized by the Mori-Tanaka scheme prescribed above, at each step.

Another Mori-Tanaka homogenisation based model (which we refer to here and later in this work as the 'Overall Elastic Moduli Homogenisation Model'), was presented by Chen et al. (1992). Here the formulation presented expresses the properties of the homogenised medium entirely in terms of the elastic properties of the constituent phases.

The premise of the material model is that the constitution of a transversely isotropic solid (in this case the fibre phase in local coordinates) may be expressed as follows:

$$\begin{bmatrix} s \\ \sigma \end{bmatrix} = \begin{bmatrix} k & l \\ l & n \end{bmatrix} \begin{bmatrix} e \\ \varepsilon \end{bmatrix}$$
$$\tau_{23} = 2m\varepsilon_{23} \tag{1.10}$$
$$\tau_{12} = 2p\varepsilon_{12}$$
$$\tau_{13} = 2p\varepsilon_{133}$$

where

$$s = \frac{1}{2}(\sigma_{22} + \sigma_{33})$$
$$\sigma = \sigma_{11} \tag{1.11}$$
$$e = \varepsilon_{22} + \varepsilon_{33}$$
$$\varepsilon = \varepsilon_{11}$$

k, l, m, n and p are Hill's elastic moduli (Hill, 1964). Specifically, k is the plane-strain bulk modulus for lateral dilation without longitudinal extension, n is the modulus for longitudinal uniaxial straining, l is the associated cross modulus, m is the shear modulus in any transverse direction and p is the shear modulus for longitudinal shearing.

In order to relate the isotropic matrix with the transversely isotropic fibre phases, we may write the following set of equations, which allow us to find the above material constants for the matrix phase:

$$\begin{aligned} k_1 &= K_1 + \frac{1}{3}G_1 \\ l_1 &= K_1 - \frac{2}{3}G_1 \\ n_1 &= K_1 + \frac{4}{3}G_1 \\ m_1 &= p_1 = G_1 \end{aligned} \tag{1.12}$$

where K_1 and G_1 are the matrix bulk and shear moduli respectively.

For composites reinforced with randomly oriented fibres, with the matrix (denoted by subscript $r=1$) and fibre phases (denoted by subscripts $r=[2,3,...,N]$) being isotropic and transversely isotropic in the local frame respectively, the overall moduli may be given by the following relations:

$$\begin{aligned} K &= K_1 + \frac{1}{3}\sum_{r=2}^{N} c_r \frac{(\delta_r - 3K_1\alpha_r)}{\left[c_1 + \sum_{r=2}^{N} c_r\alpha_r\right]} \\ G &= G_1 + \frac{1}{2}\sum_{r=2}^{N} c_r \frac{(\eta_r - 2G_1\beta_r)}{\left[c_1 + \sum_{r=2}^{N} c_r\beta_r\right]} \end{aligned} \tag{1.13}$$

where

K, G	are the overall bulk and shear moduli of the composite respectively,
c_r	are the volumetric fractions of each phase r, with the matrix phase assigned $r=1$ and the fibre phases following as $r=[2,3,...,N]$.
$\alpha_r, \beta_r, \delta_r, \eta_r$	depend on the moduli and geometry of the phases, and for cylindrical fibres are given as follows:

$$\begin{aligned} \alpha_r &= \frac{3K_1 + 3G_1 + k_r - l_r}{3G_1 + 3k_r} \\ \beta_r &= \frac{1}{5}\left[\frac{4G_1 + (2k_r + l_r)}{3G_1 + 3k_r} + \frac{4G_1}{p_r + G_1} + \frac{2(\gamma_1 + G_1}{\gamma_1 + m_r}\right] \\ \delta_r &= \frac{1}{3}\left[n_r + 2l_r + \frac{(2k_r + l_r)(3K_1 + 2G_1 - l_r}{k_r + G_1}\right] \\ \eta_r &= \frac{1}{5}\left[\frac{2}{3}(n_r - l_r) + \frac{8m_rG_1(3K_1 + 4G_1)}{m_r(3K_1 + 4G_1) + G_1(3K_1 + 3m_r + G_1)} + \frac{8p_rG_1}{p_r + G_1} + \frac{4k_rG_1 - 4l_rG_1 - 2l_r^2 + 2k_rl_r}{3k_r + 3G_1}\right] \end{aligned} \tag{1.14}$$

where, for an isotropic matrix,

$$\gamma_1 = \frac{3G_1K_1 + G_1^2}{3K_1 + 7G_1} \tag{1.15}$$

Note that the elastic modulus of the fibre phases are defined in the local coordinate frame of that fibre.

In another model, presented by Hoffmann (1995), SMC is viewed as a laminate consisting of fibre bundles embedded in the resin/filler matrix where the individual layers are assumed void free and adhere firmly to one another. The stiffness of the bundles and the matrix is expected to be reduced by the development of cracks, which is viewed as a statistical process.

A combination of the quadratic criterion in stress space and the maximum strain criterion is used to predict failure in the fibres and matrix respectively. The model also includes residual stresses arising from high curing temperatures, anisotropic fibre orientation and varying content of filler particles in the matrix inside and outside of bundles.
This model also allows for the appreciation of the quantitative influence of different materials and processing parameters on SMC behaviour and in this way to optimise its composition.

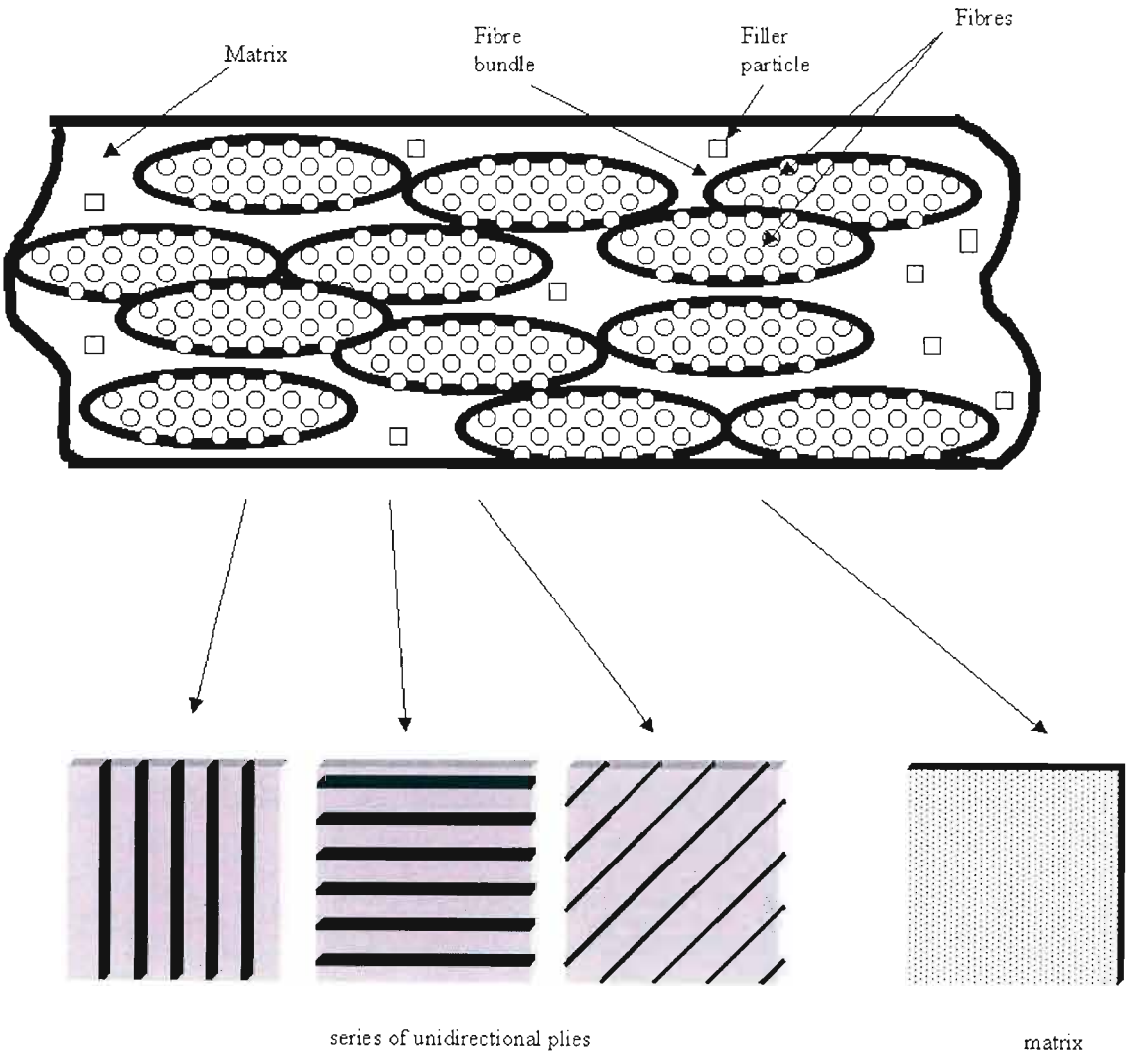

Fig. 1.2 Representation of SMC by means of a multilayer composite consisting of unidirectional plies

The fundamental element of the SMC structure is modelled here (see Fig. 1.2) as the fibre bundle saturated by the matrix material (which is assumed isotropic with elastic properties), which represents a unidirectional (UD) composite the thermo-elastic properties (TEP) of which may be calculated using formulae presented by Hashin (1979).

The TEP of the matrix may be calculated by combining the formulae of Kerner and Hashin as done in Kabelka & Ehrenstein (1992) and on the basis of the TEP's of the matrix and filler and of the filler fractions, the material properties can be calculated.

The fibre bundles saturated by the "internal" matrix are the effective reinforcing elements and can be viewed as macroscopic fibres with anisotropic properties embedded in the "external" matrix. These bundles are randomly distributed and are differently oriented.
By collecting all the bundles lying in the same direction into one ply, the stochastic structure is transformed in the multilayer composition, consisting of UD-plies having identical TEP's. The total stiffness of the laminate is then determined by summing the individual layer stiffnesses.

The following elliptic failure criterion was proposed along with the constitution described above (Hoffmann et al., 1995):

$$\frac{\sigma_T^2}{R_T^2}+\frac{\sigma_{LT}^2}{R_{LT}^2}=1 \tag{1.16}$$

where R_T and R_{LT} are tensile and shear strengths, determined experimentally.

In multilayered composites, however the local fracture propagates through the layer and causes a stress concentration in the adjacent, unfractured laminae, which arrests its further propagation. The damaged ply cannot support any transverse tensile or shear load in the vicinity of the crack and its contribution to the total stiffness is in this way reduced but its stiffness in the fibre direction is unaffected. The stiffness reduction degradation function of the bundles is accepted in the form:

$$D_b(\sigma_T,\sigma_{LT})=1-e^{-(0.707\frac{\sigma}{R})^2} \tag{1.17}$$

A similar procedure is used to assess the crack creation in the matrix surrounding the bundles where in this case the maximum strain criterion is used. The ultimate elongation was found by experimentation to have the following form:

$$\varepsilon_{mu}=1.5\sqrt{\varepsilon_{ru}}(1-1.04\sqrt[3]{\Phi_{pe}}) \tag{1.18}$$

where ε_{ru} is the tensile elongation and Φ_{pe} is the filler fraction.

So, the stiffness of each layer may be defined according to its level of stressing, and the total laminate stiffness is found as a sum of the stiffnesses of the degraded layers

The moduli of elasticity of SMC are calculated at stepwise increasing strain (ε_l) and the corresponding stress σ_l is determined for each value of strain, assuming the SMC response to be linear. Thus, the σ-ε curve is obtained to describe the damage process in SMC.

Comparative results presented by Hoffmann (1995), ostensibly show that the model is able to describe the SMC behaviour under tensile loading especially well at the beginning of loading, however when a higher level of crack density is reached, the damage process takes on a local character, which the model is not able to take into account. Also, substantial differences in the

second half of the loading cycle can also be caused by the initial anisotropy of the investigated SMC samples. It should be noted that to prevent misrepresentation due to material anisotropy, measurements on specimens cut in two mutually perpendicular directions are necessary.

In summary, this model is a rather unique approach to modelling a short fibre composite, and presents a new perspective. This layered approach at first glance seems an unwieldy and overcomplicated attempt at modelling composites that in fact would appear to perform as homogenised materials, as a representative volume model or the models already described above would suggest. However results presented by the Hoffmann et al. show fairly good correlation with experiment, especially for lower crack density values, which would indicate that further investigation into this method of modelling might be in order. It must be remembered however that the results presented are fairly artificial as the values for R_T and R_{LT} were chosen to best fit the experimental results. This evaluation is feasible though, as it could mean that a database for these values could be built up, or initial testing could be performed prior to modelling.

Moving on, the 'Interpolated Aggregate Model' as mentioned earlier, makes use of a Fibre Orientation Distribution (FOD) to model short fibre composite material. The premise of this model is that the mechanical properties of a composite material with some known FOD are determined by testing specially fabricated specimens; and then these elastic constants could be extrapolated for any other fibre orientation state.

This general concept is known as the aggregate model, originally suggested in the work of Voigt (1889) and using this concept, elastic moduli have been predicted for composites having planar random, spatial random, and transversely isotropic FODs, and has been successfully applied to polymeric short-fibre composites. In each instance the model makes use of a unit cell with transversely isotropic elastic properties.

This aggregate model has limitations, however, namely:

(1) the unit cell stiffnesses must first be estimated by micromechanical approximations
(2) it is reasonably accurate only at nearly unidirectional orientations.

The interpolated aggregate model serves to overcome these limitations. The model is based on parameters easily determined from elastic constants measured on the material in a known, but arbitrary orientation state. The need for micromechanics is thus eliminated, but strong dependence on the definition of the FOD matrix is noted and necessary.

The development of this model is described as follows. Let $M_{\alpha\beta\gamma\delta}$ be the stiffness components of the unit cell in local coordinates (x_1', x_2', x_3') associated with the reinforcement orientation as shown in Fig. 1.3. These may be transformed to the stiffnesses in the global coordinates frame (x_1, x_2, x_3) as follows:

$$B_{ijkl} = l_{i\alpha} l_{j\beta} l_{k\gamma} l_{l\delta} M_{\alpha\beta\gamma\delta} \tag{1.19}$$

where

$$l_{ij} = \cos\alpha_{ij} = \frac{\partial x_i}{\partial x_j'} \tag{1.20}$$

and α_{ij} and $x_j^{'}$ are defined as shown in Fig. 1.3.

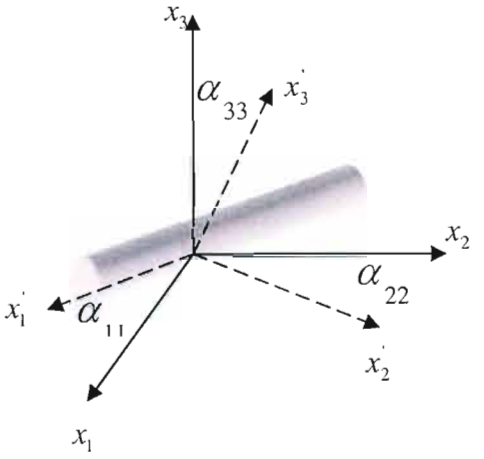

Fig. 1.3 Spatial orientation of the reinforcement for the general, 3D case

The orientation of the unit cell is defined in terms of only two Eulerian angles φ and ω (Fig. 1.4) defined as follows, since rotation about the fibre axis $x_1^{'}$ is immaterial for transverse isotropy:

$$\cos\varphi = \frac{\cos\alpha_{21}}{\sin\alpha_{11}} \tag{1.21}$$

$$\omega = \alpha_{11} \tag{1.22}$$

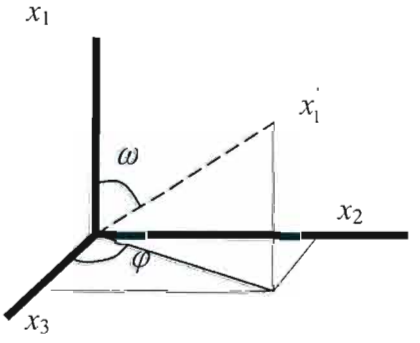

Fig. 1.4 Eulerian angles

Assuming that the stiffness of the material is equal to the volume average of the transformed stiffnesses of all unit cells, the stiffness components of the material can be calculated as

$$C_{ijkl} = \oint l_{i\alpha} l_{j\beta} l_{k\gamma} l_{l\delta} M_{\alpha\beta\gamma\delta} \psi(\boldsymbol{q}) d\boldsymbol{q} \tag{1.23}$$

where $\boldsymbol{q}$ denotes the unit cell orientation, $\oint d\boldsymbol{q}$ means integration over all possible orientations and $\psi(\boldsymbol{q})$ is the orientation distribution function defined such that the volume fraction f of the unit cells in the interval $(q, q+dq)$ is given by

$$f(\boldsymbol{q},\boldsymbol{q}+d\boldsymbol{q}) = \psi(\boldsymbol{q})d\boldsymbol{q} \tag{1.24}$$

Assume that all unit cells are identical and introduce vector $\{C\}$containing the 21 independent components of the material stiffness matrix C_{ijkl}, as

$$\{\tilde{C}\} = \begin{Bmatrix} C_{1111} \\ C_{2222} \\ C_{1212} \\ C_{1122} \\ C_{3333} \\ C_{2323} \\ C_{3131} \\ C_{1133} \\ C_{2233} \\ C_{1123} \\ C_{1131} \\ C_{1112} \\ C_{2223} \\ C_{2231} \\ C_{2212} \\ C_{3323} \\ C_{3331} \\ C_{3312} \\ C_{2331} \\ C_{2312} \\ C_{3112} \end{Bmatrix} \tag{1.25}$$

then Eq. 1.23 could be presented in the form

$$\{\tilde{C}\} = [F]\{\tilde{M}\} \tag{1.26}$$

where $[F]$ is a descriptor of the orientation state, defined by

$$F = \oint l_{i\alpha} l_{i\beta} l_{i\gamma} l_{i\delta} \psi(q) dq \tag{1.27}$$

and $\{\tilde{M}\}$ is the unit cell stiffness vector containing the independent components of $[M]$, the full unit cell stiffness tensor

$$\{\tilde{M}\} = \begin{bmatrix} M_{1111} \\ M_{3333} \\ M_{1313} \\ M_{1122} \\ M_{1133} \end{bmatrix} \tag{1.28}$$

The interpolation procedure follows as:

If $\{\tilde{C}\}$ is known for a particular orientation state [F], $\{\tilde{M}\}$ may be established; and could be employed to find $\{\tilde{C}\}$ for any other orientation state [F].

The problem lies in the fact that $\{\tilde{C}\}$ is generally not easily known. To simplify the problem, certain assumptions are made regarding the unit cell which reduces the number unit cell stiffness components to five, as described by Eq. 1.28 (Toll, 1992).

Now, the unit cell stiffness vector $\{\tilde{M}\}$ may be rewritten as:

$$\{\tilde{M}\} = [R]\begin{Bmatrix} T \\ L \end{Bmatrix} \tag{1.29}$$

where T and L are the transverse and longitudinal unit cell stiffnesses M_{1111} and M_{3333} respectively, and

$$[R] = \begin{bmatrix} 1 & 0 \\ 0 & 1 \\ (1-\frac{M_{1133}}{M_{1111}})\frac{M_{1313}}{2M_{1212}} & 0 \\ \frac{M_{1122}}{M_{1111}} & 0 \\ \frac{M_{1133}}{M_{1111}} & 0 \end{bmatrix} \tag{1.30}$$

The ratios above may be expressed in terms of Poisson's ratios:

$$\frac{M_{1122}}{M_{1111}} = \frac{\nu_{12} + \nu_{31}\nu_{13}}{1-\nu_{13}\nu_{31}} \tag{1.31}$$

$$\frac{M_{1133}}{M_{1111}} = \frac{\nu_{31} + \nu_{12}\nu_{31}}{1-\nu_{13}\nu_{31}} \tag{1.32}$$

And since the longitudinal and transverse shear stiffnesses M_{1313} and M_{1212} are usually of similar magnitude

$$\frac{M_{1313}}{M_{1212}} \approx 0.5 \tag{1.33}$$

Now, in the limit (isotropic conditions) T=L, and this requires the following:

$$\frac{M_{1122}}{M_{1111}} = \frac{M_{1133}}{M_{1111}} = \frac{\nu + \nu^2}{1 - \nu^2} \tag{1.34}$$

Where ν is the longitudinal Poisson's ratio ν_{31} (Toll, 1992).

Thus for a known ν, $\{R\}$ may be completely determined.

This model does require a 'calibration' process. Inaccuracies occur in the strain field as a result of the assumption of a non-equilibrium strain field with uniform strain. According to the minimum potential energy theorem, the inaccuracies will be overestimated, and will increase in overestimation with increasing heterogeneity of strain.
These inaccuracies in the strain field are taken into account by reducing the unit cell stiffnesses at some orientation state ψ.
The model is thus calibrated at this orientation state of calibration and errors in the engineering modulus will be smallest for orientations closest to ψ.

This calibration procedure entails the selection of two material stiffnesses (eg. C_{1111} and C_{2222}) which are measured experimentally, to act as calibration parameters. The relation $\{\tilde{C}\} = [F]\{\tilde{M}\}$ is made true for these two stiffness values, and the multipliers required to adjust the predicted stiffnesses to the measured stiffnesses is computed. These multipliers are then applied to the values of T and L to adjust them accordingly.

In summary, the dependence of this model on the experimental definition of an FOD is both clumsy and not necessarily representative. Inadequacies in this method of modelling have already been intimated to, and these remain, highlighted in this case by the need for artificially defined calibration parameters.

Another model encountered and eventually implemented (Chapter 2), due to it being the most relevant modelling option for SMC composites available in the PAM-CRASH finite element analysis package which was eventually adopted for numerical simulation study (see Chapter 3) was the relatively simple Elastic-Plastic material model with isotropic damage behaviour, as presented in PAM-CRASH Theory Manual, 2000. Here the material is initially isotropic and the software includes both a plasticity analysis algorithm and a damage mechanics law based on experimentally obtained results. For the purposes of this study only the damage law option was considered to model SMC composite behaviour.

In this model, damage is applied to the material stress tensor as follows:

$$\sigma = \left(1 - d(\varepsilon_p)\right)\sigma_0 \tag{1.35}$$

where σ is the full stress tensor for the damaged material,
$d(\varepsilon_p)$ is the isotropic scalar damage function, a function of the strain, ε_p (accounting for plasticity effects if necessary),
σ_0 is the full stress tensor as calculated according to the elastic-plastic material law (with or without strain rate effects) for the undamaged material.

The damage curve is assumed piecewise linear between the strain points, $\varepsilon_i, \varepsilon_1, \varepsilon_u$, which are obtained off an experimental stress-strain curve for the material, as shown in Fig. 1.5 for a material with plasticity taken into account. For SMC composite modelling, which includes no

plasticity effects, the material is progressively degraded by the damage function only, and there is no reduction of the modulus of the material caused by plastic deformation (Fig. 1.6).

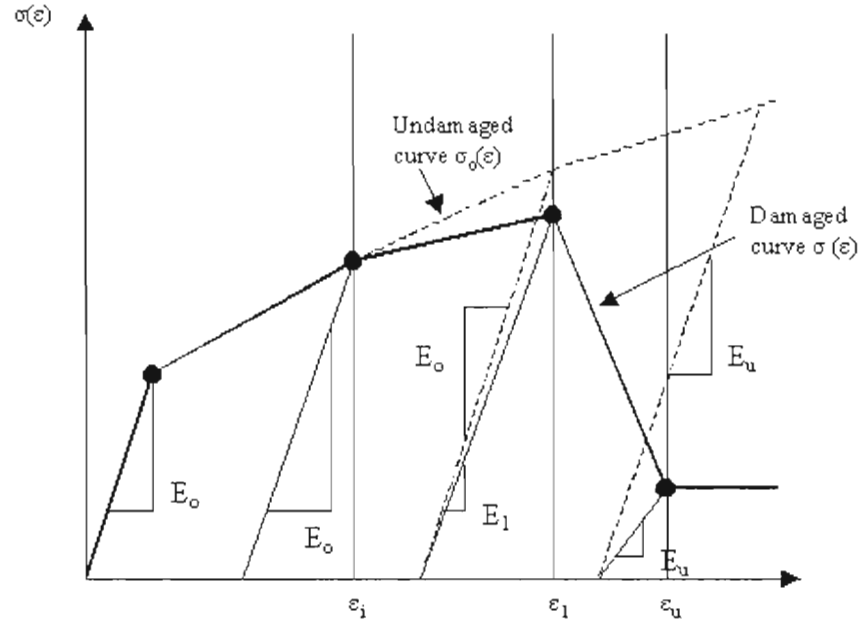

Fig. 1.5 Damaging curve for an elastic-plastic material

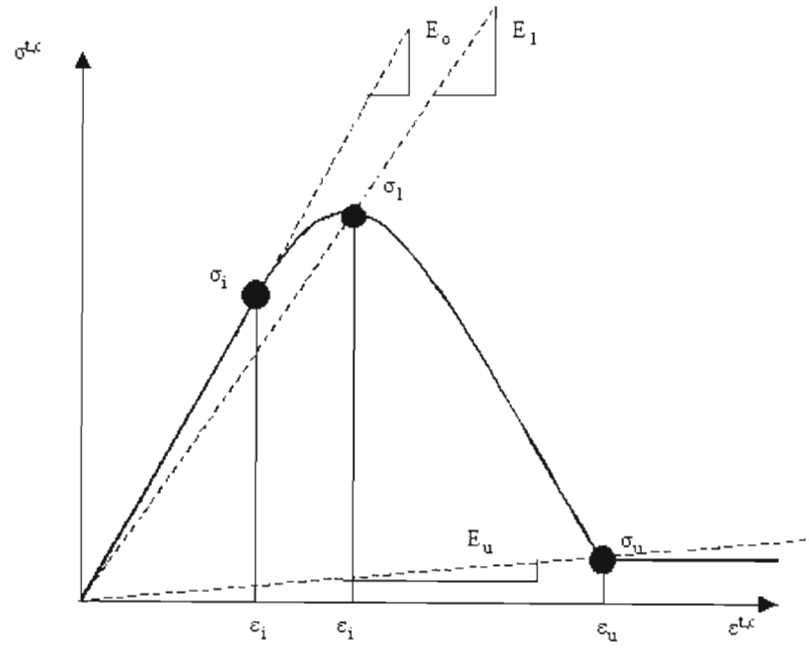

Fig. 1.6 Damaging curve used for an SMC composite material

The isotropic scalar damage, function d is defined as follows:

$$d_1 = 1 - \frac{E_1}{E_0} \tag{1.36}$$

at ε_1 and

$$d_u = 1 - \frac{E_u}{E_1} \tag{1.37}$$

at ε_u.

Between these defined points, d grows linearly from 0 to d_1 in the interval $\varepsilon_i \leq \varepsilon \leq \varepsilon_1$, and from d_1 to d_u in the interval $\varepsilon_1 \leq \varepsilon \leq \varepsilon_u$. Beyond the ultimate damage strain the damage function remains constant (see Fig. 1.7).

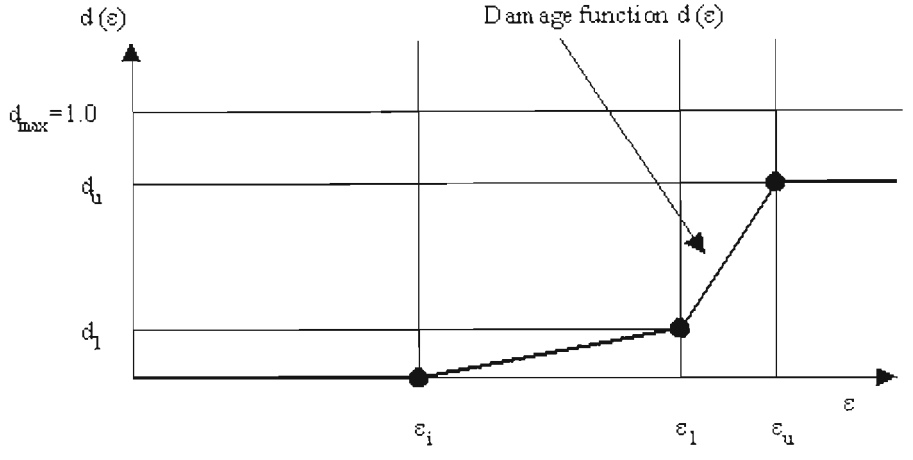

Fig. 1.7 Isotropic damage function

Definition of the values of the three key strain points is done by analysis of experimental stress-strain curves on the material in question. These curves are obtained from uniaxial testing.

Now that we have an idea of a typical model that may be used for short-fibre composite analysis, we can look at a similarly implemented model, but this time without the use of a composite specific damage function. This may at first seem rather arbitrary and not of particular relevance, but the survey in Chapter 3 will show that options by way of available implemented composite models for the class of composites we are dealing with here are particularly limited, and the 'Elastic Plastic with Kinematic Hardening' material model (LS-DYNA Theory manual, 1998) is included here as it represents the most suitable model for the progressive damage simulation of SMC composites in the LS-DYNA finite element analysis package, which was chosen as a secondary analysis tool (to be discussed in Chapter 3). This model is suitable for the modelling of isotropic and kinematic hardening plasticity with the option of including strain rate effects, and thus is loosely applicable to SMC composites. It may also serve to represent modelling options available in any basic finite element package, without any real composite options, and thus might be the only option available to some researchers/analysts who may be doing only basic analysis.

The following material properties are required to characterise the material:

- ρ, Mass density,
- E, Young's modulus,
- ν, Poisson's ratio,
- σ_Y, Yield stress,
- E_t, Tangent modulus
- β, Hardening parameter.

Isotropic, kinematic, or a combination of isotropic and kinematic hardening may be obtained by varying the hardening parameter β between 0 and 1. For β equal to 0 and 1 kinematic and isotropic hardening are obtained respectively. In isotropic hardening, the centre of the yield surface is fixed but the radius is a function of the plastic strain. In kinematic hardening, the radius of the yield surface is fixed but the centre translates in the direction of the plastic strain.

Thus, almost paradoxically, both the variety of methods available for modelling, as well as the lack of truly representative implemented modelling options is shown. The most critical result of the survey performed here is in fact the latter observation, and this forms the basis of the rest of this study. The variety of paths to take creates the first step necessary to proceed: the choice of suitable modelling options. Next, these models are to be in some way studied as to their implementabilty, and practicality. Once this has been completed, an assessment will be made as to whether a suitably representative model exists for crashworthiness modelling of SMC composites. If this analysis shows there to be any lacking in this regard, new modelling options will be approached and analysed. In this way, a suitable model, able to be practically implemented and adopted into the finite element analysis environment, such that it may be readily used to analyse crash situations, will be presented.

Chapter 2

Material Characterisation and Model Implementation Analysis

As a first step in the analysis to be performed, a selection of models was made from those discussed in Chapter One, based on their applicability to the specific problem of SMC composite crashworthiness, and their implementability within the time and budgetary constraints of this study. Various models were considered inapplicable by virtue of their being too cumbersome to execute under practical conditions, not quite being fully complete in their formulation, or not being financially viable due to costly material characterisation requirements. The discussion presented here thus looks at the physical material characterisation requirements of each model, and includes only those models that were considered both applicable, and viable.

Included below are both models that are ready-implemented into commercial modelling packages (PAM-CRASH and LS-DYNA) as well as proposed models that are based on modelling theories introduced in the previous chapter.

What becomes immediately apparent during the following analysis is the true practicality of the respective models. It is fair to say that this sort of analysis is neglected in most technical write-ups, however, as may be clearly seen, the implementation of a model sometimes entails unexpected considerations, and requires much added input. The latter models have thus been modified, coupled with relevant failure criteria, and prepared for implementation and may therefore be considered entirely new formulations.

2.1 Models available and implemented into the Finite Element Analysis environment

2.1.1 Elastic-Plastic Model with Kinematic Hardening

This model, as mentioned earlier, has, strictly speaking, been formulated for elastic-plastic isotropic materials, and the following parameters should be provided in this case. However, for SMC composite materials, some of these parameters (especially those defining the plasticity behaviour) are not applicable and must be reinterpreted within the framework of SMC composites modelling. The model is included here simply because it represents the only method for the modelling short fibre composites, namely by general isotropy, available in any basic modelling packages without any true short-fibre composite modelling options (in this case, LS-DYNA).

2.1.1.1 Material Characterisation

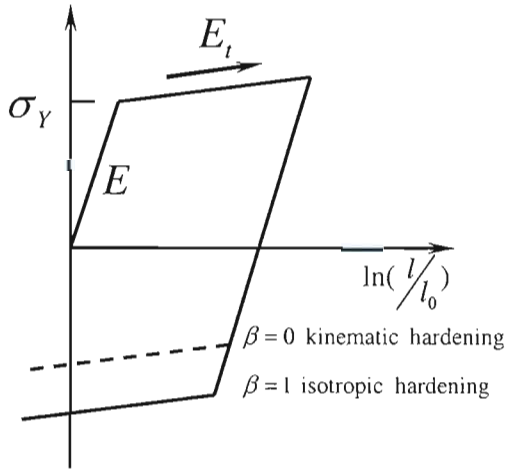

Fig. 2.1 Elastic-plastic behaviour with kinematic and isotropic hardening, where l_0 and l are undeformed and deformed lengths of uniaxial tension specimen, E_t is the slope of the bilinear stress-strain curve

An overview of the required material parameters, and their method of characterisation is presented:

- ρ : mass density of the SMC material.
- E and ν : Young's modulus and Poisson's ratio found during tensile testing of a flat specimen made from the material to be modelled.
- σ_y, E_t, β : for isotropic materials, these parameters correspond respectively to the yield stress, tangent modulus and hardening parameter. Fig. 2.1 shows how to find these parameters in the isotropic case. Obviously, for SMC composites these characteristics need to be interpreted differently. To do this, it is required to perform tensile and compression tests and plot diagrams of Stress vs. $\ln(l/l_0)$. These figures then yield the necessary parameters for SMC material.

- *D, p*: strain rate parameters for the Cowper-Symonds strain rate model. These parameters are used to best fit the simulated curves with the experimental data.

Thus, in summary, to model SMC composite behaviour using this model, we are required to test simple flat specimens:

- 1 specimen should be tested under tension to find the Young's modulus and the Poisson's ratio
- 1 specimen should be used to model SMC composite behaviour with isotropic plastic law

It is immediately obvious that such a model is in no way tailor-suited for SMC composite analysis, but as mentioned earlier, sometimes represents the entirety of modelling options available to work with, and to thus quantify the applicability and the results obtainable is a meaningful exercise. The characterisation requirements are of course simple to carry out due to the model's rather simplistic approach.

2.1.2 Elastic Model with Isotropic Damage Behaviour

Another ready implemented model, as seen in the PAM-CRASH software, this model represents a vast improvement on the last model as it adopts a specific algorithm geared towards progressive degradation, as is exhibited by composite materials, rather than relying on plasticity or hardening effects alone. This is the first truly applicable composite material model found that was immediately applicable to short-fibre composite analysis.

2.1.2.1 Material Characterisation

Tensile testing yields the following elastic properties of the SMC material:

- Modulus of elasticity, E
- Poisson's ratio, ν

Shear modulus is calculated as

$$G = \frac{E}{2(1+\nu)} \tag{2.1}$$

The isotropic damage behaviour parameters $\varepsilon_i, \varepsilon_1$ and ε_u, are interpreted as equivalent threshold strains. They are found from the stress-strain diagram as described in Chapter 1.3. Damage variable $d_1 = 1 - E_1 / E_0$ where E_0 is the initial elastic modulus and E_1 the unloading modulus determined in the test at the intermediate uniaxial strain ε_1. Damage variable d_u is the ultimate damage. Its value is usually taken less than 1 in order to assign a non-zero resistance for large strains.

2.1.2.2 Strain Rate effects

The PAM-CRASH software allows the use of different laws to model the strain rate effect (dependence of the stress-strain diagram on the rate of loading) in conjunction with this material model. Each law (as presented in PAM-CRASH Solver Notes, 2000) modifies the

original strain-rate curve $\sigma_0(\varepsilon)$ by multiplying it by a factor of amplification, which is a function of a number of parameters, depending on the complexity of the model:

- Cowper-Symonds law:

$$\sigma(\varepsilon,\dot{\varepsilon}) = \sigma_0(\varepsilon)\left[1+\left(\frac{\dot{\varepsilon}}{D}\right)^{1/p}\right] \tag{2.2}$$

where $\sigma_0(\varepsilon)$ is the original stress-strain curve (without any strain-rate influence), $\dot{\varepsilon} = \frac{d\varepsilon}{dt}$ is the strain-rate, and D and p are two parameters used to fit the simulated curve to experimental results, i.e. to reflect the observed strain-rate dependency of the material.

- Johnson-Cook law:

$$\sigma(\varepsilon,\dot{\varepsilon}) = \sigma_0(\varepsilon)\left[1+\frac{1}{p}\cdot\ln(\max(\dot{\varepsilon}/D,1))\right] \tag{2.3}$$

where all the parameters have already been described for the Cowper-Symonds law.

- Modified Jones' law:

$$\sigma(\varepsilon,\dot{\varepsilon}) = \sigma_0(\varepsilon)\left\{1+\left[\frac{(\varepsilon_u-\varepsilon_y)\dot{\varepsilon}}{D_u(\varepsilon-\varepsilon_y)+D_y(\varepsilon_u-\varepsilon)}\right]^{\frac{1}{A\varepsilon+B}}\right\} \tag{2.4}$$

where $\sigma_0(\varepsilon)$ is the original stress-strain curve (without any strain-rate influence), and $\dot{\varepsilon} = \frac{d\varepsilon}{dt}$ is the strain-rate. D_u, D_y, A and B are four constants, which are used to fit the simulated curve with the experimental data. The stress-strain diagrams corresponding to this law are shown in Fig. 2.2.

Between ε_y and ε_u, the factor of amplification is equal to $\sigma(\varepsilon,\dot{\varepsilon})/\sigma_0(\varepsilon)$ due to the variable strain rate. This law can be considered as the Cowper-Symonds law, calibrated at strains ε_y and ε_u, corresponding respectively to σ_y and σ_u where σ_y extrapolates the function σ for strains lesser than ε_y and σ_u extrapolates it for strains greater than ε_u. To avoid extrapolations, ε_y is usually set to 0 and ε_u is taken large enough to cover all strains encountered during the analysis.

- Left shifted stress-strain law :

Good approximations of strain rate dependency may be obtained by shifting a basic Stress vs. Strain curve $\sigma_0(\varepsilon)$ in the direction of negative strain by an amount of ε_0, depending on strain rate. A left shift of $\varepsilon_0(\dot{\varepsilon}_{ref}) = \varepsilon_{0ref}$ could be measured at a given reference strain rate, then approximately $\sigma(\varepsilon,\dot{\varepsilon}_{ref}) = \sigma(\varepsilon+\varepsilon_{0ref})$. The shift, ε_0, depends on the strain rate as follows: $\varepsilon_0(\dot{\varepsilon}) = \varepsilon_{0ref}(\dot{\varepsilon}/\dot{\varepsilon}_{ref})^p$. Then strain rate dependent stress-strain law is presented as:

$$\sigma(\varepsilon,\dot{\varepsilon}) = \sigma_0(\varepsilon)\left(\varepsilon + \varepsilon_{0ref}\left(\frac{\dot{\varepsilon}}{\dot{\varepsilon}_{ref}}\right)^b\right) \tag{2.5}$$

Where b is a parameter used to best fit the simulated curves to the actual observed strain rate dependency of the material.

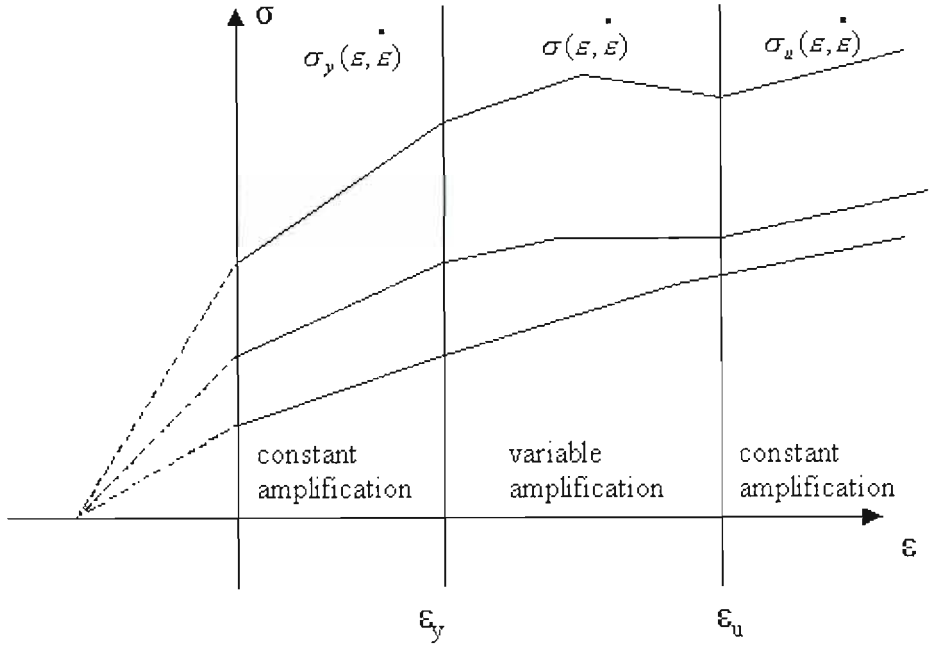

Fig. 2.2 Modified Jones' law

2.1.3 Conclusions

The two implemented models presented above represent those models readily available for short fibre composite modelling in two of the most popular finite element analysis packages available. It is obvious that the LS-DYNA implemented Hardening model is far from ideal, and whereas the PAM-CRASH implemented Isotropic Damaging model is more readily acceptable, it is clearly evident that room for improvement exists. This is to be confirmed or not by simulated results later in this work, but at this stage, it is considered a necessary task of this study to propose the implementation of possible new modelling options, based in part on existing modelling approaches, with modifications or additions to these, to prepare them for implementation within the finite element analysis environment.

The three models following were all investigated for their implementation potential, and within the scope of this work, one was chosen for further scrutiny and subsequent development into a new, complete analysis model.

2.2 Development of models proposed for implementation

2.2.1 Mori-Tanaka Homogenisation model with Statistical Failure Criteria

2.2.1.1 Algorithm for implementation

This model is based on that of Desrumaux et al. (1995) as described in Chapter 1. An algorithm for the implementation, is presented in Fig. 2.3

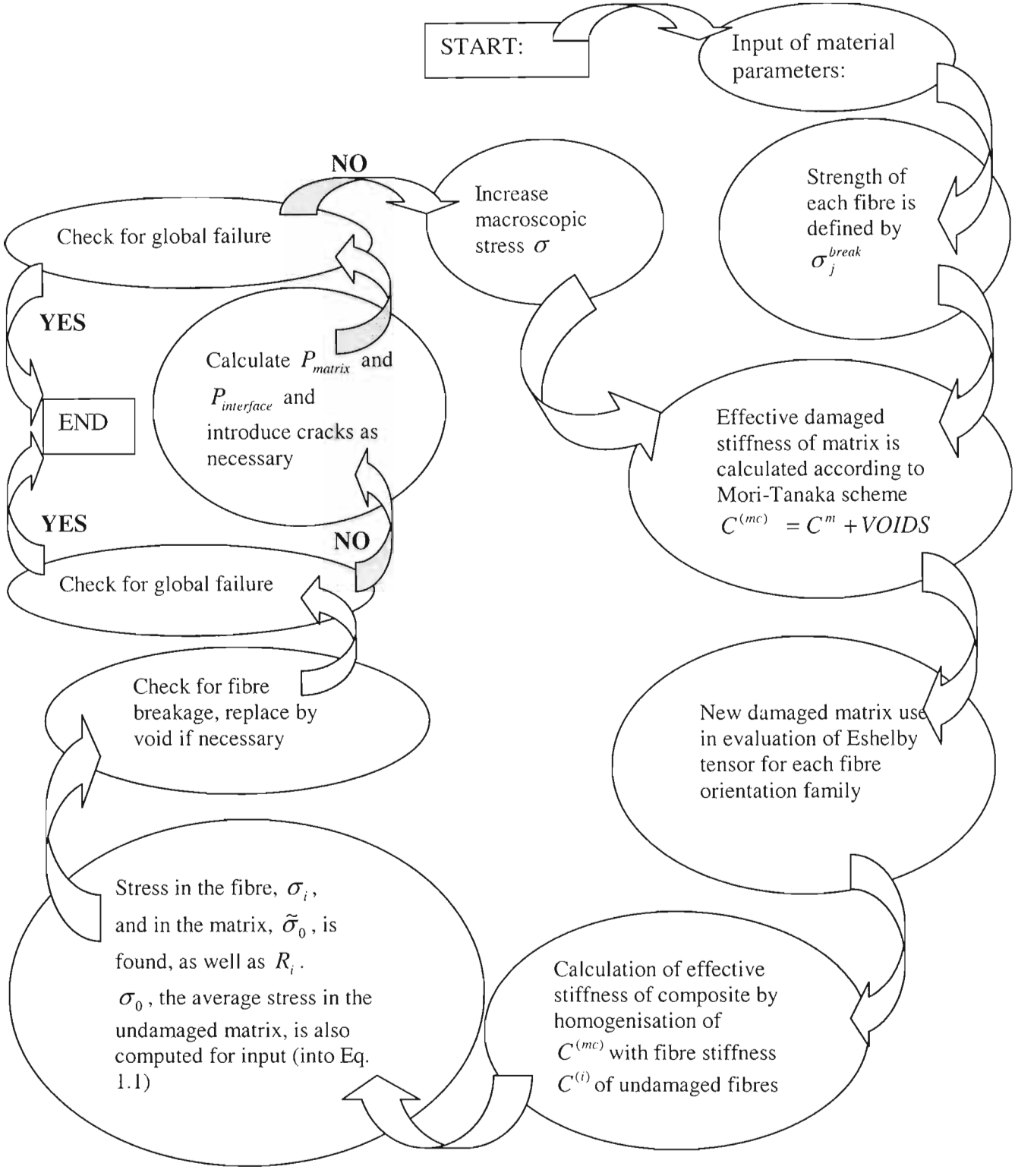

Fig. 2.3 Algorithm for integration of Mori-Tanaka model with statistical damage

The algorithm steps are described further below:

1. The material parameters are required for input as follows

$$C^{(0)}, C^{(i)}, N, L, L_0, V,$$
$$V_0, X_{matrix}, Y_{matrix},$$
$$S_{matrix}, X_{fibre}, R_0, \beta,$$
$$m_f, m_X, m_Y, m_S$$

- L_0 and d, the measured length and diameter of the fibres respectively, yield the parameter

- m_f and X_f, the Weibull shape and scale parameters respectively. Parameter m_f corresponds to the dispersion of the fibre strength about the average strength X_f. The specimen to be used is a composite with the same material composition as for the SMC material (same matrix material and same fibre material). A sufficient number of such specimens is required for representative normal strength measurements to be made by tensile testing of the unidirectional material along the fibres. The failure stress σ is determined for each specimen, and then we can plot $\ln\left(-\ln\left(1-P_f\right)\right)$ versus $\ln(\sigma)$ where P_f is the probability of failure of fibres for a given stress. This probability is obtained by counting the number of specimens that failed at the given normal stress. Parameters m_f and X_f are the slope and the y-intercept of the plotted line respectively (Parthasarathy et al., 1998).

- $C^{(i)}$, the stiffness tensor of each family of fibres, characterized by a given orientation. In a first approximation we can assume that each phase behaves like a unidirectional ply and use a corresponding tensor expression for $C^{(i)}$ (in the transversely isotropic case) (Desrumaux et al., 1995). As we are considering the modelling of thin-walled components, we neglect the transverse normal strain and in the global system of coordinates, we can then write:

$$\{\tilde{\sigma}\} = C^{(i)}\{\tilde{\varepsilon}\} \Leftrightarrow \begin{pmatrix} \sigma_{11} \\ \sigma_{22} \\ \tau_{12} \\ \tau_{13} \\ \tau_{23} \end{pmatrix} = \begin{pmatrix} C_{11} & C_{12} & C_{14} & 0 & 0 \\ C_{12} & C_{22} & C_{24} & 0 & 0 \\ C_{14} & C_{24} & C_{44} & 0 & 0 \\ 0 & 0 & 0 & C_{55} & C_{56} \\ 0 & 0 & 0 & C_{56} & C_{66} \end{pmatrix} \times \begin{pmatrix} \varepsilon_{11} \\ \varepsilon_{22} \\ \gamma_{12} \\ \gamma_{13} \\ \gamma_{23} \end{pmatrix} \tag{2.6}$$

where:

$$\begin{cases} C_{11} = \overline{E}_1 c^4 + \overline{E}_2 s^4 + 2E_{12} c^2 s^2 & C_{44} = \left(\overline{E}_1 + \overline{E}_2 - 2\overline{E}_1 \nu_{12}\right) \cdot c^2 s^2 + G_{12}\left(c^2 - s^2\right)^2 \\ C_{12} = \overline{E}_1 \nu_{12} + \left(\overline{E}_1 + \overline{E}_2 - 2E_{12}\right) \cdot c^2 s^2 & C_{55} = G_{12} c^2 + G_{23} s^2 \\ C_{14} = \left[\overline{E}_1 c^2 - \overline{E}_2 s^2 - E_{12}\left(c^2 - s^2\right)\right] \cdot cs & C_{56} = \left(G_{12} - G_{23}\right) \cdot cs \\ C_{22} = \overline{E}_1 s^4 + \overline{E}_2 c^4 + 2E_{12} c^2 s^2 & C_{66} = G_{12} s^2 + G_{23} c^2 \\ C_{24} = \left[\overline{E}_1 s^2 - \overline{E}_2 c^2 + E_{12}\left(c^2 - s^2\right)\right] \cdot cs \end{cases} \tag{2.7}$$

and $\overline{E}_1 = \dfrac{E_1}{1-\nu_{12}\nu_{21}}$, $\overline{E}_2 = \dfrac{E_2}{1-\nu_{12}\nu_{21}}$, $E_{12} = \overline{E}_1\nu_{12} + 2G_{12}$, $c = \cos\phi$ and $s = \sin\phi$, where ϕ is the angle of orientation of the fibres in the ply. Then, we have to test a unidirectional composite to find five engineering constants: E_1, E_2, G_{12}, G_{23} and ν_{21}. Another Poisson's ratio ν_{12} can be found from equation: $E_1\nu_{12} = E_2\nu_{21}$. Parameters E_1, E_2 and ν_{21} are determined from a tensile test along and across the fibres of a unidirectional composite. Shear modulus G_{12} could be obtained from a tension test on a $[\pm 45°]_{2S}$ laminate using the following equation:

$$\frac{1}{G_{12}} = \frac{4\varepsilon_{11}}{\sigma_{11}} - \frac{1}{E_{11}} - \frac{1}{E_{22}} + \frac{2\nu_{12}}{E_{11}} \tag{2.8}$$

2. Strength of each fibre in the ERV (Elementary Representative Volume) is determined according to

$$\sigma_j^{break} = X_{fibre}\left[\frac{L_0}{L}\ln\left(\frac{1}{1-z}\right)\right]^{1/m_f} \tag{2.9}$$

3. The stiffness of the effective damaged matrix, C_c, is calculated by Mori Tanaka Scheme.

   Initially there will be no voids, but as damage is predicted according to the statistical failure criteria, those phases which are predicted to fail are replaced, by voids with no material stiffness. At each step these voids are then homogenised with the matrix using

$$C^{(mc)} = C^{(0)}\left[I + \left(\sum_{i=1}^{n} f_i L^{(i)}\right)\left(\sum_{i=1}^{n} f_i\left(S^{(i)} - I\right)L^{(i)}\right)^{-1}\right]^{-1} \tag{2.10}$$

   where

   $L^{(i)}, S^{(i)}, f_i$

   are the localisation tensor, Eshelby tensor and volume fraction respectively of the each void present after failure analysis.

4. Calculate Eshelby tensor for each fibre orientation family with the new matrix $C^{(mc)}$ replacing $C^{(0)}$ in the calculation described.

5. Calculate the damaged effective stiffness of composite, $C^{(c)}$, by the Mori-Tanaka scheme.

$$C^{(c)} = C^{(mc)}\left[I + \left(\sum_{i=1}^{n} f_i L^{(i)}\right)\left(\sum_{i=1}^{n} f_i\left(S^{(i)} - I\right)L^{(i)}\right)^{-1}\right]^{-1} \tag{2.11}$$

6. Find $\sigma^{(i)}$ within each fibre family and $\sigma^{(0)}$ within the matrix by

$$\sigma^{(0)} = B^{(0)}\sigma \tag{2.12}$$

and

$$\sigma^{(i)} = B^{(i)}\sigma \tag{2.13}$$

7. Calculate the interfacial stress for each fibre

$$R_i = \sigma_N + \beta\tau \tag{2.14}$$

8. Check for fibre failure, i.e.

$$\sigma_i > \sigma_j^{break}$$

Then check for global failure, defined by complete loss of fibre contribution in the direction of loading or some pre-determined limit based on, for example, the loading condition.

9. Find P_{matrix} and $P_{\text{interface}}$ and introduce damage as designated.
The probability will define what percentage of the matrix/interface will be replaced by voids. Interface failure corresponds to the introduction of voids transversely oriented to the fibre family responsible for failure; matrix failure corresponds to the introduction of voids transverse to the direction of loading.

11. Check for global failure induced by matrix failure, marked by either the complete loss of strength of matrix phase or some pre-determined limit as for the fibre case.

12. Increase the applied stress and restart damage assessment at step 3.

With the algorithm now fairly evident, we evaluate the characterisation requirements of the model, by way of physical testing that is required for each described variable.

2.2.1.2 Material characterisation

Implementation of the modelling of the fibre phase requires elastic parameters (such as Young's modulus) and Weibull strength characteristics.

In summary, to find the parameters that are to be introduced in order to model the fibre phase, we need:

- 1 specimen of unidirectional composite: a tensile test along the fibres will be performed to find Young's modulus E_1 and Poisson's ratio ν_{12}. A tensile test across the fibres will then provide E_2.
- 1 unidirectional layer loaded at an angle of $\phi = 10°$. This will give G_{12} (off-axis test).
- Approximately 30 (or more) specimens of unidirectional ply. Failure stress measurement on each specimen will give Weibull distribution parameters m_f and X_f, allowing statistical modelling of the strength of the fibre phase.

The matrix phase is isotropic and only two elastic parameters (Poisson's ratio and Young's modulus) are to be determined. To implement this model, we also need strength (normal and shear strength) characteristics of the matrix, which are statistically described using the Weibull distribution (similarly as for the fibre phase above).

- The original measured gauge volume of the matrix material, $V_0 = f_m V_c$ where V_c is the volume of the overall composite and f_m is the matrix fraction.
- $m_x = m_y$, $X_{matrix} = Y_{matrix}$, Weibull shape and scale parameters respectively of the matrix material. A sufficient number of specimens (at least 30) made from the matrix material should be tested to determine failure stresses (corresponding to the normal strength of the material) for each specimen. Then a graph of $\ln(-\ln(1-P_f))$ versus $\ln(\sigma)$ should be plotted, where σ is the strength and P_f is the probability of failure of the material at this particular strength. This probability is obtained simply by counting the number of specimens that failed at a given level of stress. Parameter m_x is the slope of the plotted line and X_{fibre} corresponds to the y-intercept of the plot.
- m_s, S_{matrix}, Weibull shape and scale parameters respectively corresponding to the shear strength of the matrix phase. In the present case, the test will be performed on a sufficient number of specimens made from matrix material. These specimens have a cylindrical shape and should be tested under a pure shear loading. The strength corresponds to the maximum shear stress, i.e. the stress corresponding to the failure of the material. Then graph of $\ln(-\ln(1-P_f))$ versus $\ln(\sigma)$ is plotted, where σ is the strength and P_f is the probability of failure of the material at this particular level of strength. This probability is obtained by counting the number of specimens that failed at a given stress. Parameter m_s is the slope of the plotted line and S_{matrix} corresponds to the y-intercept of the plot.
- E_m, and ν_m, the Young's modulus and Poisson's ratio of the matrix could be obtained from tensile testing of a specimen made of the same material as the matrix of the composite material.
- $C^{(0)}$, the stiffness tensor of the matrix is completely determined by the knowledge of E_m and ν_m, since the matrix is considered isotropic:

$$C_0 = \begin{pmatrix} C_{11} & C_{12} & C_{12} & & & \\ C_{12} & C_{11} & C_{12} & & (0) & \\ C_{12} & C_{12} & C_{11} & & & \\ & & & \frac{C_{11}-C_{12}}{2} & & \\ & (0) & & & \frac{C_{11}-C_{12}}{2} & \\ & & & & & \frac{C_{11}-C_{12}}{2} \end{pmatrix} \tag{2.15}$$

where $C_{11} = \frac{E_m}{1-\nu_m^2}$ and $C_{12} = \frac{E_m \nu_m}{1-\nu_m^2}$.

In summary, in order to characterise the matrix phase in this model we need several flat specimens made from the matrix material of the composite to be modelled

- 1 specimen to be tested under tension to find the Young's modulus and the Poisson's ratio E_m and ν_m,
- up to 20 specimens to give the Weibull distribution of normal strength m_x and X_{matrix} (though less may indeed be justified if convergency of results is displayed),
- up to 20 specimens to give the Weibull distribution of shear strength m_s, and S_{matrix} (similarly).

To model the interfacial phase we have to provide both the normal and shear strengths of this interface. The normal strength is the stress *across* the fibre sufficient to debond the fibre from the matrix. The shear strength is the stress *along* the fibre sufficient to take the fibres and the matrix apart. The strength of this phase is once again described using a Weibull distribution (in the same way that was used for the matrix and fibre phases), with the following parameters required:

- σ_n, the interfacial normal strength. This parameter characterizes the normal stress at the interface between the fibres and the matrix. One can use a specimen as shown in Fig. 2.4 and apply a tensile load until the interface fails. This specimen (which we refer to here as a 'Type 1' specimen) allows us to determine the mode of failure. In this case, we want to find the normal stress at the boundary at which the fibre phase is separated from the matrix phase.

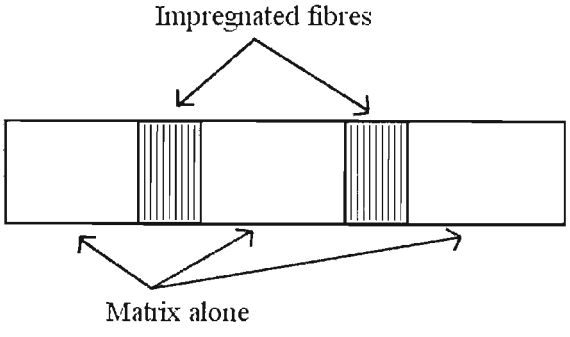

Fig. 2.4 Specimen used to determine interfacial normal strength

The test is repeated several times to find the parameters required to define the Weibull distribution of the interfacial strength, as described in the procedure described below where parameters R_0 and m_i are introduced.

- τ, the maximum shear stress. This characteristic is determined using a fibre pull-out test (Carpick et al., 1996). The sample used (which we refer to here as a 'Type 2' specimen) is a small disk of the matrix material with a fibre embedded in it. The matrix is clamped in place while the fibre is pulled out. The point of maximum load is reached just before the fibre debonds, after which, the load corresponds to the frictional forces of the fibre being pulled out. The test is made several times, with different lengths of embedded fibre. Then, a graph of the measured maximum load versus the embedded fibre length is plotted and the slope of the straight line obtained indirectly gives the shear strength of the interface between the matrix and the fibre material. Maximum shear stress τ is given by the following equation:

$$\tau = \frac{P}{2\pi r_f l_e} \tag{2.16}$$

where P is the maximum load, r_f the radius of the fibre and l_e the embedded fibre length.

In summary, two kinds of specimens are required to fully characterize the fibre-matrix interface: Type 1 to obtain the interfacial normal strength and Type 2 for interfacial shear strength:

- Several specimens of Type 2 should be tested to find the interfacial shear strength. The specimens differ from each other by the length of embedded fibre. Testing of 5 to 10 specimens may already give a good assessment of the shear strength.
- A suggested amount of up to 20 specimens of Type 1 should be tested according to the procedure described above. This will provide the value of normal strength and the Weibull distribution parameters characterising the interfacial strength.

Another characterisation requirement of this model is the computation of the Eshelby tensor as defined in Eq. 2.10, required for each inclusion (fibre or void). In this expression, C is the tensor corresponding to the phase for which we need the Eshelby tensor. As an indication of the computationally unwieldly process required to evaluate this tensor, a sample *Mathematica*™ program presented in Appendix A gives just the value of the integral of G_{1111} (which appears in the inner integral) as a function of ζ_3:

To obtain the full tensor, the same procedure is to be used to find all the different expressions for each integration of G_{ijkl}. Then, for each term of the double summation, the two integrated terms of G needed for calculation are taken, and the second numerical integration is performed using the same method (Gauss-Legendre integration). To find one term of S all previously calculated terms are to be summarised. This calculation should then be repeated for *each term* of the Eshelby tensor.

2.2.1.3 Conclusions

It is unquestionable that the Mori-Tanaka based homogenisation model described above is strongly reliant on a mathematical formulation that is not necessarily representable by clear physical phenomena. However, that said, it should be also be quite evident that the model presented here incorporates very clear 'calibrating variables', such as the pre-determined limit describing that percentage of failed fibres constitutes 'complete failure'. Such a variable is calibrated in line with actual testing, necessitating such testing as part of the model-verification prcess, but not necessarily of the model-*building* process. It may, with some justification, be argued that such a 'fitting' of the model to a finite number of experimental tests is an artificial method of aligning what could well be dubious theoretical formulations with experimentally obtained data. It is thus suggested here that a review of the model formulation should be as thorough as possible, and also that it be kept in mind that the building of a truly representative model, for any material type, necessarily includes formulations and theories of many different originators and researchers, eventually evolving into one that may be adopted with a minimum of reliance on artificial 'fitting'. When this is achieved, which, for SMC composites at least has not quite happened yet, then the 'job' of adequately modelling a material can be considered complete.

Thus, revisiting the model at hand, it is evident that there still do exist these fairly 'artificial' factors (count, as another example, the Weibull shape and size parameters), but it may be contended that if these factors (and others) are derived and calculated in a physically and statistically sensible manner, that the end result will in fact be sensible too. After all, using the example of the Weibull parameters, the purpose of these are merely to encapsulate the results of a series of experiments into two easily manipulated and adopted variables. The validity of these variables thus depends on the validity of the testing regime that originated them (since

the vailidity of the Weibull distribution itself has been well documented and generally accepted).

2.2.2 Interpolative Aggregate Model

We now go back to the Interpolative Aggregate Model, as described in Chapter 1.3. The main implementation concern of this model is shown to be the definition of the FOD matrix, which depends on the image analysis of polished specimens of the composite material in question.

2.2.2.1 Algorithm for implementation

A simple algorithm to show how this model might be implemented in a finite element package is illustrated below.

a. The components of matrix $[F]$ are calculated as

$$F_{ij} = \frac{\sum_{k=1}^{N} f_k A_{ij}(q_k)}{\sum_{k=1}^{N} f_k} \tag{2.17}$$

where N is the number of fibres,
f_k is the volume fraction of the k^{th} fibre,
A_{ij} are the components of the transformation matrix $[A]$, a function of the orientation vector $\boldsymbol{q}$, expressed for the 3D case in Eq. 2.18

b. $\{\tilde{M}\}$ (the unit cell stiffness vector) is found in terms of the longitudinal, L, and transverse, T, unit cell stiffnesses, using the matrix $[R]$, which is in turn defined in terms of the longitudinal Poisson's ratio of the material ν (described in Eqns. (1.28) - (1.32))

c. T and L are calibrated using the measured material stiffnesses, C_{1111} and C_{2222}, i.e. the expression $\{\tilde{C}\} = [F]\{\tilde{M}\} = [F][R]\{T \quad L\}^T$, is solved for the two measurable components of $[C]$, the deviation between the estimated and experimental values is expressed as a pair of multiplying factors, and these factors are applied to T and L, so that $[C]$ may be recalculated.

d. $[C]$ is then fully known for the undamaged material and may be degraded according to the chosen damage law.

Inputs:

- C_{1111} found from uniaxial tensile tests,
- C_{2222} found from uniaxial tensile tests,
- ν the longitudinal Poisson's ratio from standard material tests

$$
\begin{Bmatrix} C_{1111} \\ C_{2222} \\ C_{1212} \\ C_{1122} \\ C_{3333} \\ C_{2323} \\ C_{3131} \\ C_{1133} \\ C_{2233} \\ C_{1123} \\ C_{1131} \\ C_{1112} \\ C_{2223} \\ C_{2231} \\ C_{2212} \\ C_{3323} \\ C_{3331} \\ C_{3312} \\ C_{2331} \\ C_{2312} \\ C_{3112} \end{Bmatrix} = \oint \begin{bmatrix}
\left(m^2+m^2c^2\right)^2 & l^4s^4 & 4\left(m^2l^2s^2+l^4c^2s^2\right) & 0 & 2\left(m^2l^2s^2+l^4c^2s^2\right) \\
\left(l^2+m^2c^2\right)^2 & s^4m^4 & 4\left(m^2l^2s^2+m^4c^2s^2\right) & 0 & 2\left(m^2l^2s^2+m^4c^2s^2\right) \\
m^2l^2+m^2l^2c^4+\frac{1}{2}\left(m^2c-l^2c\right)^2 & m^2l^2s^4 & \left(m^2s-l^2s\right)^2+4m^2l^2c^2s^2 & -\frac{1}{2}\left(m^2c+l^2c\right)^2 & 2\left(m^2l^2c^2s^2-m^2l^2s^2\right) \\
\left(ml-mlc^2\right)^2 & m^2l^2s^4 & 4\left(m^2l^2c^2s^2-l^2m^2s^2\right) & \left(m^2c+l^2c\right)^2 & m^4s^2+l^4s^2+2m^2l^2c^2s^2 \\
s^4 & c^4 & 4c^2s^2 & 0 & 2c^2s^2 \\
m^2c^2s^2+\frac{1}{2}ls & m^2c^2s^2 & l^2c^2+\left(mc^2-ms^2\right)^2 & -\frac{1}{2}l^2s^2 & -2m^2c^2s^2 \\
l^2c^2s^2+\frac{1}{2}m^2s^2 & l^2c^2s^2 & m^2c^2+\left(ls^2-lc^2\right)^2 & -\frac{1}{2}m^2s^2 & -2l^2c^2s^2 \\
l^2c^2s^2 & l^2c^2s^2 & -4l^2c^2s^2 & m^2s^2 & m^2c^2+l^2s^4+l^2c^4 \\
m^2c^2s^2 & m^2c^2s^2 & -4m^2c^2s^2 & l^2s^2 & l^2c^2+m^2s^4+m^2c^4 \\
ml^2cs-ml^2c^3s & ml^2cs^3 & 2\left(ml^2c^3s-ml^2cs^3-ml^2cs\right) & -m^3cs-ml^2cs & m^3cs-ml^2cs^3+ml^2c^3s \\
l^3c^3s-m^2lcs & l^3cs^3 & 2\left(m^2lcs+l^3c^3s-l^3cs^3\right) & 0 & m^2lcs+l^3c^3s-l^3cs^3 \\
ml^3c^4-m^3l+m^3lc^2-ml^3c^2 & ml^3s^4 & 2\left(m^3ls^2-ml^3s^2+2ml^3c^2s^3\right) & 0 & m^3ls^2-ml^3s^2+2ml^3c^2s^2 \\
m^3c^3s-ml^2cs & m^3cs^2 & 2\left(ml^2cs+m^3c^3s-m^3cs^3\right) & 0 & ml^2cs+m^3c^3s-m^3cs^3 \\
m^2lcs-m^2lc^3s & m^2lcs^3 & 2\left(m^2lcs+m^2lc^3s-m^2lcs^3\right) & -l^3cs-m^2lcs & l^3cs-m^2lcs+m^2lc^3s \\
m^3lc^4-ml^3+ml^3c^2-m^3lc^2 & m^3ls^4 & 2\left(ml^3s^2-m^3ls^2+2m^3lc^2s^2\right) & 0 & ml^3s^2-m^3ls^2+2m^3lc^2s^2 \\
-mcs^3 & mc^3s & 2\left(mcs^3-mc^3s\right) & 0 & mcs^3-mc^3s \\
-lcs^3 & lc^3s & 2\left(lcs^3-lc^3s\right) & 0 & lcs^3-lc^3s \\
mlc^2s^2 & mlc^2s^2 & -4mlc^2s^2 & -mls^2 & mlc^4+mls^4-mlc^2 \\
mlc^2s^2-\frac{1}{2}mls^2 & mlc^2s^2 & mls^4+mlc^4-mlc^2-2mlc^2s^4 & \frac{1}{2}mls^2 & -2mlc^2s^2 \\
\frac{1}{2}\left(m^2lcs-l^3cs\right)-m^2lc^3s & m^2lcs^3 & l^3cs-m^2lcs+2m^2lc^3s-2m^2lcs^3 & \frac{1}{2}\left(m^2lcs+l^3cs\right) & m^2lc^3s-m^2lcs^3-m^2lcs \\
\frac{1}{2}\left(ml^2cs-m^3cs\right)-ml^2c^3s & ml^2cs^3 & m^3cs+2ml^2c^3s-2ml^2cs^3-ml^2cs & \frac{1}{2}\left(ml^2cs+m^3cs\right) & ml^2c^3s-ml^2cs^3-ml^2cs
\end{bmatrix} \psi(\mathbf{q})d\mathbf{q}[R]\begin{Bmatrix} T \\ L \end{Bmatrix}
$$

$l = \cos\varphi$

$m = \sin\varphi$

$c = \cos\nu$

$s = \sin\nu$

(2.18)

- [*A*] found by substituting fibre orientation angles, found by image analysis of a micrograph of the cross section of the material, into the transformation components shown in Eq. 2.18

- [*f*] the fibre area matrix, also found from image analysis. (The cross-sectional area of each fibre is used as an indication of its volume)

Outputs:

- The fibre orientation distribution matrix, [*F*]

- Matrix $[R]$

- Unit cell stiffness matrix, $\{\tilde{M}\}$, determined from $\{R\}$, C_{1111}, C_{2222}, and ν by Eqns. (1.27)- (1.32) and thus,

- Material stiffness matrix [*C*] determined from [*F*] and $\{\tilde{M}\}$,

- Material stiffness matrix [*C*] for any other fibre orientation set by redefining the [*F*] matrix, but retaining $\{\tilde{M}\}$, for the same material.

2.2.2.2 The Two-dimensional case

For thin-walled components, which are the focus of the current study since these are more generally employed in automotive structures, a two-dimensional definition of the fibre orientation is sufficient. Since the thickness of the component is of the same order as the fibre diameter, fibres are situated in roughly a single plane. For this reason, a derivation of the two dimensional case is presented here.

The axes of the unit cell embedding the fibres are (x_1', x_2', x_3') and the global axes of the material are denoted as (x_1, x_2, x_3). Axis x_1' is directed along the fibre direction and the fibre lies in the (x_1', x_2') plane.

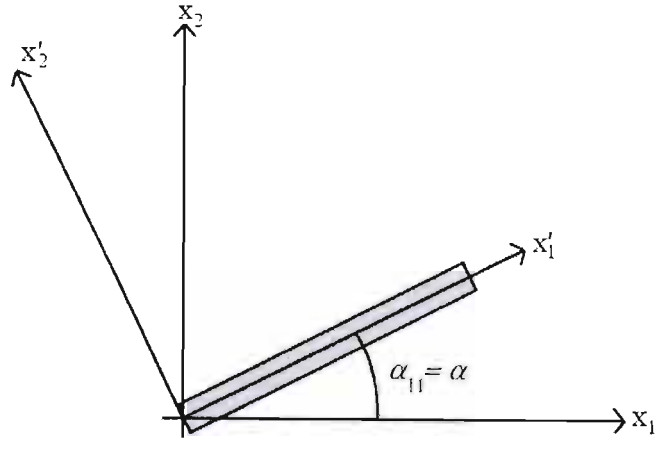

Fig. 2.5 Unit cell and axes notation

The unit cell is referred to in the local system of coordinates (x_1', x_2', x_3') as shown in Fig. 2.5. The material of the unit cell is transversely isotropic and stiffness matrix [M] may be expressed as:

$$\begin{pmatrix} \sigma_1 \\ \sigma_2 \\ \sigma_3 \\ \tau_{23} \\ \tau_{13} \\ \tau_{12} \end{pmatrix} = \begin{pmatrix} M_{11} & M_{12} & M_{12} & 0 & 0 & 0 \\ M_{12} & M_{22} & M_{23} & 0 & 0 & 0 \\ M_{12} & M_{23} & M_{22} & 0 & 0 & 0 \\ 0 & 0 & 0 & M_{44} & 0 & 0 \\ 0 & 0 & 0 & 0 & M_{55} & 0 \\ 0 & 0 & 0 & 0 & 0 & M_{55} \end{pmatrix} \times \begin{pmatrix} \varepsilon_1 \\ \varepsilon_2 \\ \varepsilon_3 \\ \gamma_{23} \\ \gamma_{13} \\ \gamma_{12} \end{pmatrix} \tag{2.19}$$

where $M_{11} = \frac{E_1}{D}(1-\nu^2)$, $M_{22} = \frac{E}{D}(1-\nu_{12}\nu_{21})$, $M_{12} = \frac{E_1\nu_{12}}{D}(1+\nu)$, $M_{23} = \frac{E}{D}(\nu+\nu_{12}\nu_{21})$, $M_{44} = G_{23} = \frac{E}{2(1+\nu)}$ and $M_{55} = G_{12}$ with $D = 1-2\nu\nu_{12}\nu_{21}-2\nu_{12}\nu_{21}-\nu^2$, $E_2 = E_3 = E$, $\nu_{23} = \nu_{32} = \nu$, $\nu_{13} = \nu_{12}$, and $E_1\nu_{12} = E_2\nu_{21}$.

For this case, the matrix l_{ij} is defined as: $l_{ij} = \begin{bmatrix} \cos\alpha & \sin\alpha & 0 \\ -\sin\alpha & \cos\alpha & 0 \\ 0 & 0 & 1 \end{bmatrix}$ and stiffness matrix B (from Eq. 1.19) is expressed as follows:

$$[\mathbf{B}] = \begin{pmatrix} c^2 & s^2 & 0 & -2cs & 0 & 0 \\ s^2 & c^2 & 0 & 2cs & 0 & 0 \\ 0 & 0 & 1 & 0 & 0 & 0 \\ cs & -cs & 0 & c^2-s^2 & 0 & 0 \\ 0 & 0 & 0 & 0 & c & -s \\ 0 & 0 & 0 & 0 & s & c \end{pmatrix} \times [\mathbf{M}] \times \begin{pmatrix} c^2 & s^2 & 0 & 2cs & 0 & 0 \\ s^2 & c^2 & 0 & -2cs & 0 & 0 \\ 0 & 0 & 1 & 0 & 0 & 0 \\ -cs & cs & 0 & c^2-s^2 & 0 & 0 \\ 0 & 0 & 0 & 0 & c & s \\ 0 & 0 & 0 & 0 & -s & c \end{pmatrix} \tag{2.20}$$

where $c = cos\ \alpha$ and $s = sin\ \alpha$. Stiffness matrix [C] of the overall material is calculated accordingly:

$$[\mathbf{C}] = \int_0^{2\pi} [\mathbf{B}] \times \psi(\alpha) d\alpha \tag{2.21}$$

This is an integral over all possible fibre orientations in the plane. Function $\psi(\alpha)$ is the orientation distribution function, which defines the volume fraction f of unit cells for a given angle α. In the case under consideration this function can be presented as shown in Fig. 2.6:

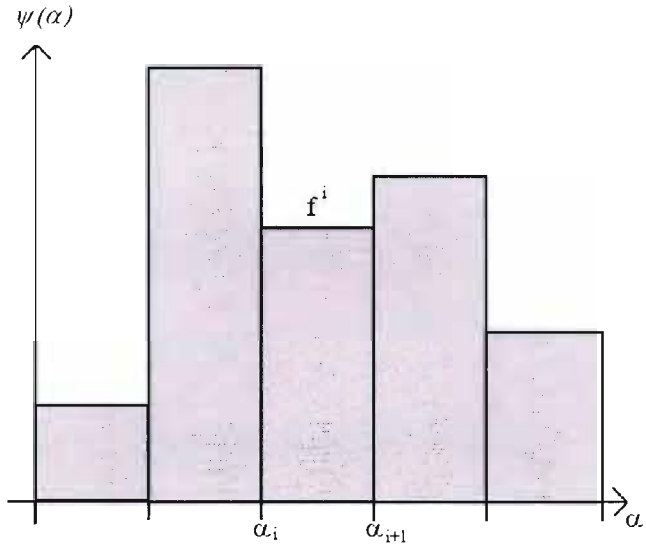

Fig. 2.6 Piecewise distribution

For $\alpha \in [\alpha_i ; \alpha_{i+1}[$, $\psi(\alpha) = f^i$. We can obtain this discrete distribution of orientation by taking micrographs of a specimen and counting the detected fibres and orientations.
According to the approach presented above for 3D case, the following vectors may then be introduced:

$$\{\tilde{M}\} = \{M_{22}, M_{11}, M_{55}, M_{23}, M_{12}\}^T$$
$$\{\tilde{C}\} = \{C_{11}, C_{22}, C_{44}, C_{12}, C_{33}, C_{66}, C_{55}, C_{13}, C_{23}, C_{16}, C_{15}, C_{14}, C_{26}, C_{25}, C_{24}, C_{36}, C_{35}, C_{34}, C_{65}, C_{64}, C_{54}\}^T$$

(2.22)

Using these notations, Eq. 1.26 may be written in the form

$$\begin{pmatrix} C_{11} \\ C_{22} \\ C_{44} \\ C_{12} \\ C_{33} \\ C_{66} \\ C_{55} \\ C_{13} \\ C_{23} \\ C_{16} \\ C_{15} \\ C_{14} \\ C_{26} \\ C_{25} \\ C_{24} \\ C_{36} \\ C_{35} \\ C_{34} \\ C_{65} \\ C_{64} \\ C_{54} \end{pmatrix} = \int_0^{2\pi} \begin{pmatrix} s^4 & c^4 & 4c^2s^2 & 0 & 2c^2s^2 \\ c^4 & s^4 & 4c^2s^2 & 0 & 2c^2s^2 \\ c^2s^2 & c^2s^2 & (s^2-c^2)^2 & 0 & -2c^2s^2 \\ cs & c^2s^2 & -4c^2s^2 & 0 & s^4+c^4 \\ 1 & 0 & 0 & 0 & 0 \\ \frac{c}{2} & 0 & s^2 & -\frac{c^2}{2} & 0 \\ \frac{s^2}{2} & 0 & c^2 & -\frac{s^2}{2} & 0 \\ 0 & 0 & 0 & s^2 & c^2 \\ 0 & 0 & 0 & c^2 & s^2 \\ 0 & 0 & 0 & 0 & 0 \\ 0 & 0 & 0 & 0 & 0 \\ -cs^3 & sc^3 & 2(s^3c-sc^3) & 0 & s^3c-sc^3 \\ 0 & 0 & 0 & 0 & 0 \\ 0 & 0 & 0 & 0 & 0 \\ -sc^3 & s^3c & 2(sc^3-s^3c) & 0 & sc^3-s^3c \\ 0 & 0 & 0 & 0 & 0 \\ 0 & 0 & 0 & 0 & 0 \\ 0 & 0 & 0 & -sc & sc \\ -\frac{cs}{2} & 0 & cs & \frac{cs}{2} & 0 \\ 0 & 0 & 0 & 0 & 0 \\ 0 & 0 & 0 & 0 & 0 \end{pmatrix} \{\tilde{M}\}\psi(\alpha)\,d\alpha \tag{2.23}$$

where $a_1 = \frac{1-\cos(4\alpha)}{4}$ and $a_2 = \frac{1+\cos(4\alpha)}{4}$. Let us then introduce the following ratios: $\omega = \frac{M_{55}}{2M_{66}} \approx 0.5$, $\rho = \frac{M_{23}}{M_{11}}$ and $\xi = \frac{M_{12}}{M_{11}}$. Then vector $\{\tilde{M}\}$ takes form $\{\tilde{M}\} = [\mathbf{R}]\begin{Bmatrix} T \\ L \end{Bmatrix}$ where

$$[\mathbf{R}] = \begin{bmatrix} 1 & 0 \\ 0 & 1 \\ (1-\xi)\omega & 0 \\ \rho & 0 \\ \xi & 0 \end{bmatrix}, \tag{2.24}$$

$T = M_{22}$ and $L = M_{11}$.

The ratios ρ and ξ may be expressed in terms of Poisson's ratios:

$$\rho = \frac{\nu_{23} + \nu_{12}\nu_{21}}{1-\nu_{21}\nu_{12}} \text{ and } \xi = \frac{\nu_{12} + \nu_{23}\nu_{12}}{1-\nu_{21}\nu_{12}} \tag{2.25}$$

And the following restrictions can be imposed on these Poisson's ratios: $0 < \nu_{21} < \nu_{12} < \nu_{23} < \nu_{21} + \nu_{23} < 1$. Which leads to the following bounds for ρ and ξ:

$$\nu < \rho < 1 \text{ and } \nu + \nu^2 < \xi < 2\nu \tag{2.26}$$

where $\nu = \nu_{12}$ is the longitudinal Poisson's ratio that could be approximated as the volume average of the Poisson's ratios of the constituents. Since ν is fairly independent on the unit-cell stiffnesses, and so is [R], then [R] = constant. Now, in the limit $T = L$, and the unit-cell must be isotropic, which requires that:

$$\omega = 0.5 \text{ and } \rho = \xi = \frac{\nu + \nu^2}{1 - \nu^2} \tag{2.27}$$

Thus, $[R]$ is determined solely by ν. The experimental procedure is then the same as that in the general three-dimensional case.

2.2.2.3 Damage introduction

Damage may be introduced into the defined material by applying or adapting either of the following damage laws:

Interpolated Damage Model

An isotropic damage law, as introduced in the Elastic Model with Isotropic Damage Behaviour discussed above may be applied. Once the stiffness matrix $[C]$ is known for the material, the undamaged stiffness components may then be calculated. Stresses and strains are computed for given loading and boundary/initial conditions.

Three points of reference in terms of limit stresses are to be taken from the stress-strain diagram and introduced into the code. Once an element of the material is found to have reached the first critical stress limit, σ_i, a reduction in that element's stiffness properties is applied, by introduction of a damage factor on the material stiffness. This damage factor is computed in terms of the original modulus value of the material and the new reduced material modulus. Input may take the form of either this reduced modulus value or the damage factor. Once the element has been degraded, recalculation of the material stresses is carried out, and the process of redefining the now degraded material properties is carried out. (T and L will have to be adjusted according to the new stiffnesses, i.e. recomputed according to the new values of C_{1111} and C_{2222}).

Three points of degradation, defined by the elastic limit, the maximum stress level and the ultimate failure level are used to calibrate the progressive degradation, with degradation interpolated between these points.

Statistical Damage Law

Damage may also be introduced in terms of a statistical law. Since the material constitution includes the identification of each fibre and its orientation in the matrix, a Weibull-type distribution may be used to estimate the failure parameters for the fibres, matrix, and even interfaces, exactly as described for the Mori Tanaka Model with Statistical Damage Criteria discussed earlier.

The probability of failure, defined in terms of the strength of the individual phases, the current stress level and Weibull shape and scale factors, as shown above, is used to fail the fibres/matrix/interface by removing their stiffness contributions but not their mass/volume. The material stiffness must then be recalculated after removing these contributions. This, in the case of fibre failure, will correspond to the removal of the specific fibres' contribution from the [*F*] matrix and the subsequent recalculation of the [*C*] matrix. In the case of matrix failure, the respective volume of matrix, transverse to the direction of loading, found to have failed, will be removed and replaced with voids/cracks of zero stiffness, but occupying the same volume as the removed material. Interfacial failure would be accompanied by the introduction of such cracks transversely oriented to the direction of the fibre family responsible for failure.

Interfacial strength is defined in terms of the normal and shear stress required to pullout a fibre, from single filament pull-out testing, while shear and volumetric strength are defined in the usual way. The process is continually repeated as the loading increases, until the entire composite fails (100% failure), or a predetermined limit level is attained in any phase.

2.2.2.4 Material characterisation

Since thin-walled components are the specific area of study here, only the material characterisation related to the two-dimensional case is discussed below.

- ν, the Poisson's ratio of the material is obtained from a tensile test on a flat specimen made from the SMC material we wish to model.

- M_{11} and M_{22}, the longitudinal and transverse moduli respectively, are measured using testing of flat SMC specimens that are assumed to be fairly homogeneous with respect to FOD.

- [**F**] is obtained from micrographs of polished surfaces parallel to the (x_1, x_2) plane of the specimen at (say)10 different levels along the thickness. Image-analysis provides values of angles $\alpha^{(k)}$ (these angles are used to compute the components of [**A**]) and cross-sectional areas $f^{(k)}$ of each fibre. The components of [**F**] may then be calculated by Eq. 2.17.

In summary, in order to implement the two-dimension interpolative-aggregate model we physically require:

- 1 flat SMC specimen on which is performed a tensile test to find the Poisson's ratio,
- 1 flat SMC specimen to measure the interpolation parameters, M_{11} and M_{22}.
- 1 flat SMC specimen from which micrographs will be taken (at each key area of the component in question) (though a greater number of these may be prudent so that an indication is made of the make-up of the entire composite)

2.2.2.5 Conclusions

The basis of this model remains the definition of the FOD matrix, and herein lies both the model's pros and cons. As has been discussed in Chapter One, an FOD is sensible when considering short fibre composites, as it is a means of accurately representing the fibre phase, not necessarily truly reflected by homogenisation processes. More importantly, it allows for the more accurate rendering of the fibre orientations that may be present in a moulded part, since moulding results in anisotropic effects and alignment of fibres, particularly in thin

walled components, the type of which are being investigated here. With this flexibility however comes the price of requiring a laboured characterisation process which requires the use of image analysis hardware and software, and multiple specimens depending on the specific geometry being analysed. This in effect dilutes the purpose of modelling and simulation, and the characterisation costs must be offset against traditional experimentation and crash tests costs to test whether implementation of such a model is justifiable. Streamlining of the characterisation process is possible however, and delineation of the required specimens in terms of geometries, and a build up of a knowledge base with regards to SMC materials will further add to the benefits enjoyed.

2.2.3 Overall Elastic Moduli Homogenisation Model

The relatively simple constitutive model (in presentation and implementation, if not in development), which, like the Desrumaux et al. (1995) model described above, makes use of a Mori-Tanaka based homogenisation was discussed at length in Chapter One. Here we propose two damage models to be incorporated with this constitutive model, and a material characterisation synopsis is once again included here.

2.2.3.1 Damage introduction

It is proposed that damage is introduced in the material defined by the formulation presented in Chapter 1.3 in the following ways:

Statistical damage law

A Weibull-type distribution (as in the Mori Tanaka Model with Statistical Failure Criteria described above) may be used to statistically fail the composite material, but suitably adapted for the parameters presented in this model. Such an adaptation is presented in Chapter Four of this study as a newly proposed composite damage model for implementation into finite element analysis software.

Interpolated Damage Model

Damage might also be introduced as already discussed for the Interpolative Aggregate Model and for the Elastic-Plastic Model with Isotropic Damage.

2.2.3.2 Material characterisation

Explicit formulae are used to calculate the effective elastic moduli of multiphase composite materials, and particularly for composites with randomly oriented fibres. In the case of randomly reinforced composites we must take two different phases into account: the isotropic matrix phase and the transversely isotropic fibre inclusions phase.

- $E^{(1)}, \nu^{(1)}$, the Young's modulus and Poisson's ratio respectively of the matrix material may be obtained from a tensile test on a specimen made from the same material as the matrix,
- $E_1, E_2, \nu_{12}, \nu_{23}$, and G_{12}, which fully characterise the transversely isotropic fibre inclusions phase. Once they are known we can derive k, l, m, n and p for the fibre phase, according to Eq. 2.28:

$$k=\frac{E_2\left(1-\nu_{12}\nu_{21}+\nu_{23}+\nu_{23}^2\right)}{2D},\ l=\frac{E_1\nu_{12}}{D}\left(1+\nu_{23}\right),$$
$$m=\frac{E_2}{2\left(1+\nu_{23}\right)},\ n=\frac{E_1}{D}\left(1-\nu_{23}^2\right),\ \text{and}\ p=G_{12} \tag{2.28}$$

where $D=1-2\nu_{23}\nu_{12}\nu_{21}-2\nu_{12}\nu_{21}-\nu_{23}^2$, E_1 and ν_{12} are respectively the longitudinal Young's modulus and the Poisson's ratio of the fibre material, obtained from a tension test of a unidirectional material along the fibres, E_2 is the transverse Young's modulus of the fibre material, obtained from a tension test of a unidirectional material across the fibres, G_{12} is the shear modulus of the fibre material, obtained from a tension test on a $[\pm 45°]_{2S}$ laminate using the following equation:

$$\frac{1}{G_{12}}=\frac{4\varepsilon_{11}}{\sigma_{11}}-\frac{1}{E_1}-\frac{1}{E_2}+\frac{2\nu_{12}}{E_1} \tag{2.29}$$

In summary, to implement this model, we need to test two types of specimens: one made from the matrix material and another made from unidirectional composite.

- 1 specimen made from the matrix material will be tested under tension to find Poisson's ratio and Young's modulus of the matrix phase
- 1 specimen made from unidirectional material will give longitudinal Poisson's ratio and Young's modulus from tension test along the fibres
- 1 specimen made from unidirectional material will give transverse Young's modulus from tension test across the fibres
- 1 $[\pm 45°]_{2S}$ laminate will give G_{12} from a tension test.

2.2.3.3 Conclusions

The formulation as presented in Chapter One is based on the same Mori-Tanaka scheme as discussed for the first of our proposed models; thus validation of the theory behind the homogenisation process is applicable to both. Being a homogenisation model, questions regarding the mathematical nature of such formulations are once again applicable. One advantage is that in this presentation of homogenisation, we are able to directly compare the properties of the individual constituents and the final medium. As far as characterisation goes, the requirements are, like the material formulation, very clear and uncomplicated, and would be simple to implement. The damage models are both repeated from other models and the analyses of these have thus already been discussed.

2.2.4 Conclusions

As opposed to the two models discussed in Chapter 2.1, we see the necessity for those models that have been proposed only theoretically to be carefully analysed for their implementabilty and practicality. Models that appear theoretically viable are sometimes impossible to actually carry out and it is considered critical that such considerations be made prior to any judgements being passed. It is true to say that some theoretical formulations defeat the essence of modelling by engendering characterisation requirements that are both cumbersome and sometimes inapplicable. The models described here were all considered applicable to the particular problem being studied here, and by analysing and discussing the implementation of each in detail, it is possible to have a fair idea of their practicality, as well as time and labour requirements. This is seen to be sorely lacking in most model proposals, yet would appear a

critical avenue of research and criteria for judgement when deciding on which model may be best to employ. The three models proposed here are considered to reflect most of the options available in terms of SMC composite modelling, and coupled with the implementation analysis presented, and the addition of progressive damage models in some instances, may now be truly considered to be complete formulations. The only next step required is the preparation for and adoption into the finite element analysis so that numerical simulation may be performed and be compared with other model results, as well iteratively improved. One such formulation is presented later in this work (Chapter Five) , which demonstrates the work involved in taking a model the next step towards complete integration.

In Chapter Four simulation is performed using the two already implemented models, focusing on the more applicable Elastic Model with Isotropic Damage; thus showing the numerical simulation process, the array of results that may be expected from those models already available within the finite element analysis environment, and where room for improvement in the available models may exist, paving the way for adoption of one of these newly proposed models.

In preparation for simulation however, intensive physical characterisation and experimentation is required, as defined by the model requirements. The process of physically obtaining the these parameters is discussed in Chapter Three, and it is shown that once again, any analyses of modelling strategies necessarily include much consideration geared towards issues of practical physical testing.

Chapter Three

Material Analysis and Experimental Characterisation

3.1 Selection of suitable material for experimentation

Material selection was initially chiefly governed by the requirements of the industrial partner involved with the project of which this study represents some portion. It was tasked that the final material to be used for fabrication of a prototype demonstrator should mirror the content and characteristics of the sample supplied by *Renault*-in other the words material used in all testing should be comparable in properties to the material *Renault* itself is considering for use in its automotive structures. With no useful data being supplied along with the sample, efforts were undertaken to characterise the material using whatever techniques were readily available.

A sample was analysed and stripped (with the aid of the *University of Natal Chemistry Department* and the *University of Natal (School of Mechanical Engineering) Metallurgy Department* to its basic constituents.

An infrared analysis was performed to determine the physical characteristics of the sample, including the fibre and filler material composition. The initial infrared scan indicated the presence of a large percentage of calcium carbonate filler, which masked the polymer of the matrix. The material was thus placed into diluted nitric acid to separate the $CaCO_3$ filler from the polymer.

The results of a second infrared scan indicated that the matrix was composed primarily of polyvinyl-acetate, and a polystyrene co-polymer. The compound was then placed into dichloromethane, so as to extract the polystyrene co-polymer.

A final infrared scan of the remaining material confirmed that the main constituent of the matrix was polyvinyl-acetate (PVA). As a matter of interest, the infrared scan results

showing the $CaCO_3$ is shown in Fig. 3.1. Fig. 3.2 shows the scan of the polyvinyl - acetate and Fig. 3.3, the scan of the co-polymer.

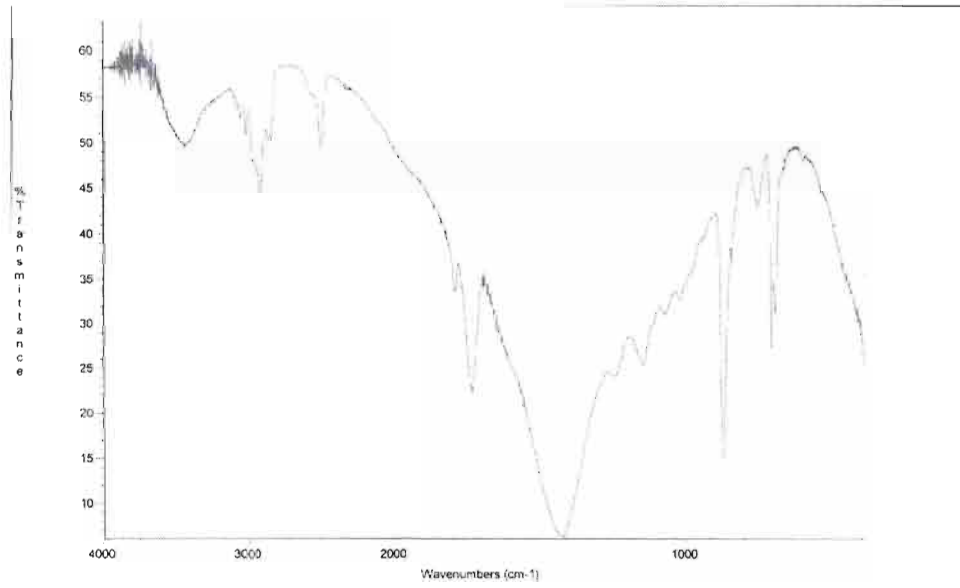

Fig. 3.1 Infrared analysis of material sample showing $CaCO_3$

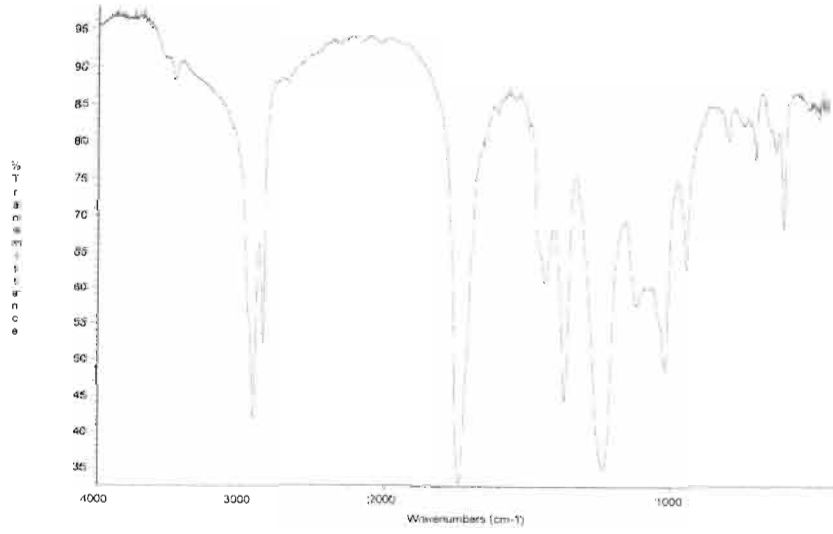

Fig. 3.2 Infrared analysis of polyvinyl acetate

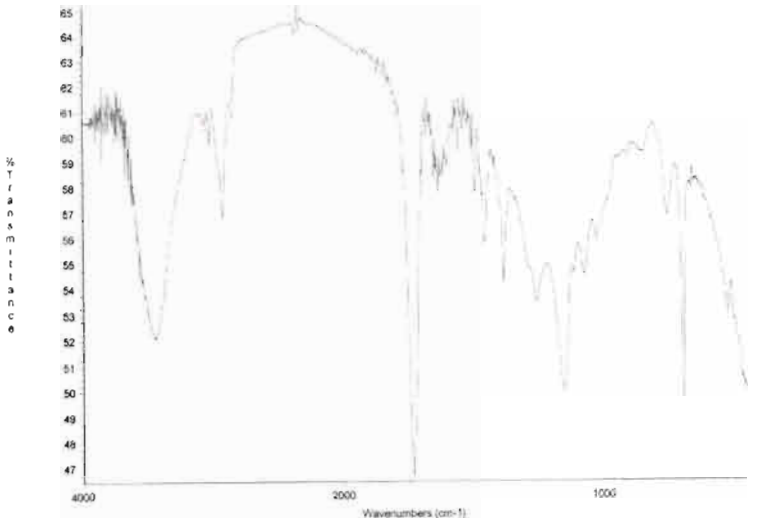

Fig. 3.3 Infrared analysis of polystyrene co-polymer

The collected results of the tests thus indicated that the composite in question was in fact a polyvinyl-acetate-polystyrene co-polymer composite material.

A mass analysis was then performed to determine the percentage compositions of each of the constituents. The composition by mass was determined to be:

$$\%Polymer = \frac{[Weight_{total} - (fibre + CaCO_3)]}{Weight_{total}} = 45\% \text{ by mass}$$

$$\%Glass = \frac{Fibre}{Weight_{total}} = 24\% \text{ by mass}$$

$$\%CaCO_3 = \frac{[(Fibre + CaCO_3) - Fibre]}{Weight_{total}} = 31\% \text{ by mass}$$

Using this information, investigation was made into a suitable similar material for experimental testing. The exact polyvinyl-acetate-polystyrene polymer composite was found to be unavailable, thus it was decided to find a suitable substitute material that was both readily available, and of minimum associated expense, with physical properties that were comparable to the supplied material.

The decision was eventually taken to proceed using pre-mixed sheets of glass-fibre/polyester resin SMC material. This form of SMC negates the need for physical mixing of the constituents, is readily available in set fibre volume percentages, and relatively easy to store and transport. Most importantly it was decided that this type of material most closely mirrored the make-up and finish of the supplied material. Drawbacks included the need for a pre-heat process, and less flexibility with regards to fibre volume percentage, however these were considered justifiable when weighed up against the time and labour saving.

The SMC sheets in question were supplied in 20% and 35% fibre volume compositions. These were calculated to be the compositions most representative of the required material properties. (At a later stage refinement of these percentages was always possible.) The material properties of this material are shown in the Table 3.1.

Table 3.1 Properties of SMC composite being used

Property	UP GF 25	UP GF 50
Tensile Strength (MPa)	65-80	124-204
Tensile Modulus (Gpa)	8.5	12.2-19.1
Flexural Strength (MPa)	155-200	248-380
Flexural Modulus (MPa)	8.5-14.0	11.6-16.4
Density (g/cm^3)	1.7-2.0	1.85-2.00

To cure, the material requires both heating and pressure. Heating is achieved by the pre-heat of the moulds being used, whilst pressure is applied using a suitable press. During the curing process the layers bond together and fill up the mould cavity, thus allowing for variable thicknesses to be achieved, depending on the actual volume of material placed in the mould. Curing time is approximately 40 seconds per millimetre of thickness, under temperatures ranging from 130 °C to 170 °C and pressures in the range of 7-15 MPa.

Options identified and initially considered for the purposes of mould pre-heating, included steam and oil heating, but heating by means of electrical cartridge heaters (pictured in Fig. 3.4) embedded into the mould itself (as opposed to being placed into a separate platen) was adopted as the most viable method due to its flexibility and relative ease of implementation. Such cartridges are readily available, and facilitate the option of using the same elements in multiple moulds (by simply making them removable), require no complicated machining (as would be the case if steam or oil heating were to be implemented), are custom-made as dictated by the heating requirements (length, diameter, shape, power output), and are relatively durable.

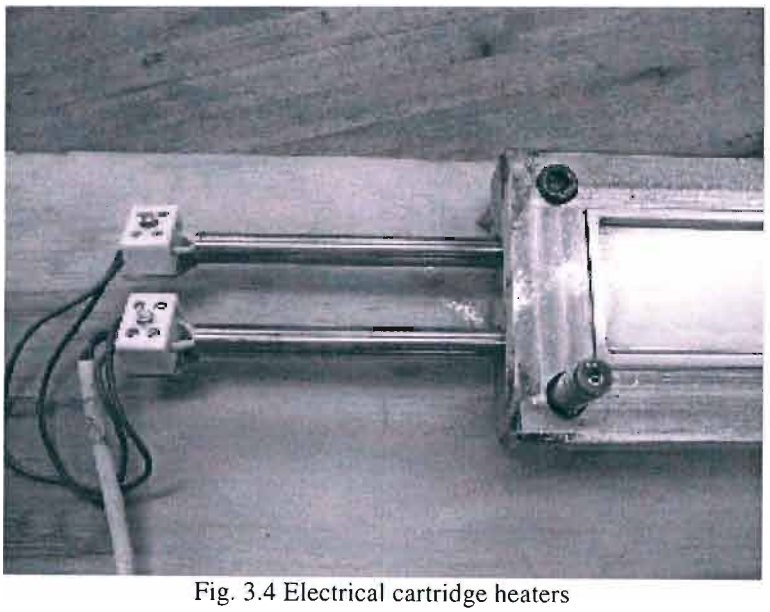

Fig. 3.4 Electrical cartridge heaters

3.2 Specimen Geometry

Tensile specimens were designed with a dumb-bell (or 'dog-bone') shaped, straight-sided configuration, with a thickness of 4 mm. The length and width of these specimens were constrained by available fixturing and the test-rig dimensions.

In the case of compression testing, the specimens were of a simple rectangular shape, the length to thickness ratio of which was kept as low as possible, so as to avoid the introduction of buckling phenomena during testing.

3.3 Design and implementation of manufacturing process

The SMC material being used (as described previously, and as is representative of materials of this family of composites) requires both pre-heating of the moulds being used, and the application of a suitable pressure. The pre-heat requirement dictates that the moulds be manufactured out of metal, and that a suitable heating process be incorporated into these moulds. Additionally, since specific temperatures are required, a heating control system has to be set in place.

Below is pictured a schematic of the complete mould, including fittings necessary to fix the mould to the hydraulic press being used to apply the required pressure.

The mould eventually designed was a semi-positive type matched mould, with each half designed to be bolted to the upper and lower platens of the press to be used.

The placement and number of the heating elements, as well as the actual diameter and power output required of the individual cartridges was determined from data sheets supplied by the manufacturer and a *FLUENT* computational flow design analysis, and the elements were supplied as such. Typically, the spacing for 600-watt elements in steel is one per 100 mm.

Temperature control was achieved using a set of thermocouples embedded in the mould at identified key points (Fig. 3.6), together with a pair of temperature controllers (see Fig. 3.7) which allow for the setting and maintaining of specific temperatures through feedback control (Fig. 3.8).

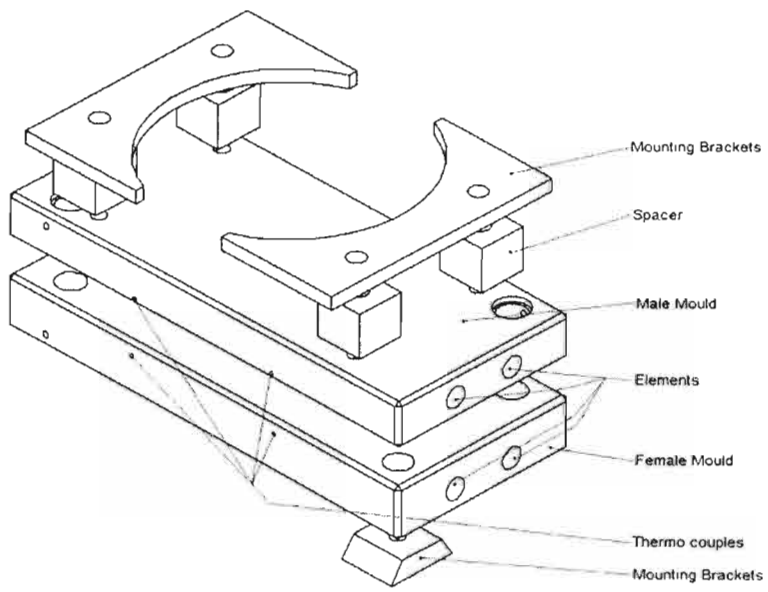

Fig. 3.5 Specimen mould design including required fixtures

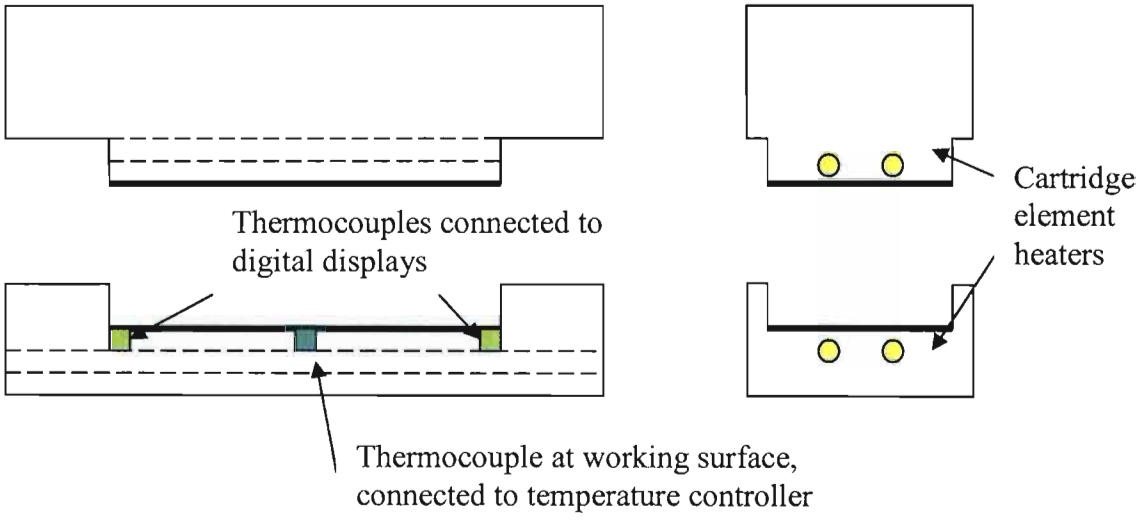

Fig. 3.6 Schematic of the heated moulds showing thermocouple and element positions

Fig. 3.7 Temperature controller (*ATC*, South Africa) and secondary temperature display (*Zenith*, South Africa)

Specifications:
Cartridge Heaters
Manufactured by *Kaytherm*, 15 mm diameter, 300 mm length, 1000W output, 220V

Controllers
Manufactured by *ATC*, J-type controllers (0-400 °C), 220V, Digital display with analogue temperature setting

Contactors
Manufactured by *Lavato*, 40 A, up to 4 points of contact

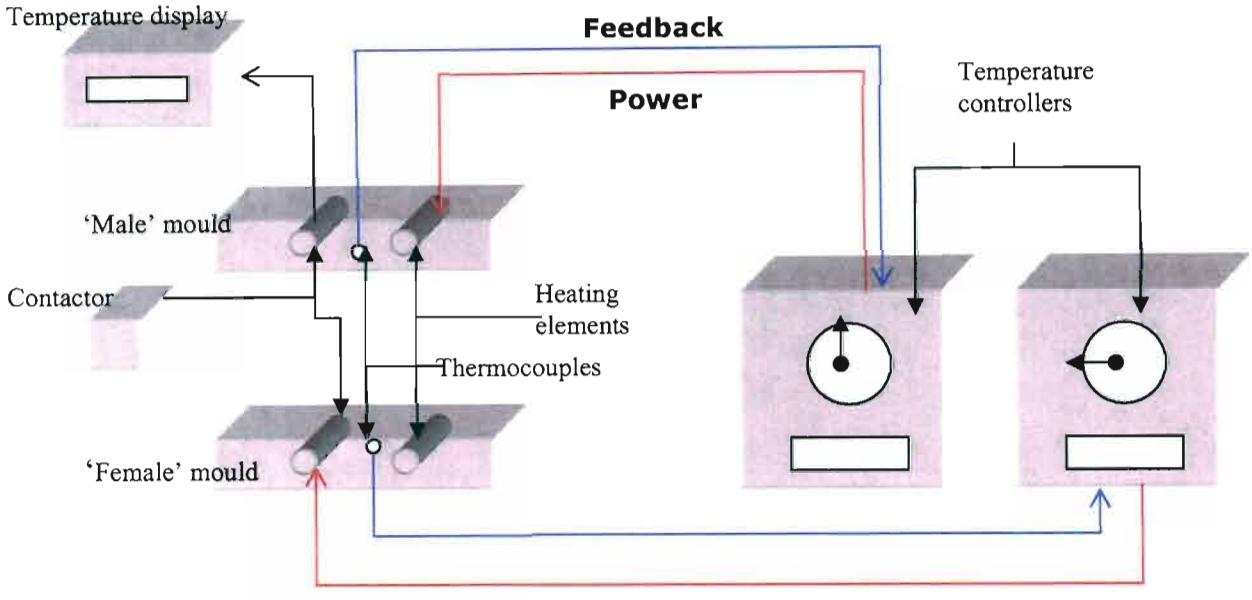

Fig. 3.8 Temperature control system

The specimens were designed to be cut out of a cured plate of SMC, thus allowing for any dimensional changes to the specimens at a later stage, the difference in sizing of compression and tension samples, as well as preventing the possibility of damage to the specimen shape during the moulding and ejection processes. Allowance in the mould size for the heating elements, an ejection mechanism, guide pins, and alignment with the hydraulic press fittings, together with the primary strength requirements SMC volumetric requirements and shrinkage dictated the dimensions of the plate to be moulded at a time to be 230 mm by 60 mm, with variable thicknesses possible. The completed mould drawings are shown in Figs. 3.10 and 3.11, with the actual product, as manufactured at the *University of Natal*, shown in Fig. 3.9.

Included in the design of the mould are two guide-pins, located diagonally opposite each other, which maintained the correct relative positioning of the mould halves. Also, to aid in removal of the specimen from the moulds after curing, a 1° draft angle is incorporated into the walls of the mould. The mould was also designed such that the thermocouples and heating elements may be easily removed as necessary, for possible maintenance or adjustment.

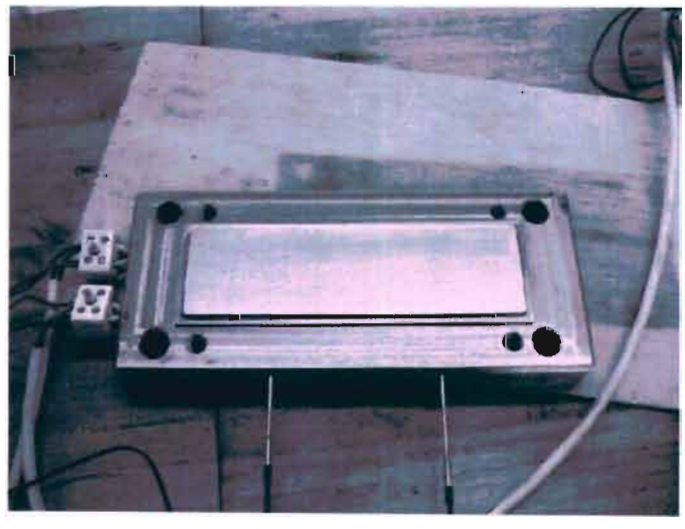

(a)

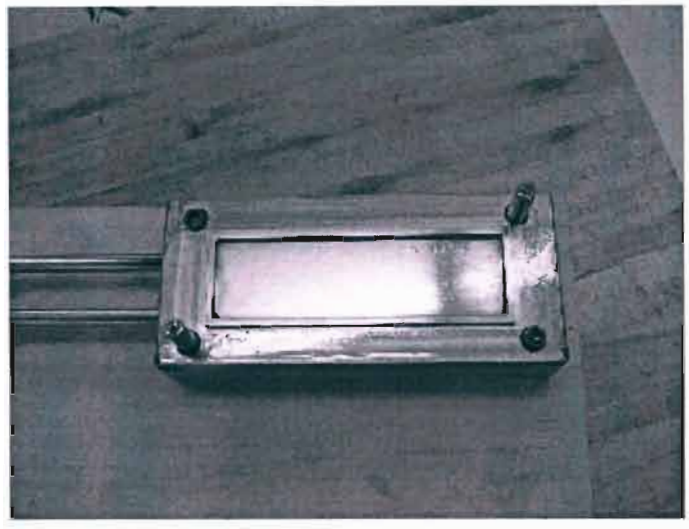

(b)

Fig. 3.9 Completed specimen mould (a) 'Male' section (b) 'Female' section

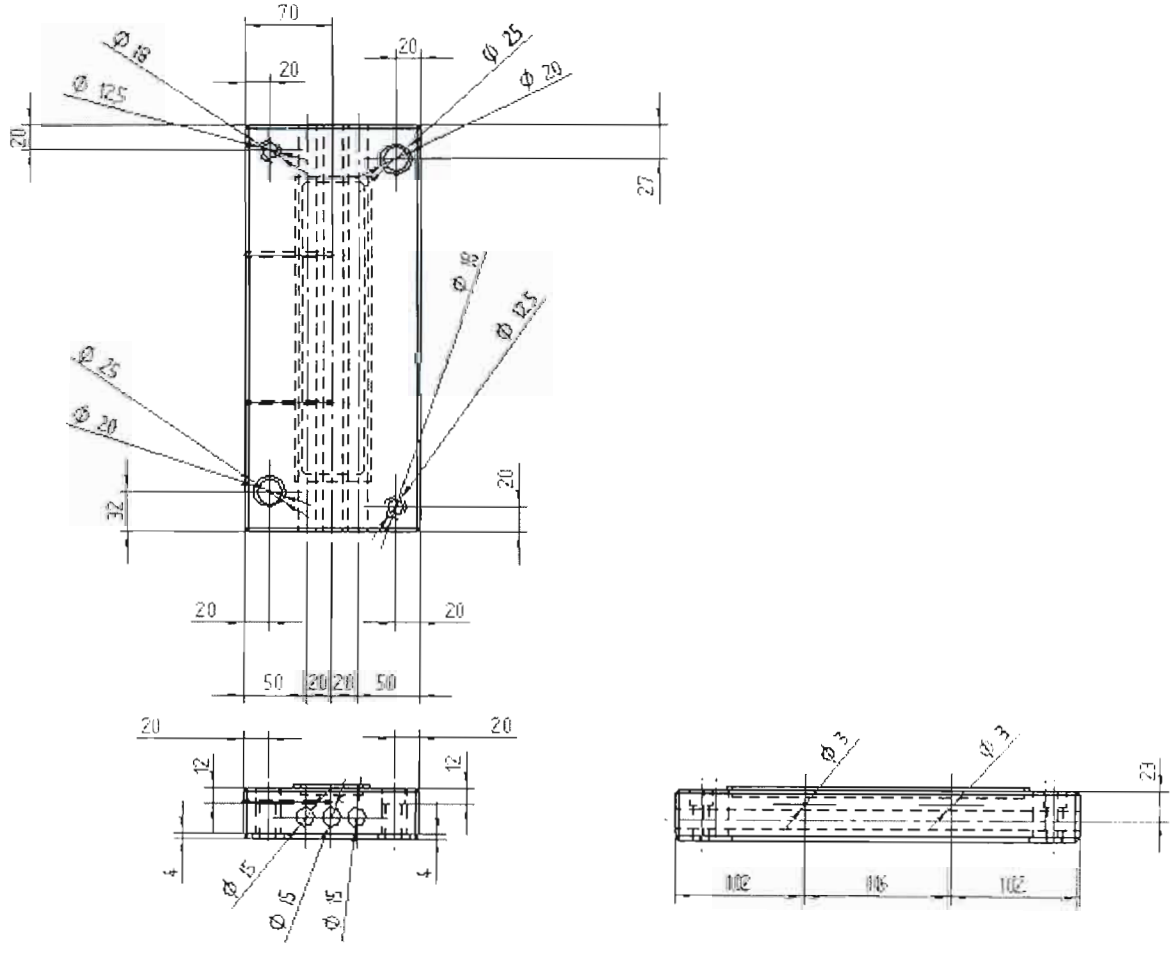

Fig. 3.10 Specimen mould drawings-'female' section

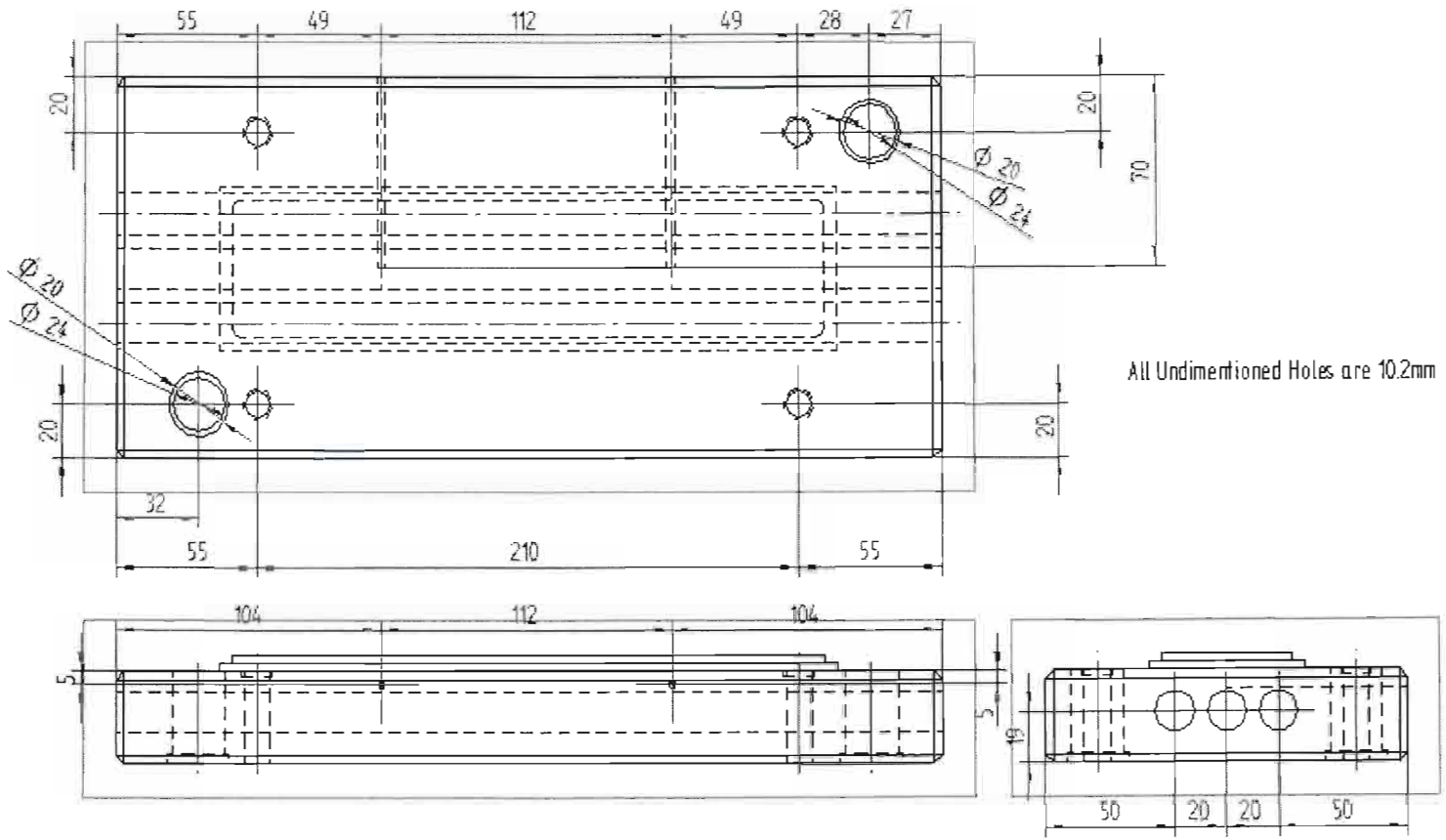

Fig. 3.11 Specimen mould drawings-'male' section

For the required size of SMC plate to be produced, the moulding process required the following:

Temperature: 130 °C
Pressure: 110 kN
Curing time: 90 s
(calculated according to supplier's data- *ABB, Bloemfontein*)

The two halves of the mould are first installed on the press to be used for manufacturing (Figs. 3.12-3.13), through the use of spacers and brackets as necessary.

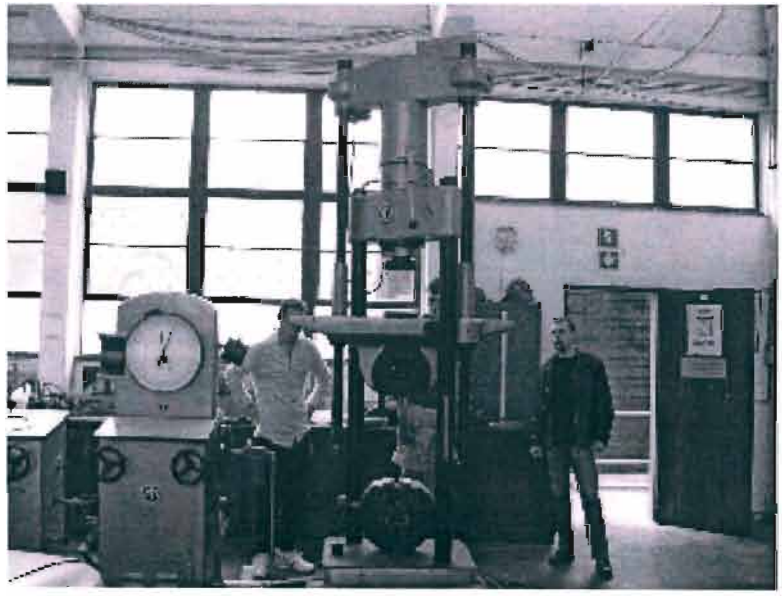

Fig. 3.12 Hydraulic press used for specimen manufacture

Fig. 3.13 Press control

Once the moulds are installed onto the press, the two halves are aligned using the guide pins (Figs. 3.14-3.15).

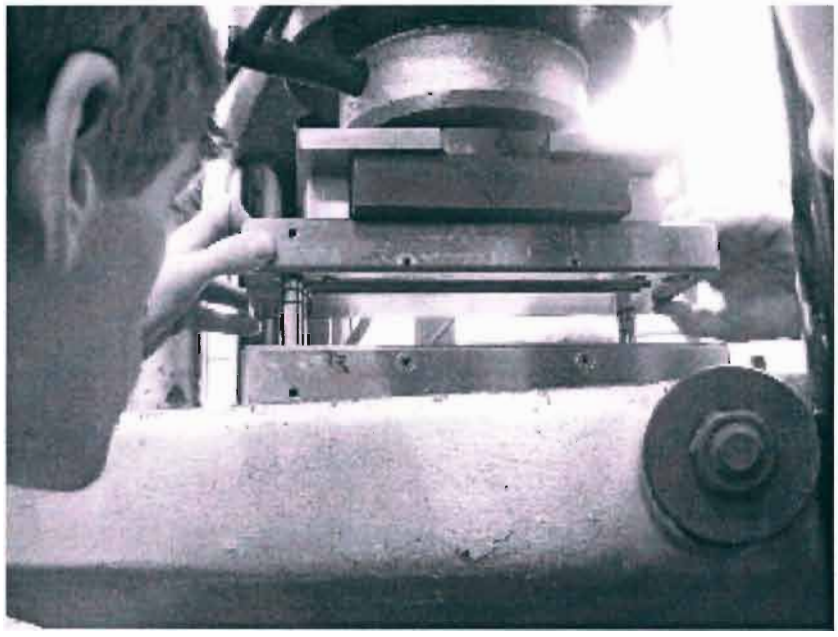

Fig. 3.14 Alignment of mould using guide pins

Fig. 3.15 Mould fitted and aligned

The thermocouples and heating elements were then installed in the mould (Fig. 3.16).

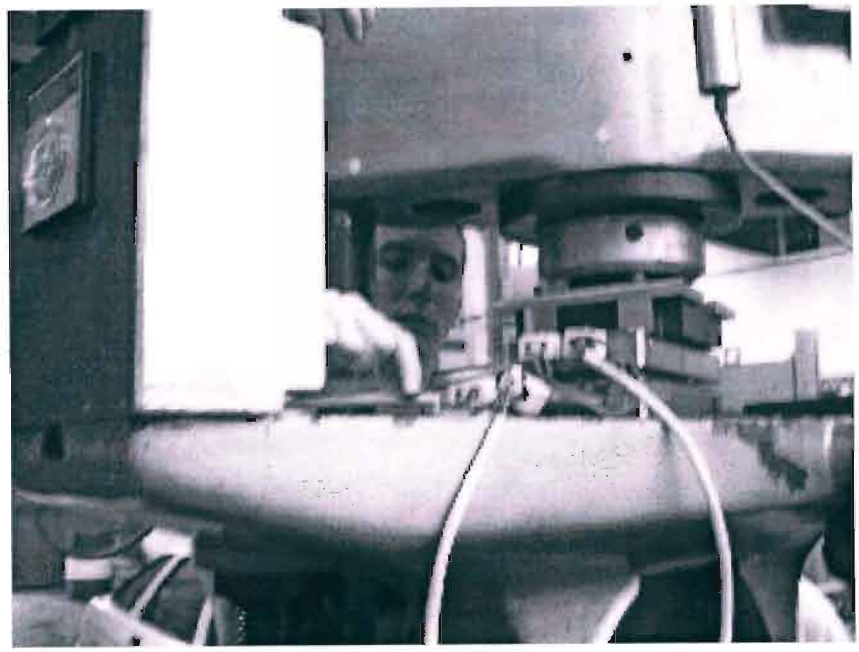

Fig. 3.16 Installation of thermocouples and heating elements

The heating control system was installed next to the press (Fig. 3.17).

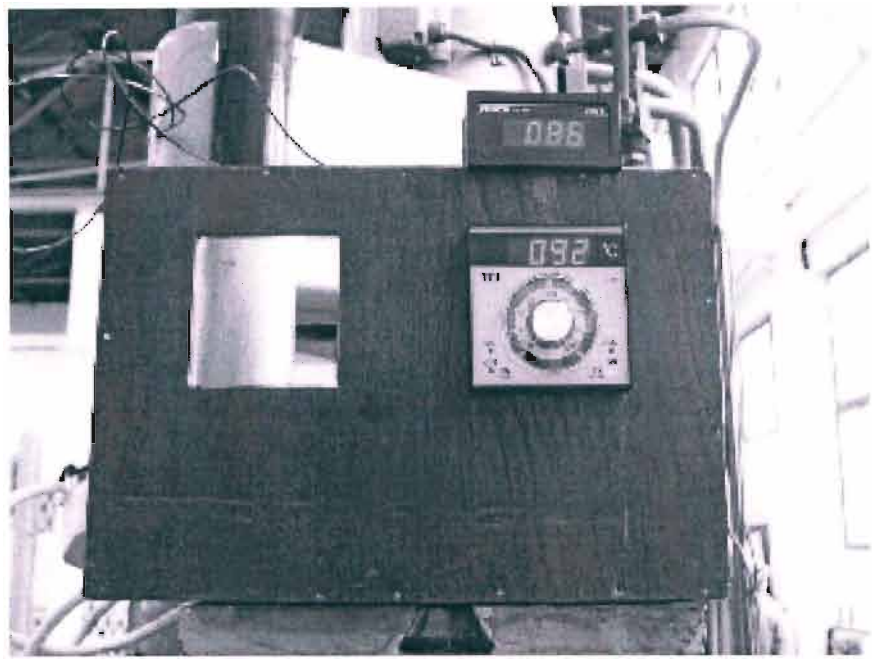

Fig. 3.17 Temperature controller and temperature display

Once the set-up was complete, the temperature was set to the necessary level, and the mould was heated up. Once the required temperature was attained, the necessary volume of SMC material was placed in the mould cavity, and the mould closed under the required pressure so that the material may be cured (Fig. 3.18).

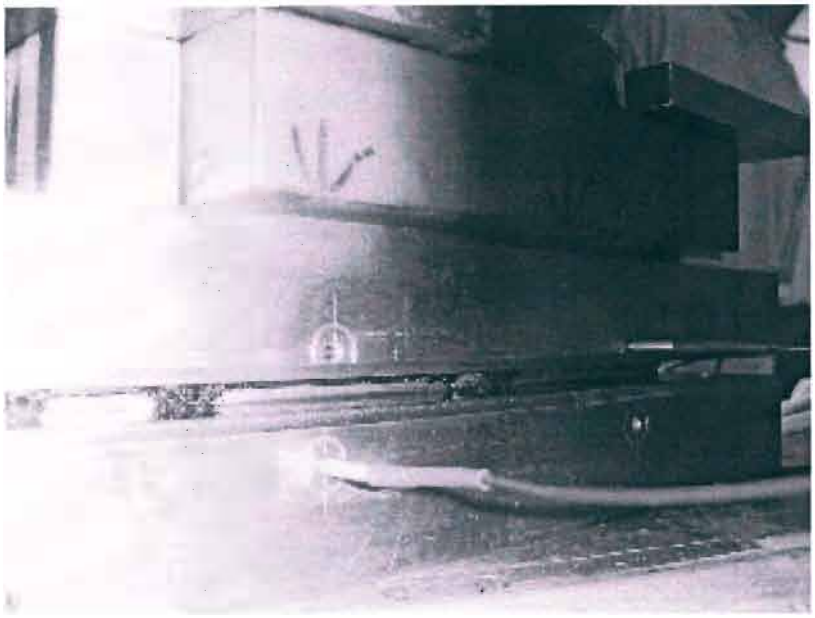

Fig. 3.18 The SMC material being cured under temperature and pressure

The curing process is completed after just 90 seconds, after which time the press is re-opened, the specimen allowed to cool slightly and removal effected by means of a compressed air ejection system.

After the required 90 seconds under temperature and pressure, the moulded plate (Fig.3.19) is allowed to cool and is then removed with the aid of a compressed air ejection system.

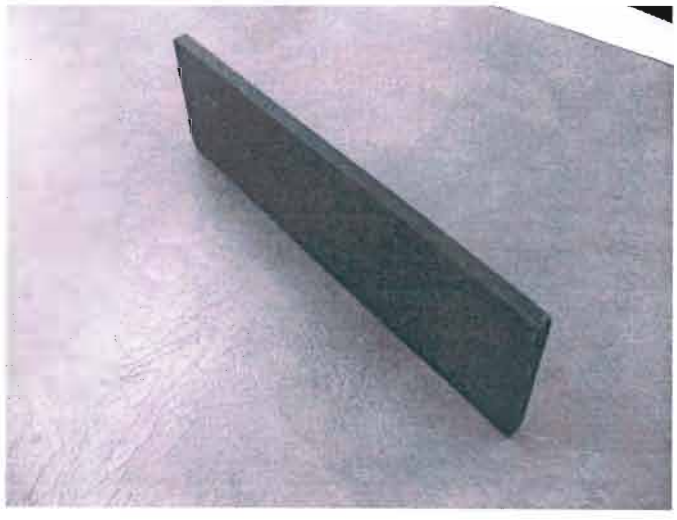

Fig. 3.19 Moulded SMC plate

The required specimen geometry was then cut out of this plate according to the geometry described earlier in this chapter.

3.4 Specimen test set-up

All testing of the test samples was initially performed on an MTS Series 412 test rig, pictured, schematically, in Fig. 3.20.

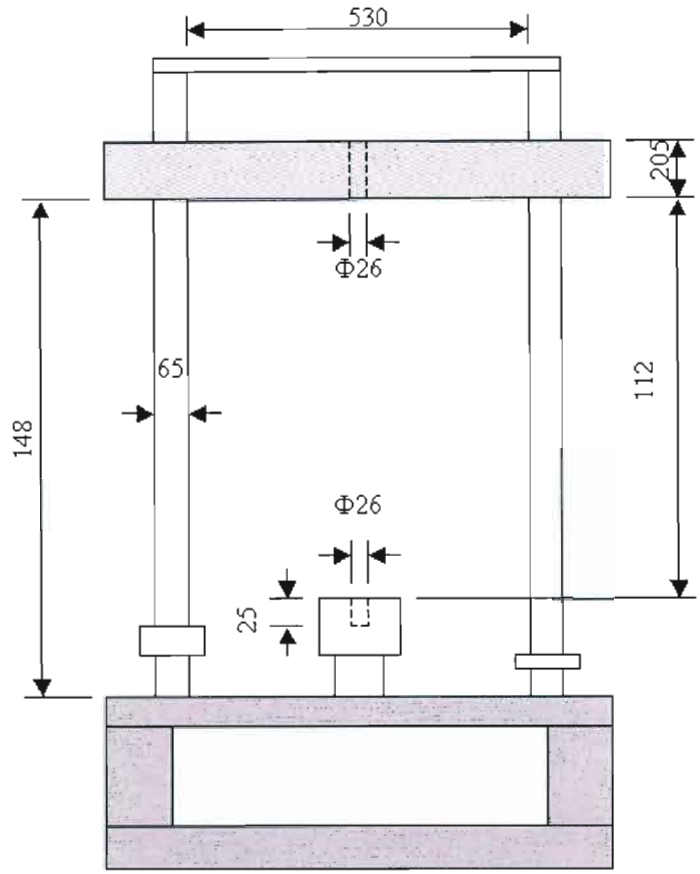

Fig. 3.20 MTS Series 412 test rig

The test rig is rated at 100kN, with a rated frequency range of 0.01 Hz to 1100 Hz. Specimen testing was performed by way of velocity prescription; the velocity of loading kept at a prescribed value, and the resultant stress-strain plot at each loading velocity then be plotted through the use of a data acquisition system.

Bending tests were also decided to be performed, to add to the validation analysis and to act as another point of comparison. A 3-point bend test set-up was decided on, and fixtures for this purpose were manufactured at the university (see Fig. 3.21).

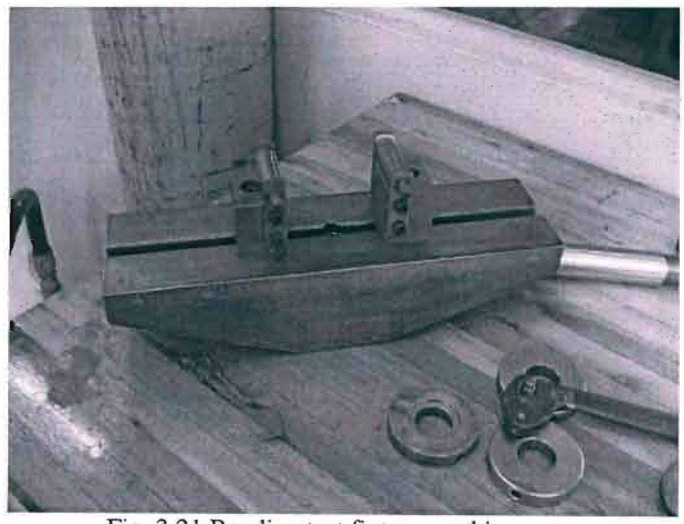

Fig. 3.21 Bending test fixtures and impactor

The data acquisition system utilised incorporated the use of the *Wavebook* hardware (Fig 3.22) and its related software to obtain the required information during the testing process. Most critically, the data acquisition system must be able to deliver accurately a stress-strain curve for the material specimens, either directly or indirectly.

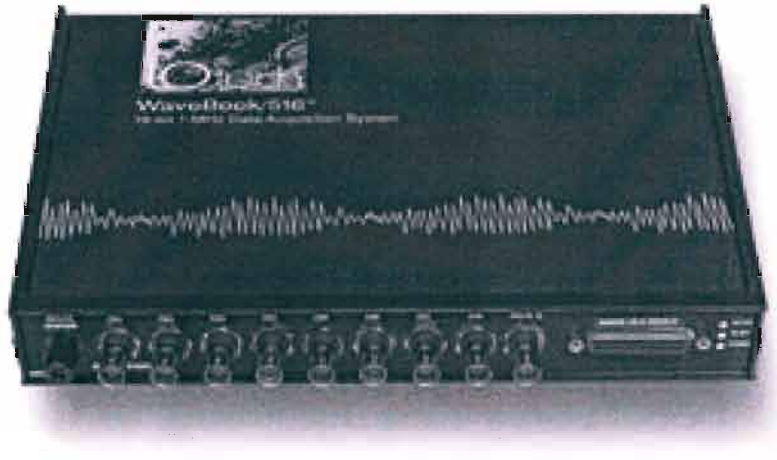

Fig. 3.22 The Wavebook hardware

Wavebook's strain gauge module allows for a number of bridge options and these are relatively simple to set up. For the purposes of this study, a full-bridge configuration was exclusively used as this was deemed to have the highest output and best performance. Of the numerous full-bridge wiring set-ups available, the 'remote sense' option (Fig. 3.24) is the option that was adopted, as in this case the excitation voltage is regulated at the strain gauge, which eliminates errors due to cable losses (which may be significant for long cables).

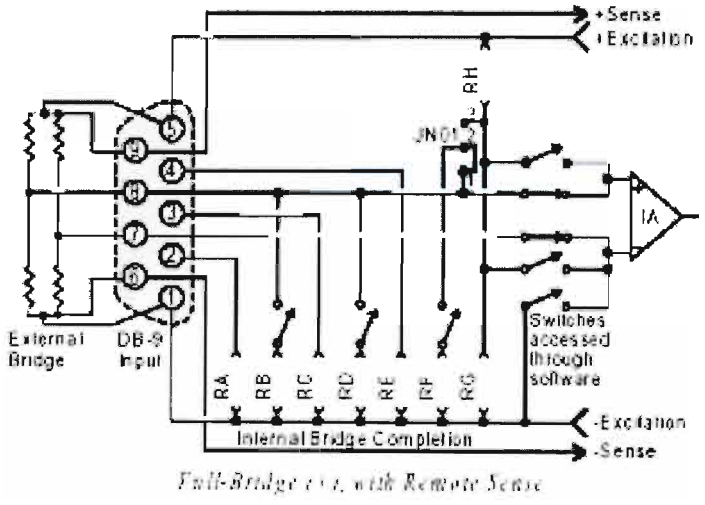

Fig. 3.23 'Remote-sense' full-bridge configuration for Wavebook strain gauge module (Wavebook Manual, 2000)

The strain gauges used were specified according to the test rig being used. For the testing performed on the MTS rig, 120Ω paper strain gauges were specified and utilised.

3.5 Proposed algorithm for incorporation of dynamic effects

The influence of strain rate was incorporated into this study by analysing the theoretical strain rate models presented in Chapter Two, as available within the PAM-CRASH finite element code environment. Quasi-static tests were performed, but these results, used in conjunction with these available strain-rate models, may be used to predict the material dynamic behaviour, when time, budgetary and logistical constraints do not allow for true dynamic testing.

A proposed characterisation algorithm incorporating these effects may thus be drawn up.

Firstly, a static stress-strain curve is obtainable from quasi-static testing. (Fig. 3.24)

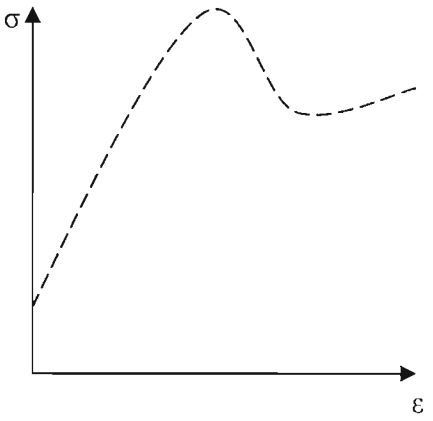

Fig. 3.24 Quasi-static stress-strain curve

A 'dynamic' stress strain curve may be obtained from dynamic testing at some pre-determined velocity (Fig. 3.25).

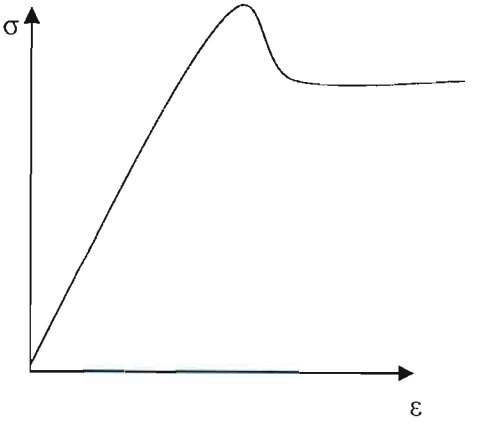

Fig. 3.25 Dynamic stress-strain curve

Each strain-rate law is adopted, and the parameters determined for best matching the quasi-static results with the dynamic results, calibrated at the velocity at which the dynamic test is performed (Fig. 3.26).

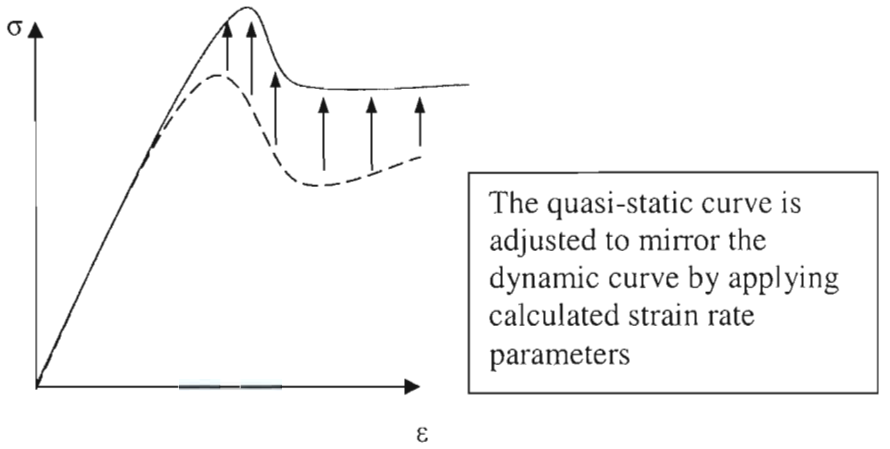

Fig. 3.26 Curve adjustment

These parameters may then be used as inputs into the finite element package. Simulations of the test are performed at the velocity of dynamic loading, and results compared and evaluated. For this work, to eliminate the strain-rate model influence on the accuracy of the results (thus, to merely evaluate the material model validity), quasi-static tests were performed with no strain rate laws applied and compared to the quasi-static test results.

At the conclusion of this chapter, borne initially only out of the need for experimental results, it is noted that certain key areas have been encompassed that might not have been if this study was limited to only theoretical formulations. An indication has been given of the depth of consideration that is required to be given to the manufacturing process so that meaningful results will be obtained. Not taking into account design concerns such as the method of temperature control, or the data acquisition system to be implemented, early on in the analysis process may in fact lead to key limitations being overlooked, and this may in turn lead to critical delays and the need for re-analysis. It is thus made evident that the manufacturing process, especially in the case of the family of composite materials, has a direct bearing on the usefulness of data that is obtained. With the required characterisation and testing complete, we may then move onto the primary purpose of the modelling, namely the numerical simulation of various loading cases.

Chapter 4

Numerical Modelling and Simulation

Simulation was performed at numerous key junctures during the study, but primarily as a basis for the evaluation of existing and implemented material and damage models for SMC composite materials (as referred to in Chapter 2 of this work), as a means of analysing experimental data, and at a latter stage, as a basis for implementation and evaluation of a newly developed SMC composite model (as will be discussed in the following chapter).

The simulation process necessarily began with the selection of suitable finite element analysis software. Such packages were initially researched and relatively evaluated using criteria listed in Table 1, and, based on this evaluation, a selection of software was made for further research, and then implementation. Selection was limited to those software packages that offered dynamic analysis capabilities and composite-specific analysis models, and the survey yielded four plausible options viz. ESI Software's PAM-CRASH, Livermore Software Technology Corporation's LS-DYA, MSC. Software's DYTRAN and Abaqus Incorporated's ABAQUS/Standard.

Table 4.1 Comparison of finite element software packages

	PAM-CRASH	LS-DYNA	DYTRAN/ PATRAN	ABAQUS
Availability	2	3	1	4
Built-in Composite Models	1	3	4	2
User-Definability	2	3	4	1
Compatibility/Implementability	3	2	1	4
Cost	3	2	1	4
RANK	**1**	**3**	**1**	**4**

Although from this simple evaluation, the DYTRAN/PATRAN option yielded what proved to be the joint lowest (and thus, best) score, after further research and evaluation to separate the two top-ranked choices, this package was removed as an option due to a lack of supporting research material and current studies utilising the software. It was thus decided to proceed using ESI's PAM-CRASH software as the basis for analysis, and also to use LS-DYNA to a lesser extent, to enable comparative analyses and allow for a broader knowledge base on which to base these analysis evaluations.

The starting point of the numerical analysis would be to explore the built-in SMC composite modelling capabilities within the selected package, and to verify the validity of results obtained from using this model by comparing them with experimental results. This would thus also satisfy one of the objectives of this study, namely the evaluation of already-implemented SMC composite modelling options (a brief survey of models present in other available packages is included in Chapter 2, but of these PAM-CRASH did in fact include what was considered to be the most promising ready-included model). A survey of the built-in models present within PAM-CRASH yielded only one appropriate for crashworthiness analysis of SMC composites; an Elastic Plastic Model with Isotropic Damage Behaviour (see Chapter 2) (corresponding to PAM-CRASH material type 105), and so analysis was performed using this model and the results were compared, for different loading conditions, with the LS-DYNA modelled results (using the Kinematic Model, also described in Chapter 2), and also with experimental results.

4.1 Initial Simulation Validation

At the initial stage, the actual simulation process and methodology, as well as the functionality of the implemented material model, was investigated. As mentioned in the description of this model in Chapter 2, the mechanical properties of the SMC material being used are determined experimentally by the uniaxial testing of flat specimens. It was considered worthwhile to thus carry out simulation of this testing as well, as this allowed for familiarisation with the analysis process parameters while simulating a relatively simple and computationally quick test.

4.1.1 Material Characterisation

The simulated material (Glass-Epoxy SMC) had the following properties, as required for input into PAM-CRASH. The damage properties were at this stage arbitrarily assigned, since the purpose of this initial investigation was merely to validate the material model and the software, rather than analyse the results themselves. Thus no testing was performed, and the other required characteristics were calculated using suitable techniques discussed below.

Density:			$1.8e^{-9}$ t/mm^3
Young's Modulus:			$2.328e^{4}$ MPa
Yield Stress:			465.6 MPa
Thickness:			5 mm
ε_i:	0.02		
ε_l:	0.06	d_l:	0.2
ε_u:	0.09	d_u:	0.9

4.1.2 Derivation of material characterisation

The material properties were calculated using data tables (Vasiliev and Morozov, 2001) for Glass Fibre and Epoxy separately, and then applying the method of mixtures law using a fibre percentage of 30% (as was supplied). The damage and yield stress values were found from testing.

The raw data for the material characterization was thus separated properties for the two phases of the composite material, namely glass fibres and epoxy matrix.

Glass Fibres:
Volume Fraction: 30%
Young's Modulus: 72 GPa
Mass Density: 0.245 kg/m^3

Epoxy Matrix:
Young's Modulus: 2.4 GPa
Mass Density: 0.122 kg/m^3

Poisson's ratio for the composite material was taken to be 0.3, a value characteristic of this type of composite material.

From this data the composite material properties were extrapolated using the following relations.

$$E_{comp} = E_f v_f + E_m v_m$$
$$G_{comp} = \frac{E_{comp}}{2(1+v_c)}$$
$$\rho_{comp} = \rho_f v_f + \rho_m v_m \qquad (4.1)$$

The tensile test was simulated by the application of a constant velocity motion of the nodes at one end of the rectangular specimen, while the nodes at the other are constrained to be fixed in position. Testing was simulated at different velocities (0.3, 3.3, 33 and 330 mm/s), to monitor the effect of loading velocity on the response.

The schematic test setup is shown in Fig. 4.1, the finite element mesh in Fig. 4.2, and the progressive deformation at 33mm/s in Fig. 4.3. The simulations yielded the results shown in Figs. 4.4. Figs 4.5 to 4.7 show similar plots for simulations at progressively increasing loading velocities.

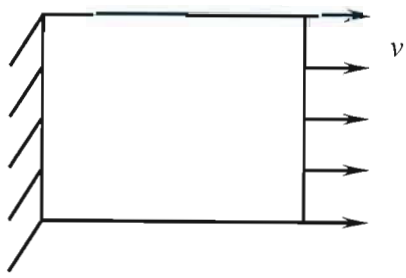

Fig. 4.1 Tensile test schematic

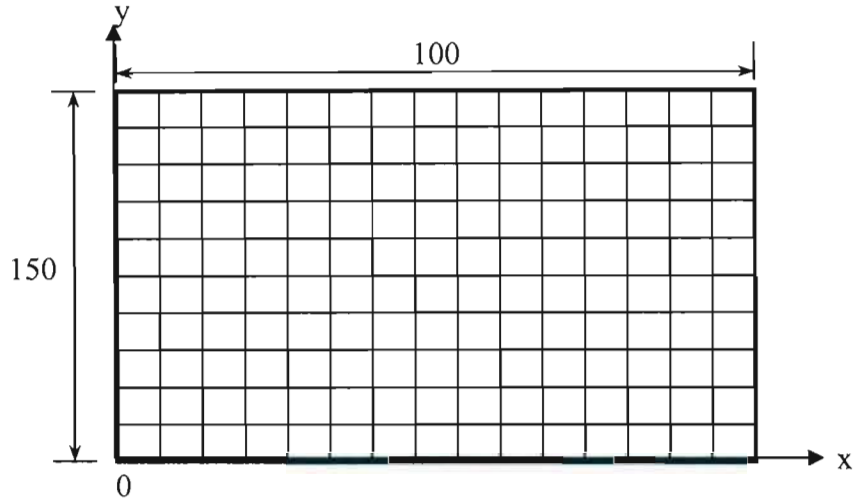

Fig. 4.2 Tensile test specimen finite element mesh

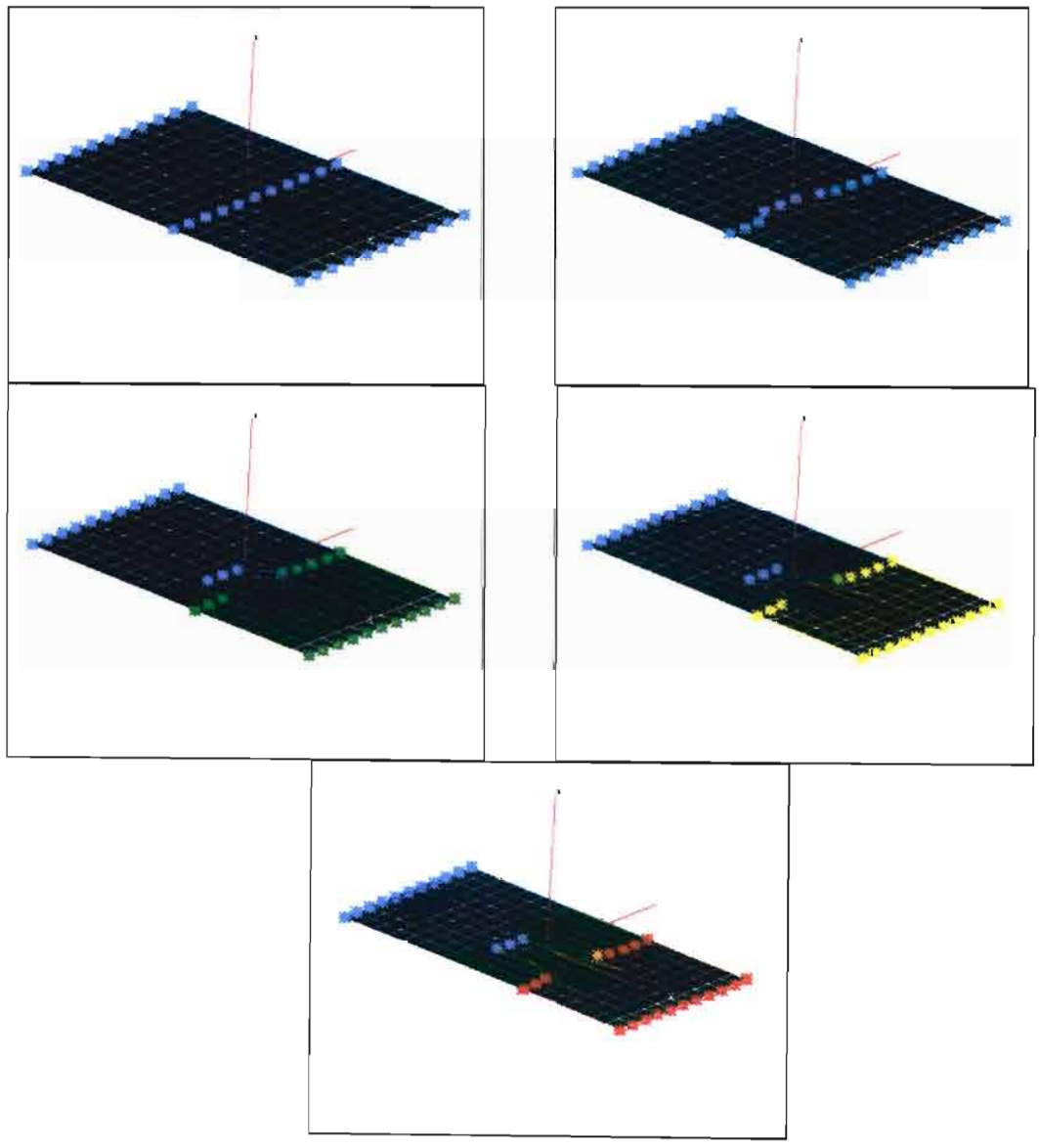

Fig. 4.3 Progressive deformation of SMC under tensile test at 33mm/s

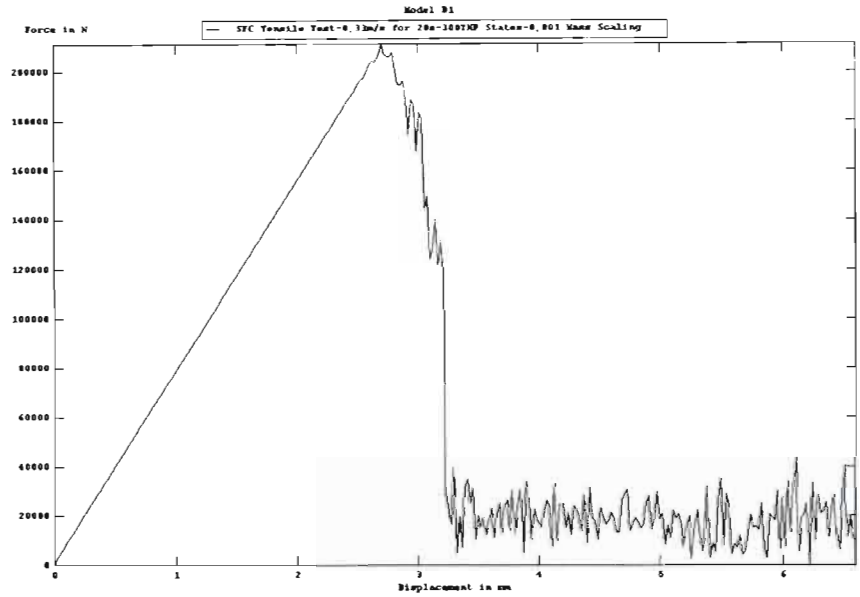

Fig. 4.4 Force-Displacement plot at a simulated applied constant velocity of 0.33mm/s

Fig. 4.4 shows the simulated result for an applied constant velocity of 0.33mm/s. It is seen that the material is clearly elastic up to a load of ±150 kN, reaches a maximum force of ±200 kN before the initiation of catastrophic failure, and has an ultimate displacement limit of ±3.3 mm (corresponding to a 20 kN load) before ultimate failure (complete loss of significant load-carrying ability).

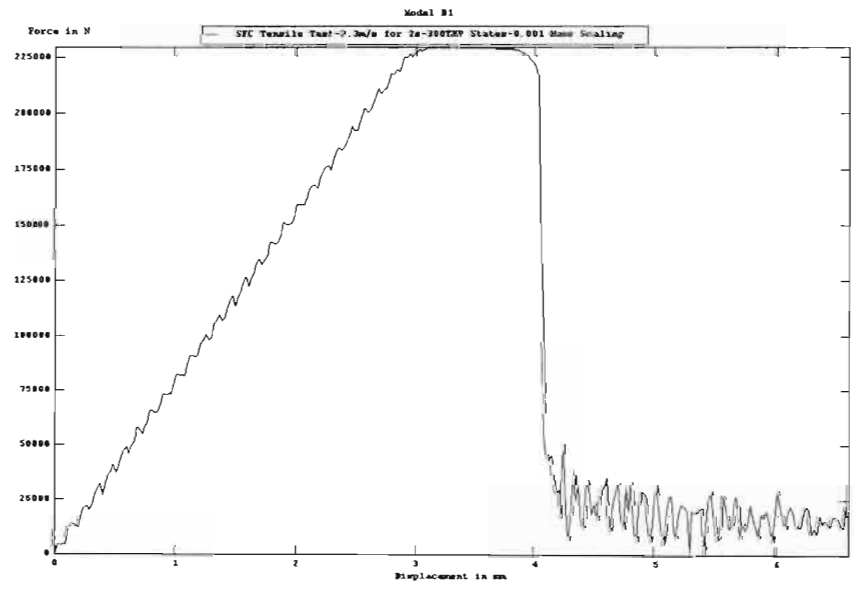

Fig. 4.5 Force-Displacement plot at a simulated applied constant velocity of 3.3mm/s

In Fig. 4.5 the applied velocity is now magnified by a factor of 10, with the result of increased values for each phase of the material. The elasticity limit now appears to be ±215 kN, a new maximum force level of 2227 kN is in evidence, and ultimate failure occurs at an increased displacement of ±4.5mm (corresponding to 20 kN again).

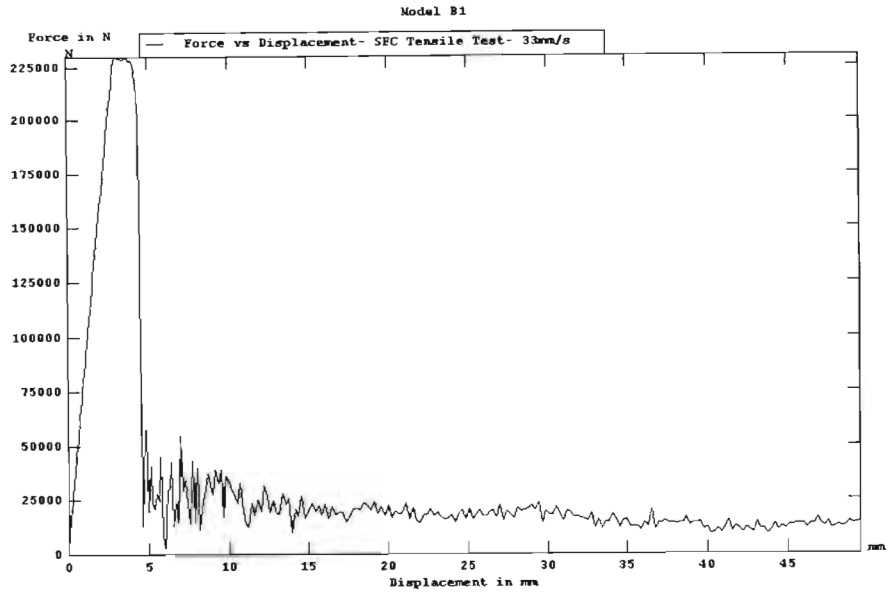

Fig. 4.6 Force-Displacement plot at a simulated applied constant velocity of 33mm/s

Fig. 4.6 (33mm/s simulation) again shows the increase of the maximum force experienced (±228kN), with a similar trend to the above plot.

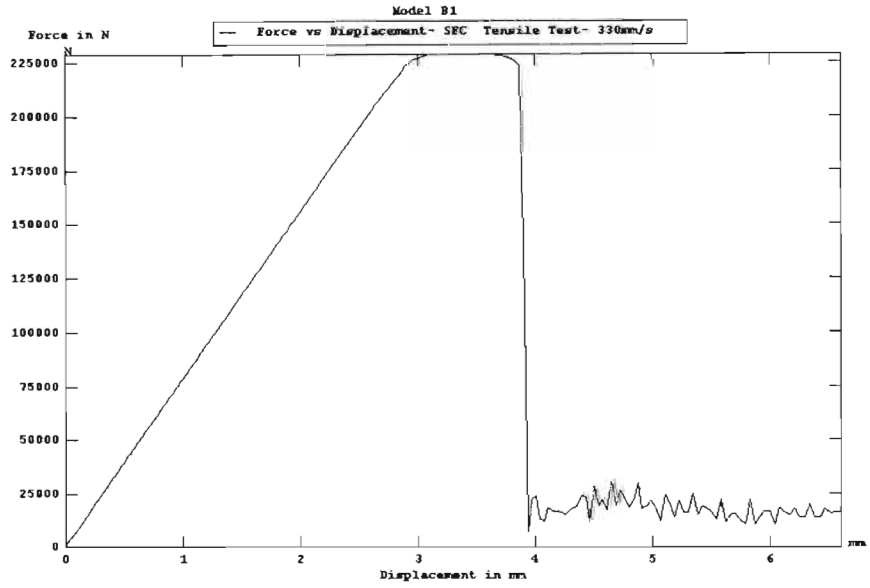

Fig. 4.7 Force-Displacement plot at a simulated applied constant velocity of 330mm/s

Finally, Fig 4.7 (330 mm/s) fairly mirrors the previous one, showing a similar trend as well as a similar maximum force point. In each case, the load of approximately 20 kN remaining at the point of ultimate failure is due to the implemented ultimate damage factor being input as 90% rather than complete or 100% failure.

Thus, the simulated responses for the tensile tests at different loading velocities show results that are physically reasonable and characteristic of the nature of this type of material. By way of comparison, and as an initial validation of the simulated results, similar simulation was performed in the LS-DYNA software, using the Elastic Plastic Model with Kinematic Hardening Model, with comparative results shown in Tables 4.2 and 4.3 for two of the loading velocities, at two of the key load points, namely the 'elastic limit' (indicated by the

end of the initial linear region of the material stress-strain curve, and thus corresponding to the point of initiation of damage) and the maximum stress point.

.

Table 4.2. Tensile test simulated results for SMC material. (330 mm/s prescribed velocity).

Simulation results	Elastic limit (MPa)	Displacement at elastic limit (mm)	Maximum Stress (MPa)	Displacement at maximum stress (mm)
PAM-CRASH	442	2.85	456	3.50
LS-DYNA	424	3.34	424	3.34
% Deviation	4	17	7	5

Table 4.3. Tensile test simulated results for SMC material.(33 mm/s prescribed velocity)

Simulation results	Elastic limit (MPa)	Displacement at elastic limit (mm)	Maximum Stress (MPa)	Displacement at maximum stress (mm)
PAM-CRASH	457	3.20	460	4.00
LS-DYNA	391	2.63	430	4.12
% Deviation	14	18	7	3

The results show fairly good correlation, within 7% discrepancy for the maximum stress value and 14% for the so-called elastic limit/damage initiation point. This coherency provides a basis of confidence in both the respectively implemented models, at least at this simplified level of analysis and justifies moving on to the next level of complexity.

As a second step, a more complex loading condition, the three-point bend test, was comparatively simulated, using both simulation packages and the material characterisation described above. As can be seen from the graphed results shown in Figs. 4.8 and 4.9, the discrepancy between the two sets of results is substantial for this loading case.

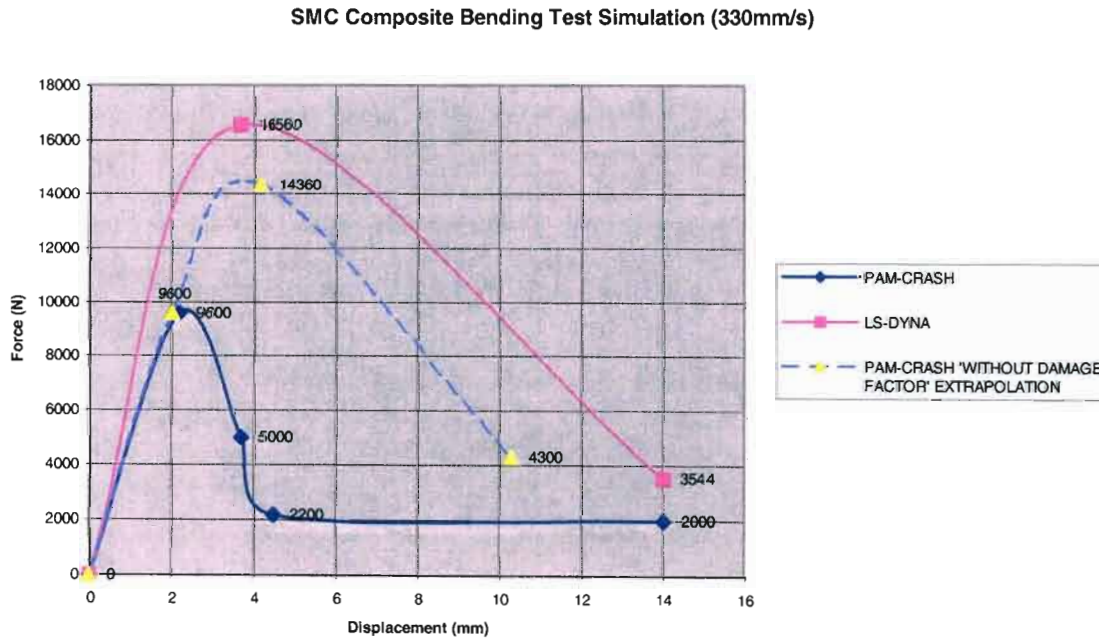

Fig. 4.8 SMC composite bending simulation comparison (330mm/s)

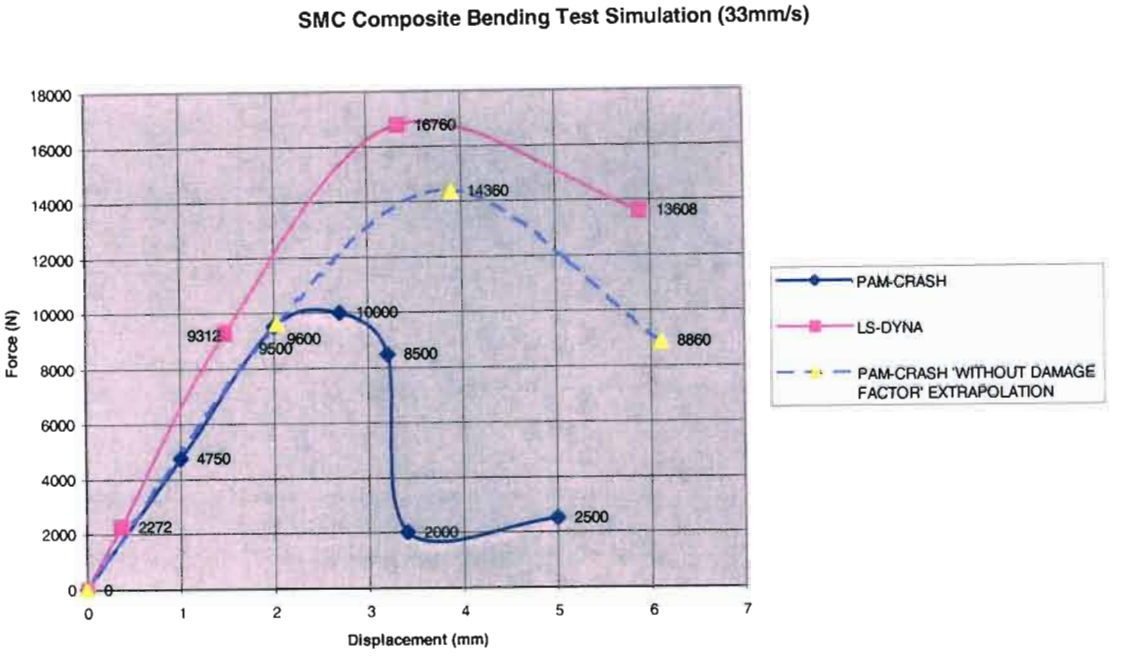

Fig. 4.9 SMC composite bending simulation comparison (33mm/s)

A third plot (shown with dashed line) is included on both plots to emphasise the effect of the input damage variables on the output of the PAM-CRASH simulation. As explained in the model description in Chapter 2, the damage variable degrades the value of the modulus of the material, which serves to decrease the maximum bending moment, as now can clearly be seen. Without these damage variables, which were rather arbitrarily chosen for the SMC composite material for this initial investigation, the two plots would follow very similar trends as shown. The value of the maximum bending moment would be increased without the effect of damaging the material, and the degradation of the material would prove to be gradual, as in the LS-DYNA case.

4.2 Bending Test Validation

At this stage, with a suitable level of confidence and understanding gained in the simulation process, and simple validation analysis being performed, the task was taken on to validate a set of simulated results by comparison with representative experimental data. Though suitable for initial exploration and validation analysis, simple uniaxial test simulation does not explore the full range of dynamic analysis or mirror the more complex loading conditions that would exist in a typical crashworthiness situation. A more suitable demonstrator test was thus chosen to better exhibit the conditions of an actual crash, and this test was then simulated in the finite element analysis environment, applying the same material model as for the uniaxial tests above.

The bending test was chosen since in this case the loaded specimen exhibits a combination of tensile, compressive and shear effects, is indicative of the type of loading that may result from certain types of collisions, and is relatively easy to set up experimentally.

4.2.1 Material characterisation

As is required by PAM-CRASH material type 105 (which makes use of the Elastic Plastic Material Model with Isotropic Damage discussed in the previous Chapters) characterisation by way of tensile testing had to be performed. Having previously arbitrarily chosen or

calculated these values from the constituent material data, tensile testing was now performed, and these results were used as the basis for the material characterisation, yielding the required values for the material elastic moduli and damage factors.

The mechanical properties of the SMC material, and specifically the values associated with the three key stress-strain points described in the model formulation, are determined experimentally by the quasi-static, uni-axial testing of flat specimens. As these properties depend on the manufacturing process parameters, to obtain adequate material characteristics that may be used for the analysis of structural components, the specimens should be fabricated using the same processes that are used to manufacture such structural elements. The material selected for analysis was an unsaturated polyester resin matrix filled with 20% glass fibres by volume, length of fibres is 25mm.

4.2.1.1 Sample Manufacture

As has already been described in detail in the previous chapter, the samples were manufactured using a hot moulding process, as required for the material to cure. The moulds were designed and manufactured specifically for this task, with cylindrical cartridge elements inserted directly into the moulds providing the necessary heating.

The moulding process occurs at a temperature of 130-170°C and a pressure of between 50 and 100 bar, and the curing process is completed in between 30 and 150 seconds (depending primarily on the thickness of the moulded part). Plates of material of dimensions 230x190x4mm were produced, from which the tensile, compressive and bending test specimens of suitable dimensions and shape were cut. Appropriate fixturing had to also be manufactured, and the test specimens appropriately strain-gauged.

4.2.1.2 Test Results

Results obtained from the tensile testing with constant velocity 0.5 mm/min are output in the form of a stress-strain graph, which is used to obtain the damage law parameters and elastic constants as mentioned in the model description. The experimental stress-strain plot specifically detailing the required model parameters is shown in Fig. 4.10.

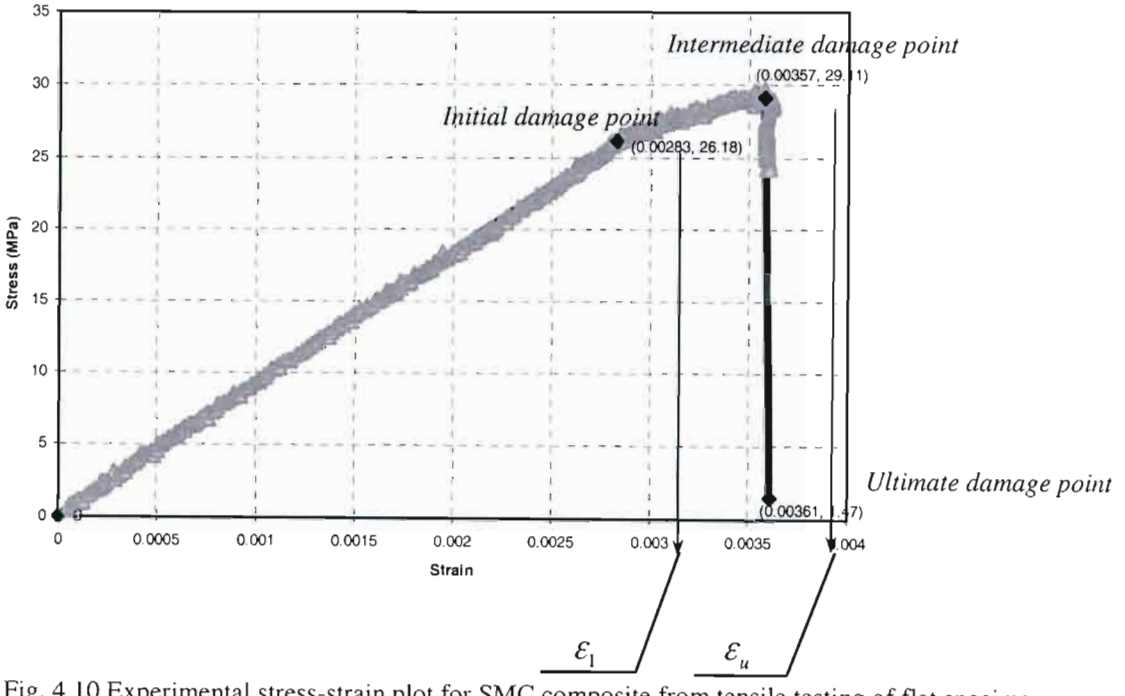

Fig. 4.10 Experimental stress-strain plot for SMC composite from tensile testing of flat specimen

From this approximated plot the intermediate and ultimate damage coefficients are calculated to be $d_1 = 0.12$ and $d_u = 0.95$ respectively, and these were thus used as the inputs into our damage model.

4.2.2 Bending test validation analysis

A three-point bending test was chosen as a basis for validation of the progressive failure model, as this mode of loading is considered to be more representative of the complex nature of loading in structural components subjected to crushing loads, especially since the bending test brings about both tensile and compressive effects in the test specimen. However, the material damage model in question is limited to the application of a single failure pattern, based on either of these test circumstances, thus the tensile loading case was chosen as the basis for the damage parameters in the material law. This choice would appear logical since failure would most probably be initiated in tension, so this would be the more conservative option.

The three point bending test was performed on both MTS and INSTRON testing equipment (for the purposes of comparison). A schematic set-up is described in Fig. 4.11, and the actual set-up is pictured in Fig. 4.12. Constant loading velocities of 2 mm/s and 100 mm/s have been applied to the simply supported plate. The destroyed test specimen is shown in Fig. 4.13.

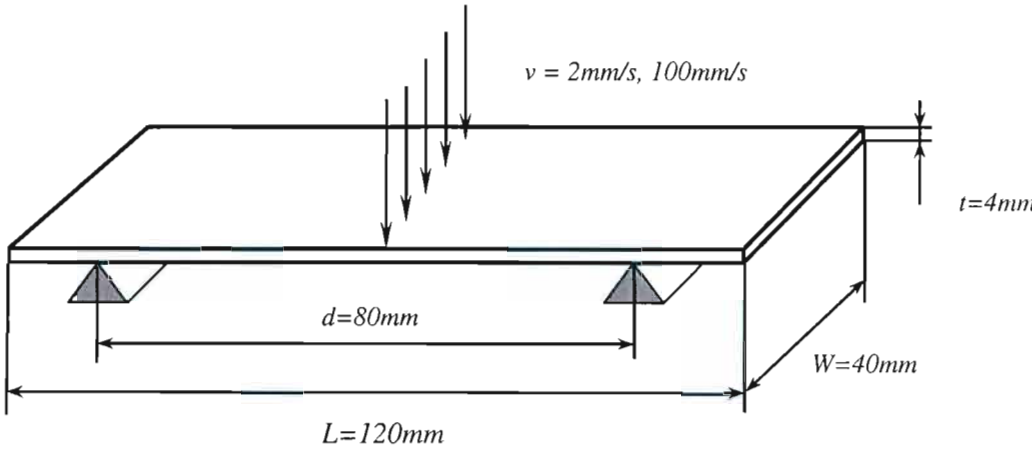

Fig. 4.11 Bending test set-up (schematic)

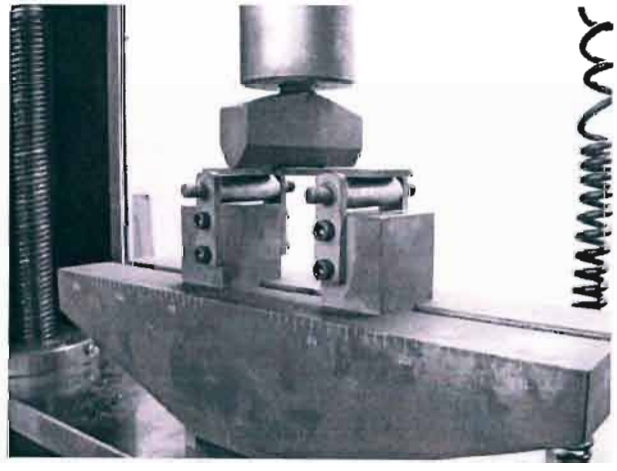

Fig. 4.12 Bending test set-up (actual)

Fig. 4.13 Destroyed specimen

The test was similarly instituted in numerical simulation using the PAM-CRASH software. The mesh (Fig. 4.14), created using MSC. NASTRAN, comprises 48 plate elements, with each element having dimensions 10x10mm. Loading is applied using the software's constant velocity boundary condition, whilst the simple supports are modelled using a displacement boundary condition.

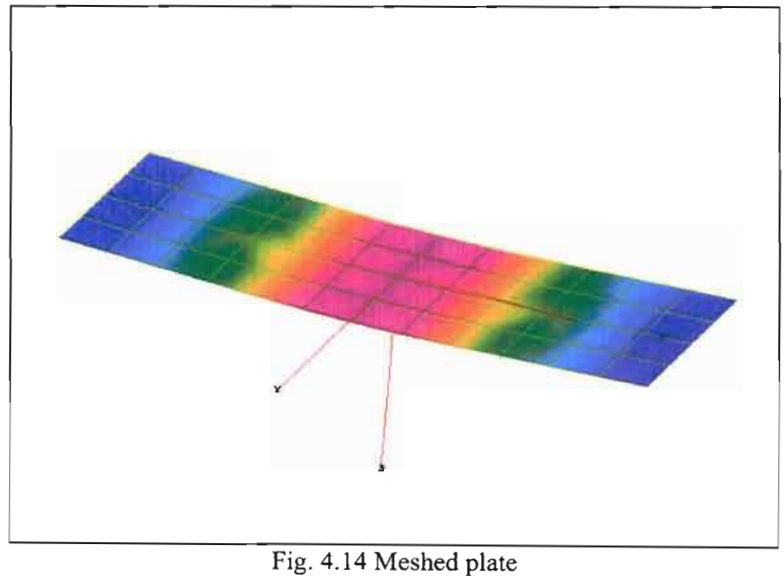

Fig. 4.14 Meshed plate

Comparative results, showing the simulation results at a test speed of 2mm/sec and 100mm/sec are included in Fig. 4.15 and Fig. 4.16.

The results indicate that the numerical simulation shows substantial discrepancy from the experimental results obtained. The validity of the experimental results was verified by carrying out the second test using different testing apparatus and data acquisition techniques. With both test runs yielding similar results, it is concluded that the inaccuracy lies in the simulated results

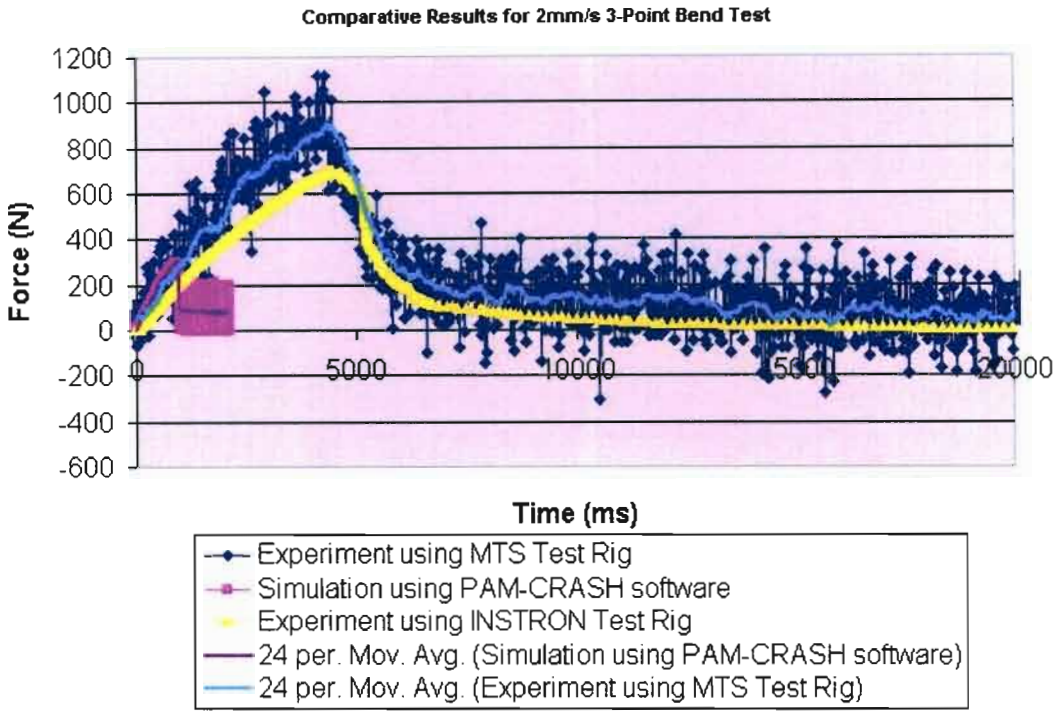

Fig. 4.15 Comparative results for 3-point-bending test with velocity 2mm/sec

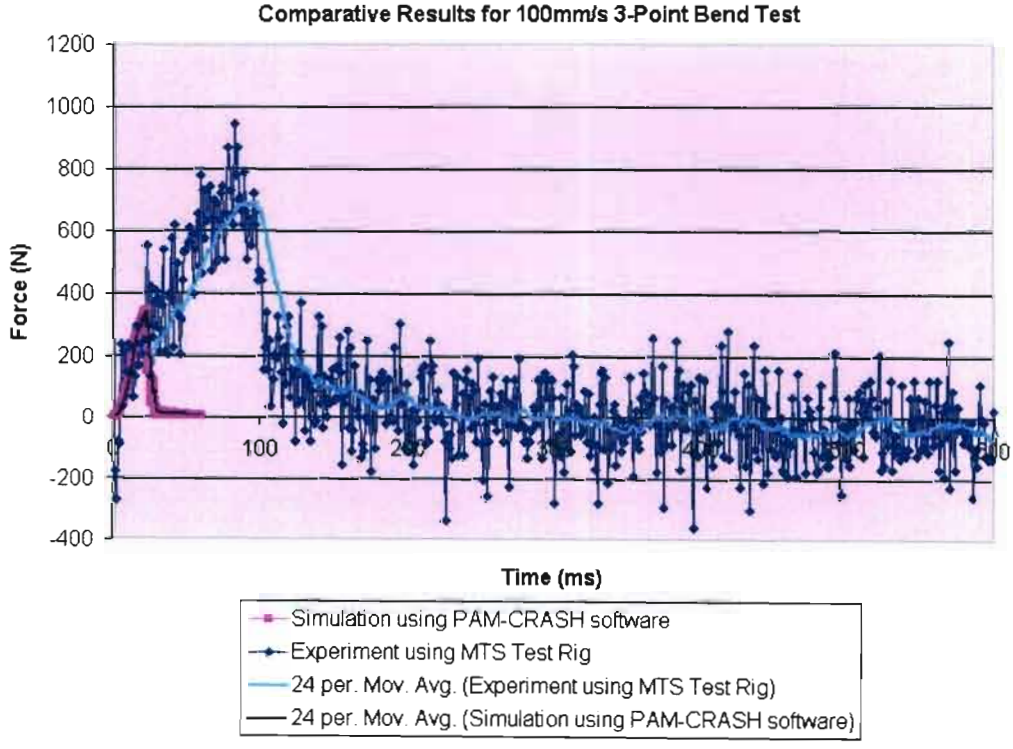

Fig. 4.16 Comparative results for 3-point bending test with velocity 100mm/sec

4.2.3 Model refinement

The numerical simulation was then scrutinized and refined, with the next iterations of simulations using a refined mesh and different element types.

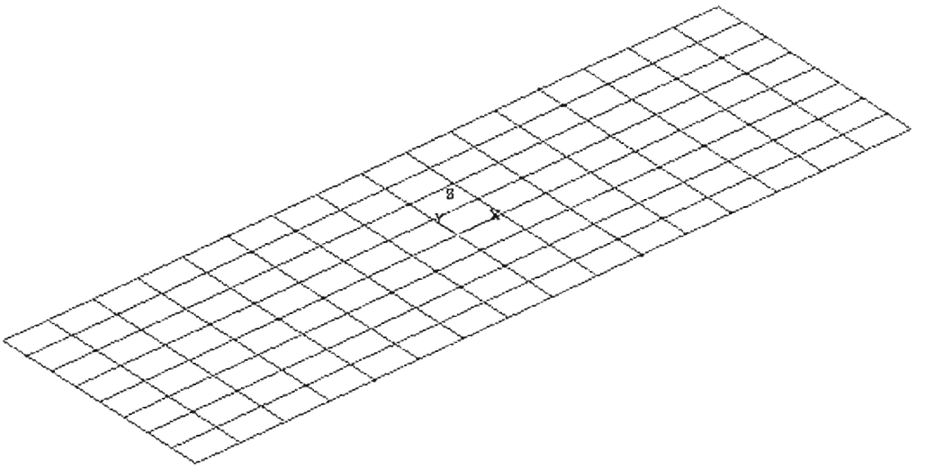

Fig. 4.17 Plate meshed with 128 plate elements (element size 5mm x 5mm)

Firstly a refinement of the plate element mesh was performed, increasing the 48 plate elements originally employed to 128 square plate elements with side length of 5 mm (Fig. 4.17). It was found that a finer mesh visibly improved the accuracy of results, (see Fig. 4.20), until too fine a mesh introduced numerical problems. With discrepancy still evident, other options to improve the simulated response were then considered.

As a second avenue for refinement, a solid element mesh was explored as an alternative to the previously adopted plate elements. PAM-CRASH Material Type 16, the solid element equivalent of plate Material Type 105, which employs identical characterisation and damage behaviour, was selected.

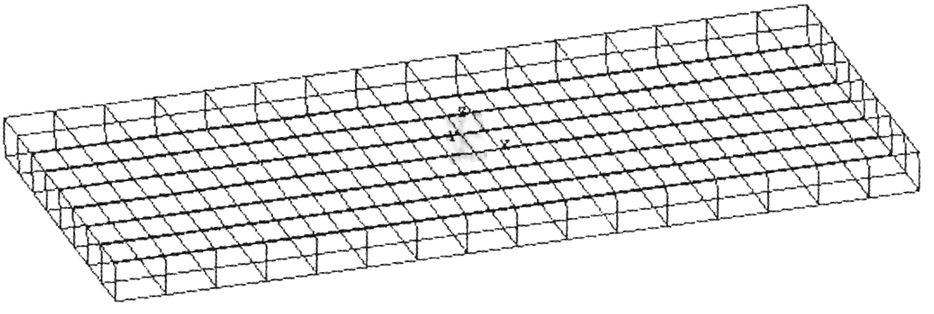

Fig. 4.18 Plate meshed with 128 solid elements (element size 5mm x 5mm x 4mm)

At first the mesh utilised consisted of only one element across the thickness of the plate (Fig. 4.18), and produced poor results. The solid element size was then reduced so that two elements (with size 2 x 2 x 2 mm) now made up the thickness of the plate (Fig. 4.19).

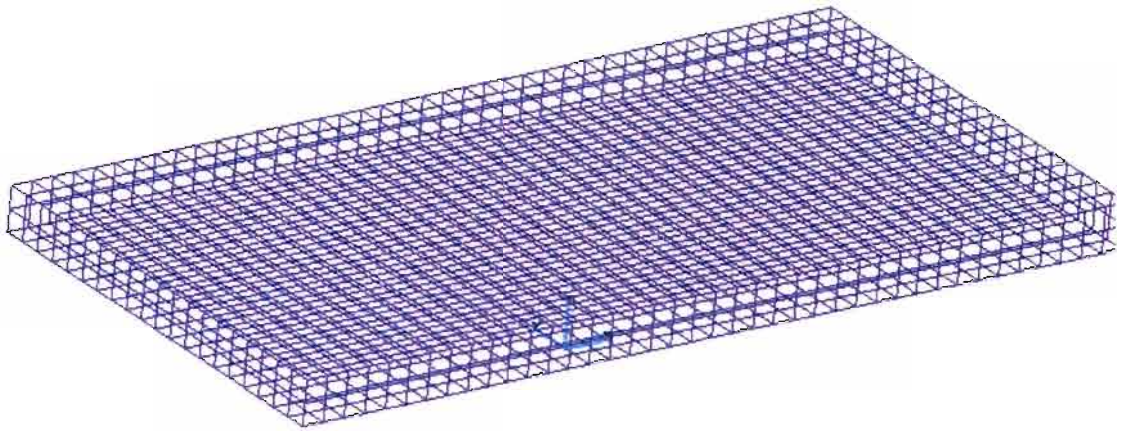

Fig. 4.19 Plate meshed with 1600 solid elements (element size 2mm x 2mm x 2mm)

The results obtained from this simulation, employing 2 x 2 x 2 mm solid elements, proved to be the closest yet to those obtained from the three point bending experiment, with a predicted peak load of 630 kN compared to a measured peak of 700 kN (a 10% error) (see Fig. 4.20).

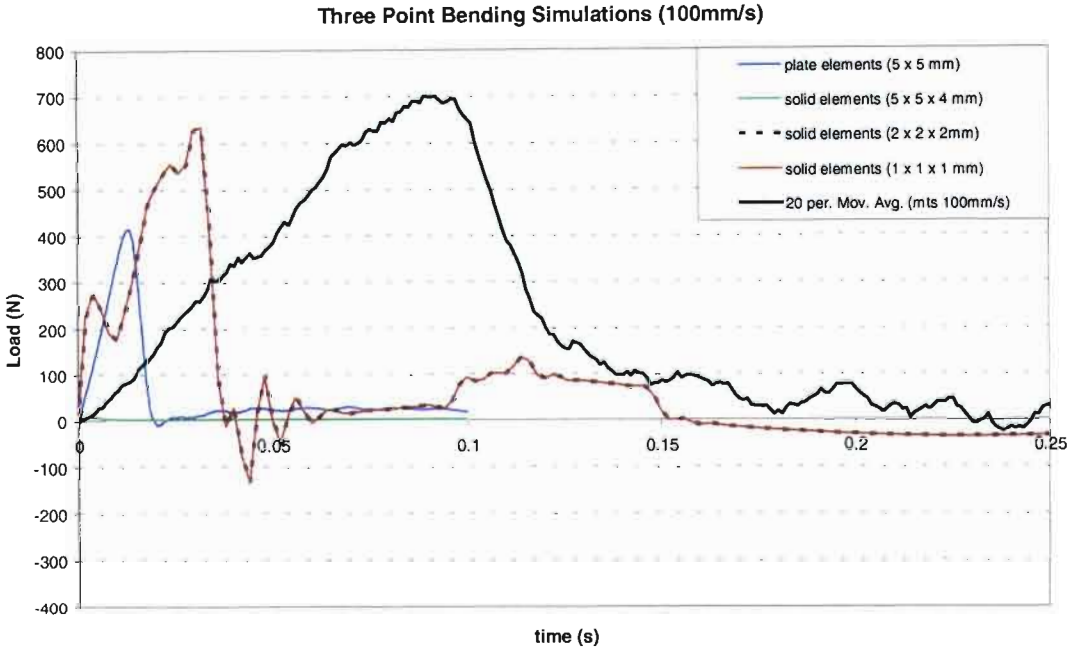

Fig. 4.20 Comparative results

The time to peak was also improved but remained less than 50% of the value recorded from experiment. Results, obtained from simulation using an even finer mesh, 1 x 1 x 1 mm elements with 4 elements across the thickness, are virtually the same as results for the 2 x 2 x 2 mm elements, thus exhibiting convergency, so that further refinement of the solid element mesh is deemed unnecessary. Deformation states as obtained from the simulation are shown for the plate and solid models in Fig. 4.21 and Fig. 4.22, respectively. The output demonstrates realistic deformation as experienced by the plate under three point bending.

Fig.4.21 Progression of deformation, solid model

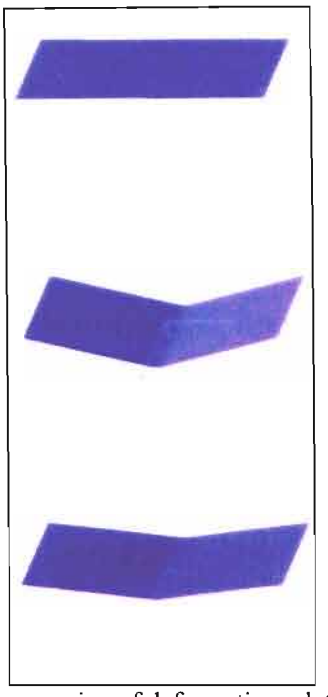

Fig.4.22 Progression of deformation, plate model

At this juncture, with a fair level of confidence that the mesh selection and refinement process had revealed the optimum available options in these areas, but with comparative results, though improved, still showing discrepancy from the experimentally obtained curve, the material characterisation process and parameters were investigated for possible refinement or adaptation. Firstly, additional quasi-static tensile testing was performed, with each test set up with identical parameters to that used in the original characterisation test (which resulted in Fig. 4.10), such that a family of curves, shown in Fig. 4.23, was yielded for the SMC material under consideration.

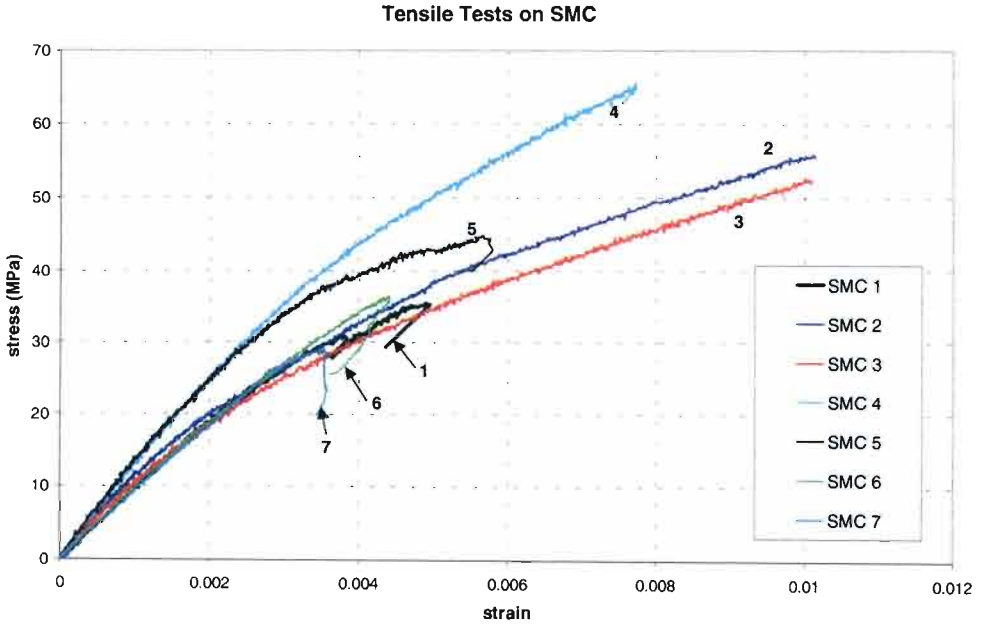

Fig. 4.23 Multiple tensile test data

The scatter evident indicates room for relatively flexible definition of the material characterisation parameters, providing a possible explanation for the lack of concurrency of

simulated results with experimentation. As a means to evaluate the effect of this scatter on our final results, the upper and lower limits of the band (see Fig. 4.24) were analysed to yield values for the material characterisation parameters, viz.

ε_i^l =0.002, ε_1^l = 0.004, ε_u^l =0.01, d_1^l =0.25, d_u^l =1, for the lower limit curve

ε_i^u =0.0023, ε_1^u = 0.00457, ε_u^u =0.0078, d_1^u =0.2, d_u^u =1, for the upper limit curve

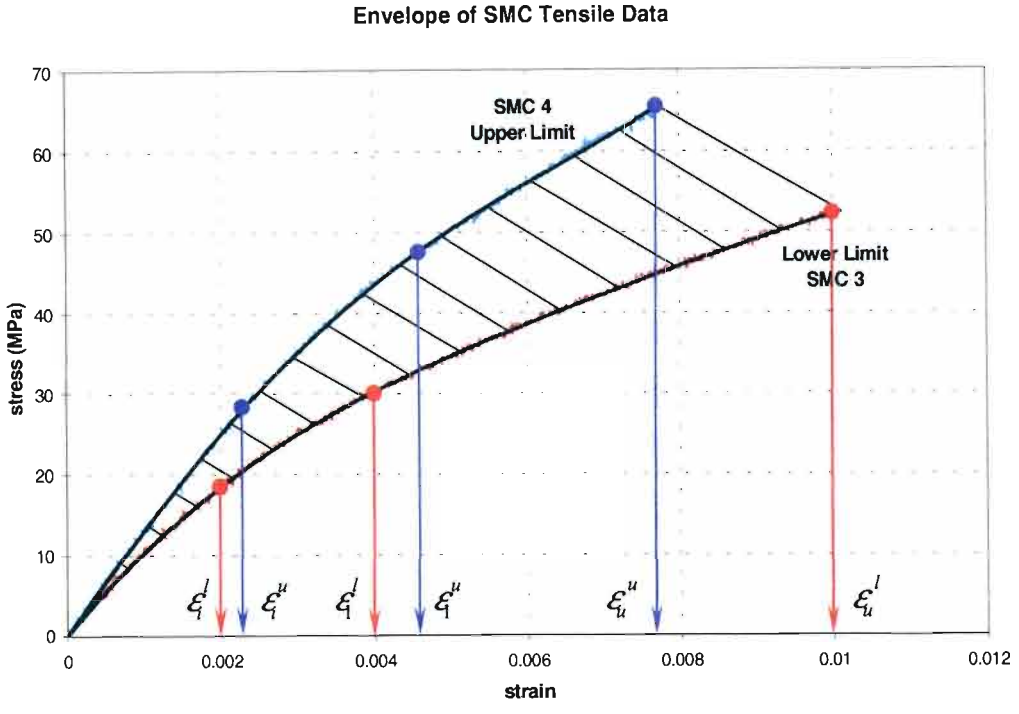

Fig. 4.24 Envelope of experimental results for SMC tensile data

Numerical simulation was then repeated, adopting each of these two sets of parameters as input data for the material characterisation, with the respective results included in Fig. 4.26. The resultant Load vs. Time curves for these two cases shows the significant effect this data has on the final material response for the bending simulation, with the maximum load for the experimental data now clearly lying between these two 'extreme' cases; as would be expected. Thus choice of a representative set of experimental data to characterise the material in question is shown to be of foremost significance; as is the need for a series of experiments in order to obtain representative results.

As a further step it was reasoned that tensile data alone would not be sufficient to characterise the response of a structure loaded under bending, as this mode of loading necessarily incorporates both tensile and compressive effects. Thus, it is justifiable to contend that characterisation of the material by way of tensile testing alone does not fully reflect the nature of those elements that are subjected to compressive loads, and are thus subject to compressive failure. It is thus considered reasonable to expect that characterisation of the material by way of compression test results would yield another 'limit' for our response. A curve obtained from compression testing (Fig. 3.27) was thus analysed, and yielded the following set of material characterisation parameters:

ε_i^c =0.006, ε_1^c = 0.044, ε_u^c =0.046, d_1^c =0.33, d_u^c =1

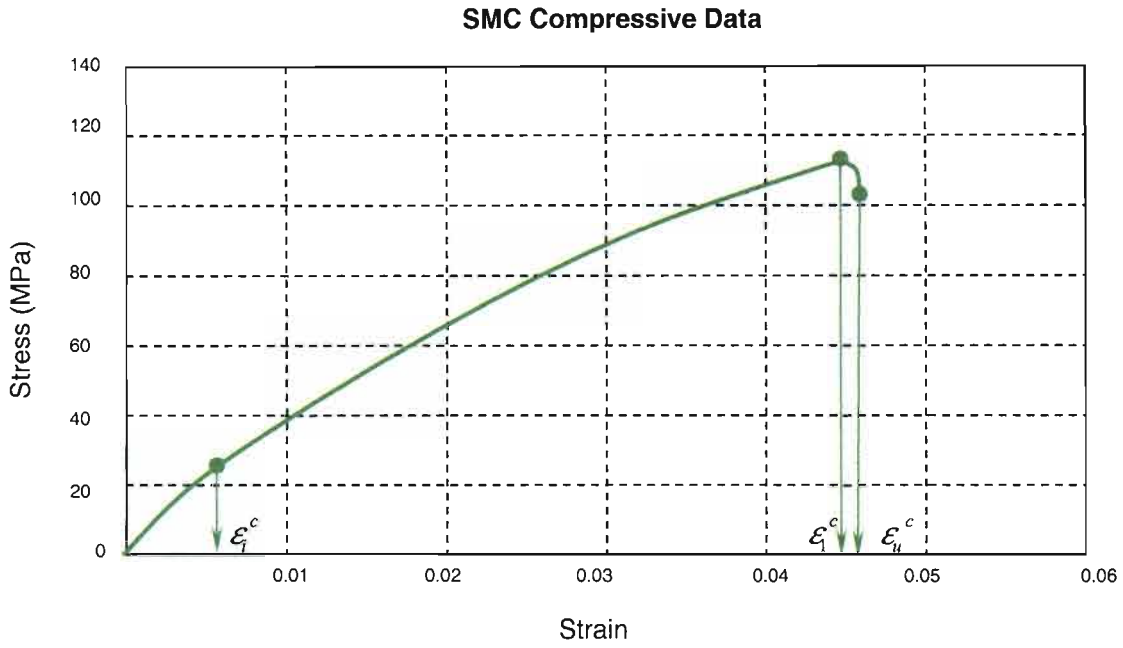

Fig. 4.25 Compression test data

The numerical simulation was again repeated, now employing these 'compression characteristics', yielding the 'compression' curve indicated on Fig. 4.26.

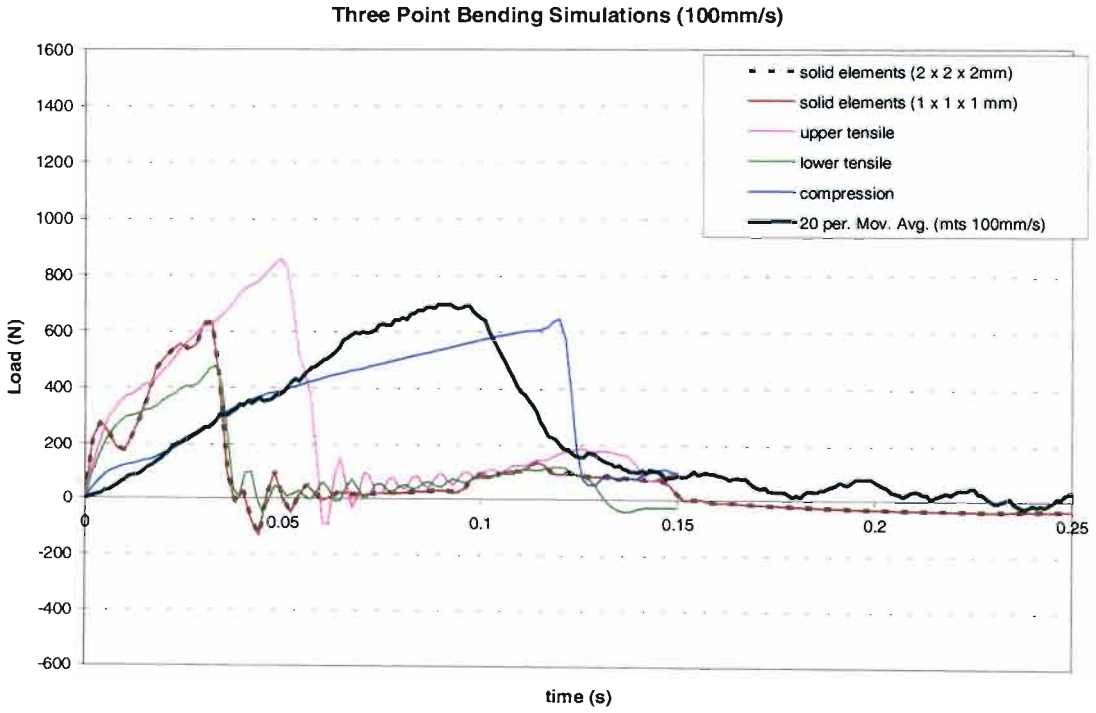

Fig. 4.26 Complete comparative results incorporating tensile limit characterisation and compression characterisation

The expectation that these results would provide another 'limit' possibility for the simulation is shown to be justified, with the strain at maximum load for the experimental results clearly lying between the 'compression' and 'tensile' characterisation results.

4.3 Simulation of Dynamic Crash Test

As a final validation, and a necessary conclusion to investigation into crash modelling, a simulation was set up as might be performed during industrial vehicle crashworthiness analysis. This involved instituting a simulation incorporating an added weight criterion, to simulate the impact of a separate object, the so-called 'impactor', and an initial velocity condition attached to this impactor, to mirror the effect of impact with subsequent deceleration.

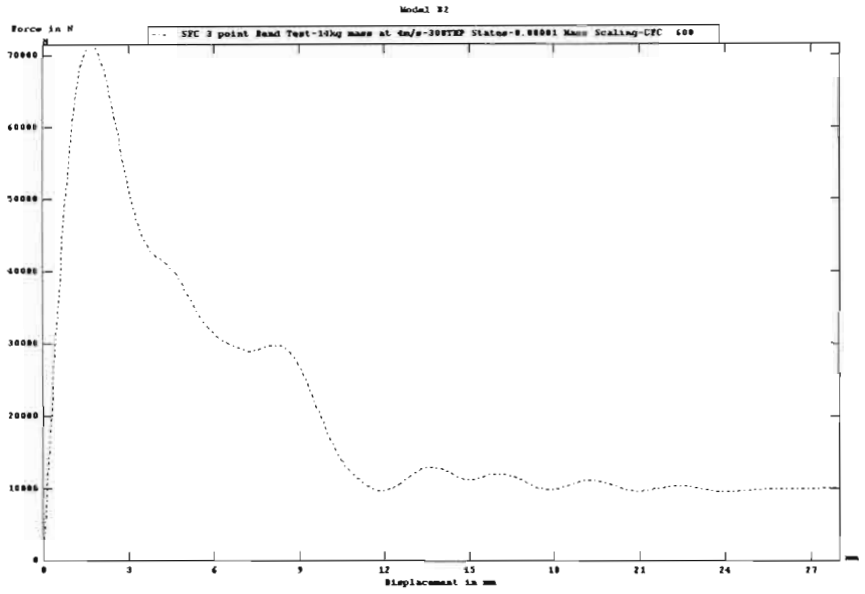

Fig. 4.27 Force-Displacement plot for added mass (14kg) with initial velocity (4m/s) simulation of SMC material

The values for the weight and velocity conditions were at first arbitrarily chosen, and the resultant Force-Displacement curve for an added mass of 14kg with an initial velocity of 4m/s, is shown in Fig. 4.27. Significantly, the plot successfully shows the distinct phases of the material, and the associated progressive degradation evident in composite materials.

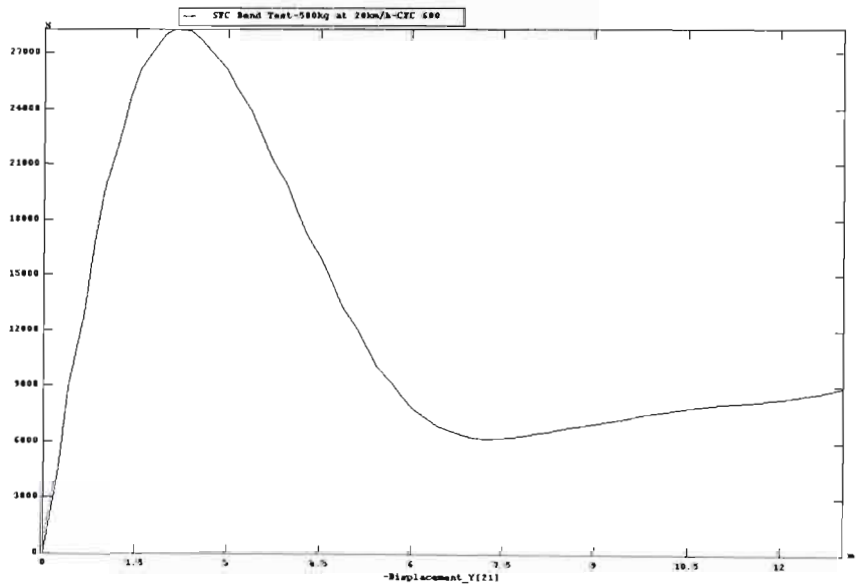

Fig. 4.28 Force-Displacement plot for added mass (500kg) with initial velocity (20km/h) simulation of SMC material

The simulation was then repeated; with loading more in line with that of a typical automotive crash situation: half a ton added weight impacting at a velocity of 20km/h. Once again the distinct failure zones of the material are observed (see Fig. 4.28) and reasonable force values are obtained. Significantly, as would be expected, a lower maximum force value is achieved. This is of particular significance as this may be interpreted to provide evidence that crashing momentum has a real effect on the response of the material, and should thus be considered during both modelling and simulation. The incorporation of the strain rate models already mentioned earlier in this work, and specifically the algorithm proposed in Chapter Three would thus seem justified; where an experimental analysis of the response of the specific material in use under suitably higher strain rates than the static case should ideally be made, so that first, the material's strain-rate sensitivity may be verified, and then quantified using the described laws. Such an analysis necessarily requires the use of strain-rate analysis equipment such as the Hopkinson's split bar apparatus. For the purposes of this study, focusing on material modelling trends, the associated strain rate models discussed in Chapter Two, and the algorithm proposed, were considered and discussed, but actual quantification of these parameters is a relevant proposal for future work; especially that dealing with multiple material types which may show distinctly different strain rate responses and sensitivity.

4.4 Conclusions

It is clear from the comparative results displayed that the modelling of SMC composite by the ready-implemented material model yields results, which, whilst certainly showing a similar trend and failure profile, yields some discrepancy when compared to the experimental results. Even though simulated results have been improved through multiple simulation iterations and refinement, results still show deviation from experimental results and this might point to a need for experimentation with regard to primary material characterisation to be more closely investigated and refined, so that a fair level of confidence in the exact evaluation and definition of these parameters is justified. This once again shows the necessity for the type of analysis performed in Chapter Three. A theoretical formulation remains only conjecture until it has been carried out and validated, and this must be preceded by specifying exactly what is required, and determining how to most relevantly define the proposed parameters.

The nature of randomly reinforced materials ensures that this task is both necessary and complex, since scatter in the exhibited properties of the material is usually apparent, due to its inherent inhomogeneity. An obvious future area of investigation would be to accommodate into the model the option of characterisation of the material by both tensile and compressive failure modes simultaneously, so that the applicable failure pattern is instituted for each element, depending on its loading. In the present model, failure is characterised solely on the basis of the either of these modes, which is shown to represent the limits for a band of material response. Experimentation should also be repeated as often as is feasible, to create a set of data that is reflective of the average nature of the material being analysed.

This said, the implemented model does show an ability to reasonably model the crash process, as depicted in Figs. 4.27 and 4.28. It is the calibration of this data and the usefulness compared to actual crash testing of complicated component shapes, which bring about highly dynamic loading effects that is debatable. Thus, another possible recommendation for future study might be the design and development of such a crash process. Within the scope of this work however, tasked with the modelling process itself, it may be concluded that existing material and progressive fracture models do exhibit the ability to adequately model the crash process, but with possible room for refinement and addition evident. This is especially necessary to preclude the possibility of obtaining results which are simply too process-specific to be of any assistance in predicting crash response without significant validating experimental data.

Thus, with these conclusions in mind, the obvious next step is to consider how existing formulations could be either improved or added to, such that firstly more options would be available to prospective modellers, and also, to provide a complete modelling scheme with every step carefully considered. At the same time, however, this must be done in such a manner that the model may be clearly implemented into an analysis environment, such as a finite element code, with a degree of confidence that it remains both relevant and flexible.

Chapter 5

Progressive Failure Model Development

This chapter deals with the development of an SMC composite material model, incorporating a homogenisation model and statistical damage criteria, after the investigation into currently available models in the previous chapters yielded results which indicate that alternative modelling concepts may indeed provide further avenues that have not yet been fully explored.

An overview of the progressive damage models that have been developed for the analysis of SMC composite materials, such as that presented earlier in this work reveals two distinct methods of modelling. Firstly, the material may be modelled on the basis of microscopic characterisation of the material constituents, viz. the fibres and matrix, with these two constituents then homogenised to result in a single material with the theoretically averaged properties of the two. Secondly, the SMC material may be characterised by way of macroscopic testing on a sample of the actual material itself, with the properties obtained from simple testing used to derive the nature of the material under more complex loading, through typical finite element analysis. The model developed here is an example of the former, with the material constitution adopted from work carried by Chen et al. (1992), and a newly proposed damaging model based on the work of Desrumaux et al. (1995).

The model theory and the basis for implementation of the model into a commercial finite element analysis package are both presented here. Coarse model validation is performed by evaluating the model parameters for a set of sample data, and applying these to the modelling of the progressive fracture of an SMC plate under tensile loading.

5.1 Model development

The model makes use of the Mori-Tanaka homogenisation scheme (see Chen et al., 1992) to express the overall properties of a randomly reinforced short fibre composite in terms of the properties of its constituents.

5.1.1 Material constitution

The material constitution for this model is as described in Chapter 1 for the model developed by Chen et al. (1992). However here we introduce a new formulation for the damaging process applied to this constitution, based on the statistical failure criteria described by Desrumaux et al. (1995). Most importantly, the actual implementation of the damaging criteria is included in a set-by-step algorithm, so that the formulation is truly complete in its presentation, and in a position to be adopted into a finite element analysis code. This is considered a key result, underpinned in importance by the lack of truly representative material models implemented into the numerical simulation environment being available, as shown through this work.

Another consideration and recommendation is that it is also considered easily possible, by slightly modifying and interpreting the described formulation, to incorporate the possibility of the inclusion phases being so called 'composite fibres', made up of cylindrical unidirectional fibre composite material. The advantages of this modelling option are immediately evident. Typically, characterisation of the individual component phases of a composite is inconsistent and sometimes even unrealistic. The characteristics of the dry fibre are for example not necessarily reflective of the same fibre impregnated with matrix material, thus it makes sense to rather test samples that take this impregnated effect into account. To thus replace our fibre phase in the above formulation by a unidirectional composite, which is simpler to test and also takes into account the composite nature of the very inclusion itself, would appear justifiable.

5.1.2 Statistical Damage Law

It is proposed that damage is introduced in the material defined by the above formulation by introducing statistical theory based on that presented by Desrumaux et al. (1995), which makes use of the Weibull distribution. The application of this distribution to characterise the failure of brittle materials particularly is fairly well established (see Bury, 1975). The distribution may be imposed to statistically control the failure pattern of the composite material, by extrapolating the results of testing of standard samples to the analysis of structures under a variety of loading, through certain statistical relations. Statistical analysis also in some way accounts for the large scatter in experimental results that usually exists in the testing of randomly reinforced composites particularly, attributable to the material's inherent structural inhomogeneity, the random distribution of the inclusion phase, and difficulty in maintaining manufacturing precision and repeatability.

The general statement for probability of failure of the material in question may be expressed as

$$P = 1 - [1 - F(\sigma)] \tag{5.1}$$

where P is the distribution function for the probability of failure of the material under the action of stress σ, which is defined by the specific strength criteria in place.

For example, for the three dimensional case, when applying the shear strain energy (Von Mises) criterion

$$\sigma = \frac{1}{\sqrt{2}}\sqrt{(\sigma_1 - \sigma_2)^2 + (\sigma_2 - \sigma_3)^2 + (\sigma_3 - \sigma_1)^2} \tag{5.2}$$

where σ_1, σ_2 and σ_3 are principal stresses. The function F in Eq. 4.7 is the probability function, expressed in terms of the Weibull distribution.

$$F(\sigma) = 1 - \exp\left[-\frac{V}{V_0}\left(\frac{\sigma}{S}\right)^m\right] \tag{5.3}$$

where m is the Weibull shape parameter, S is the Weibull scale parameter, V_0 is the original volume of the samples used for testing to obtain the Weibull distribution parameters, and V is the volume of the structure to which the distribution is extrapolated.

Whichever strength criterion is adopted, once a pre-determined limit for the overall probability, P, is attained, the material in question is considered 'failed' and either holds no more load carrying capability or is gradually degraded by the lowering of its stiffness properties, until the material is rendered completely failed.

5.2 Model implementation

Implementation in a finite element analysis environment requires, as a first step, definitions of the inputs of the model. From the above description, the following inputs are revealed:

The bulk and shear moduli, K_l and G_l, of the matrix, where $K_1 = \frac{E}{3(1-2\nu)}$ and $G_1 = \frac{E}{2(1+\nu)}$ respectively, and where E is the elastic modulus, and ν the Poisson's ratio of the matrix material. These parameters may be obtained from standard specimen tensile testing, or, for commonly used materials such as polyester matrix, such data is readily available.

Parameters k, l, m, n, p for the fibre material can be found as follows. The model definition allows for the possibility that the reinforcement phase may be made up of different materials, but since usually only one fibre material is included, only one set of these constants is required. Once again, these material properties may be obtained from testing, however for traditionally used materials, such as glass fibres, such material constants are available from reference. The constants may be related to more commonly adopted stresses by manipulating the original constitutive equation (Eq. 1.10), the first portion of which may be rewritten as

$$\begin{bmatrix} k & l \\ l & n \end{bmatrix} = \begin{bmatrix} s \\ \sigma \end{bmatrix}\begin{bmatrix} e \\ \varepsilon \end{bmatrix}^{-1} = \begin{bmatrix} \frac{1}{2}(\sigma_{22} + \sigma_{33}) \\ \sigma_{11} \end{bmatrix}\begin{bmatrix} \varepsilon_{22} + \varepsilon_{33} \\ \varepsilon_{11} \end{bmatrix}^{-1} = \begin{bmatrix} \frac{1}{2}\sigma_{22} \\ \sigma_{11} \end{bmatrix}\begin{bmatrix} \varepsilon_{22} \\ \varepsilon_{11} \end{bmatrix}^{-1} \tag{5.4}$$

(Assuming no stress and strain contributions along third axis (two-dimensional case))

Thus we need the strain response of the material under loading (stress), which allows us to find the moduli (k, l, n). This may be obtained, once again, from standard specimen testing.

The only shear term that applies for our two-dimensional case is τ_{12}, and since $\tau_{12} = 2p\varepsilon_{12}$ (Eq. 1.10), this implies that $2p$ corresponds with the material shear modulus G_{12}, which is also obtainable from testing or reference.

The outputs of the material model, which will in fact serve as inputs to a finite element analysis solver, are the overall bulk and shear moduli, K and G respectively, of the SMC composite material in question. These moduli are defined in a similar manner to which the Young's modulus, E, and the shear modulus, G, are defined for an isotropic material, within the solver. The proposed progressive failure model may then be applied.

Data derived from sample tensile testing is extrapolated to component analysis by applying the Weibull distribution function expressed in Eqns. 1.7 and 1.9. The purpose of the sample testing is to statistically describe the distribution of the material strength, by evaluation of the Weibull shape and scale parameters. The shape parameter m, may be found by plotting a graph of ($ln(-ln\ (1-F))$) vs. ln (σ), where F corresponds to the percentage of samples that fails at stress σ. The slope of the graph may be shown to be equal to m, and the scale parameter S, is then obtainable from functions relating the scale and shape parameters (see Eq. 5.5 for example).

Depending on the number of samples tested, the range of failure for the samples should thus first be sub-divided into appropriate intervals. The cumulative number of failures at each interval is then noted and plotted, as shown in Fig. 5.1 for a set of data corresponding to eight tensile tests on SMC specimens.

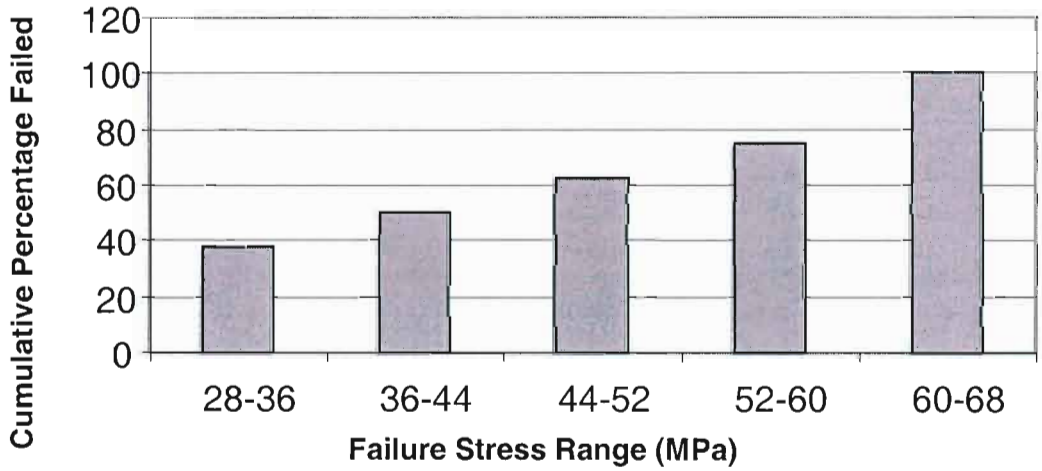

Fig. 5.1 Cumulative distribution for failure stress of samples

Each interval may then be characterised by its median stress, σ_{fm}, and the cumulative percentage failures (which corresponds to F for the sample distribution) may be plotted against these in the form ($ln(-ln\ (1-F))$) vs. $ln\ (\sigma_{fm})$ (Fig. 5.2) so that the corresponding value of m, the shape parameter, may be found.

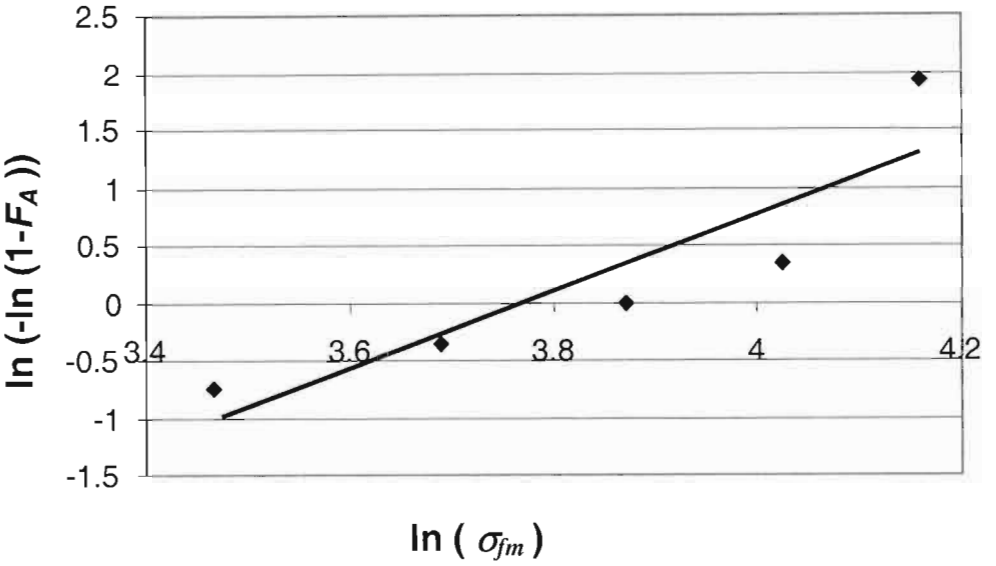

Fig. 5.2 Weibull parameter identification

The Weibull shape parameter for the set of data used in this study is thus found to be 3.37 (by suitably approximating the slope of the graph). The scale parameter, S, may then be evaluated, since it may be shown (from Eq. 5.3), that when $ln\,(\sigma_{fm}) = 0$,

$$(ln(-ln\,(1-F))) = -m\,ln\,(S) \tag{5.5}$$

The scale parameter S is thus evaluated for our set of experimental data to be 43 MPa.

Alternative methods are also applicable, one such method being an iterative process for finding suitable shape and scale pairs for a given set of experimental data. This involves selecting one of the two variables and then calculating the second, and repeating until convergence of the selected and calculated values occurs (see Bury (1975)). Using this technique, values of m and S were found to be 3.5 and 51 MPa respectively for the set of data presented here.

It should also be noted that a so called small-sample 'unbiasing factor', a function of the number of samples taken, N, is usually applied to the shape parameter for relatively small values of N i.e. a low number of observations, typically less than 120. The unbiasing factor for N=8 samples here is given as 0.82 (see Bury, 1975).

The suitably unbiased shape parameter and the calculated scale parameter may then be substituted into the expression for F (Eq. 5.3) to find the probability of failure of the analysed component. The Von Mises stresses (for the shear strain strength criterion) in the material are calculated by the finite element analysis solver, and we may then apply the probability of failure (P), as governed by the above derived formulae, to determine whether an element fails (and therefore either does not contribute any load-carrying capability in the next solver iteration, or is degraded), or not.

For the purposes of an illustrative example, a 150x100x5 mm SMC plate, loaded in tension was used. The associated volume of this specimen, 7500 mm^3 represents our value V_0, the original volume. We take our analysis volume, V, here to be equal to the volume of each element of the finite element analysis. Thus, failure is attributable at the element level and we may then observe the progressive degradation of the structure as elements are progressively degraded. Since our analysis uses an 8x8 mesh, the fraction V/V_0 is thus 1/64 here.

We use the values for the shape and scale parameter yielded by the iterative technique described above and then draw up a table of Probability of Failure vs. Von Mises Stress, for any level of stress, and define that stress level (according to the corresponding probability) that denotes failure of the element. Setting 70 % as our probability limit here, we see that a stress level of 230 MPa corresponds to this limit (Fig. 5.3).

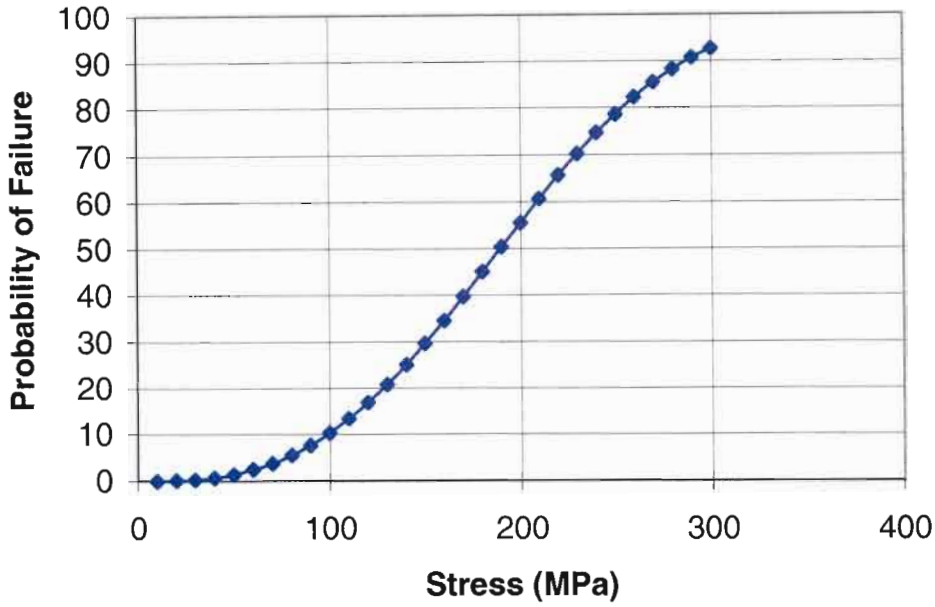

Fig. 5.3 Probability of Failure vs. Stress

Thus, above a stressed level of 230MPa, we define that the element in question is rendered failed, and 'removed' (converted to so called 'null' elements which contribute to volume but not strength), or degraded for the next iteration. Once all the failed elements are 'removed' or degraded, the solver is to recalculate the stresses in the material at the next iteration step. We choose to merely degrade the stiffness properties of the failed elements by a factor of 50%, which might be more applicable to more ductile materials. The stress levels in the specimen are computed at each step by finite element analysis, as shown in Fig. 5.4.

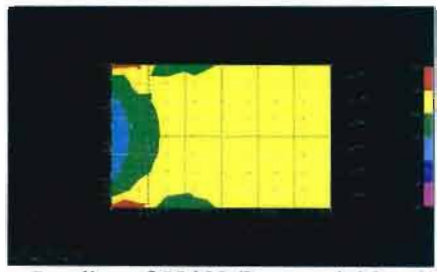

a. Loading of 55 kN. Damage initiated. Only 1 element fails

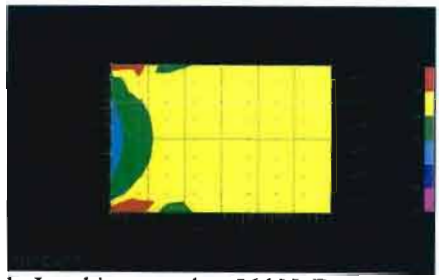

b. Load increased to 56 kN. Damage progresses to incorporate second element

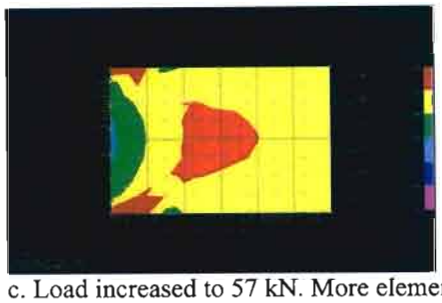

c. Load increased to 57 kN. More elements fail.

d. Load increased to 57.5 kN. The two right quarters now almost completely meet the criteria and are both degraded by halving their stiffness properties.

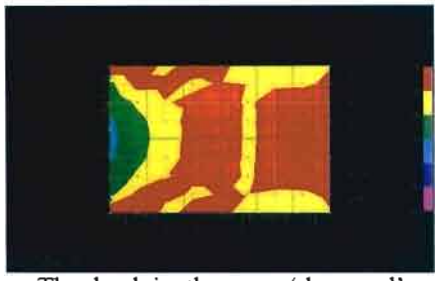

e. The load in the new 'damaged' material is increased to 57.6 kN and the stresses redistribute accordingly. The right half meets degradation criteria again and its stiffness is again degraded by half. The left half is degraded for the first time.

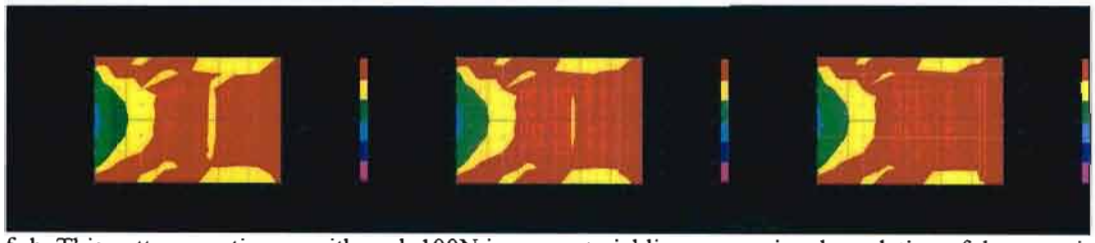

f.-h. This pattern continues, with each 100N increment yielding successive degradation of the material.

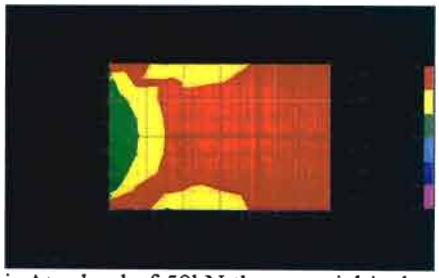

i. At a load of 58kN the material is degraded fully to some limit level (10% stiffness chosen here) and then enters the accelerated fracture phase, characterised by catastrophic degradation of the material stiffness.

Fig. 5.4 Progression of stress damage in tensile specimen

For computational ease, the example shown here degrades the specimen by groups of 16 elements at a time (quarters of the model), but of course, a more refined degradation (which would require individual elements being assigned individual material properties) is simple to institute-especially in a tailor-made analysis algorithm within a user-defined material in a suitable finite element analysis package. The darkest areas of the specimen as shown in Fig. 5.4 correspond to the areas where stress has exceeded the limit stress of 230 MPa, and is thus degraded appropriately. For this relatively coarse example, once more than 50% of the elements in any quarter exceeded the limit, the entire quarter was degraded by halving the material stiffness properties of that quarter.

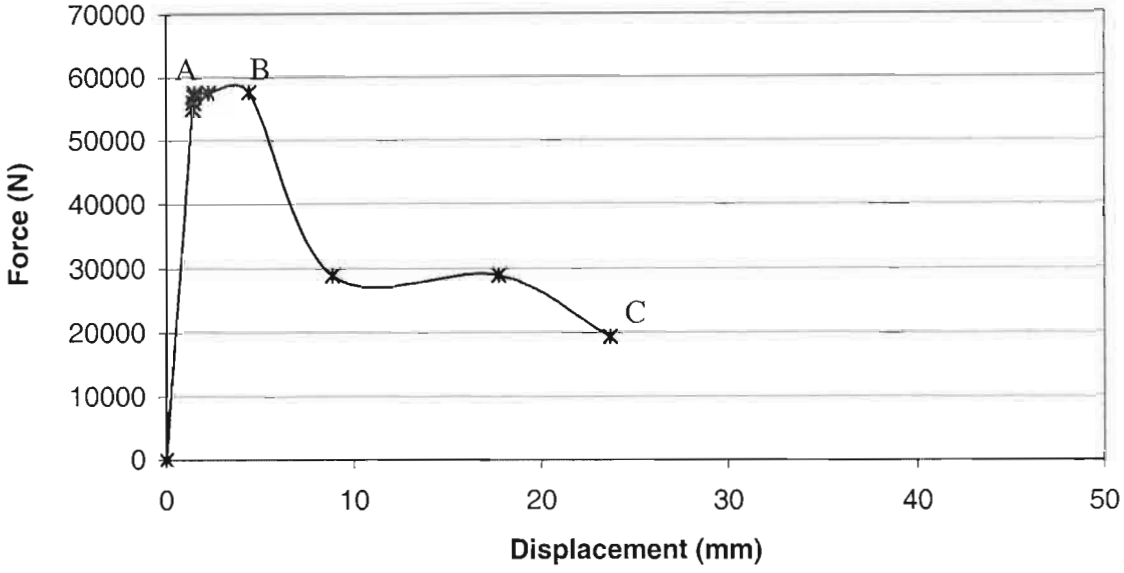

Fig. 5.5 Applied Force vs. Displacement curve for illustrative example

The force vs. displacement curve shown in Fig. 5.5 shows the nature of the material behaviour as it undergoes progressive degradation. Point A represents the initiation of damage (initial reduction in stiffness in a portion of the structure, as described in Fig. 5.4). Point B represents the initiation of catastrophic loss of load carrying ability. The region B-C is modelled by an inverse analysis, where the material stiffness is degraded by a factor of 50% at each increment, and the corresponding force calculated at regular displacement intervals.

5.3 Conclusions

At present those material models used for the analysis of SMC composite materials within commercially available finite element software packages take advantage of the overall isotropic nature of these materials. Though this approximation is indicative of the general response of SMC composite materials, it does not allow for any analysis in terms of the material constituents. A model developing a relation between the properties of the constituent phases allows for comparative analysis using various fibre materials, resin materials, and fibre volume percentages.

The next phase of implementation of such a model presented here is complete integration into a commercial finite element analysis package as a user-defined option for analysis, so that real-time degradation of each element may be performed as and when it meets the failure criteria.

Such a model as presented here displays just a few options for further development in the field of SMC composite modelling. The model takes advantage of the ease of analysis of an isotropic material, but allows for this homogenisation to be governed by the individual properties of the constituent phases, thus allowing further flexibility during comparative analysis of various SMC composites. The incorporation of further analysis and modelling concepts, such as the inclusion of strain rate effect modelling, is readily applicable and easily appended to the formulation as presented. This may thus be a consideration for future study, but at this juncture, the formulation presented is considered to successfully incorporate the most applicable and relevant aspects of SMC composite modelling, and to have been suitably readied for direct integration into the finite element analysis environment.

Chapter 6

Conclusions

It may be seen from both the initial literature survey and from the results and discussions presented in the latter sections of this work that the field of SMC composite modelling is, relatively speaking, still in its infancy. Modelling of structures fabricated of 'traditionally' used materials such as steel has advanced to a point of some confidence and modelling practices are now quite standard considerations.

Laminated materials represent the most widely integrated composites, speaking strictly in terms of implemented material models. It would appear that more focus has been previously placed on these materials, in lieu of their more economical SMC brethren, due surely in most part to their generally superior material characteristics. It would make sense that attention would be placed on such materials in the learning stages of a relatively new science (namely composite technology), but as a suitable knowledge base is created and researched and broadened, so too, inevitably, does the mindset of the researcher, with the more practical considerations of cost, practicality and ease of manufacturing beginning to take on larger significance, where previously the pursuit of superior performance alone may have been the driving factor.

The realisation has thus come through that sometimes the 'best' must give way to the 'best necessary', especially when considering that the former almost always comes with a significantly larger price tag, and that sometimes the gap between the two is not wide enough to be justifiable in the face of a specific operation. It is as this realisation has become more and more wide-spread, that the utilisation of SMC composite material has become similarly so, with a lack of sufficient knowledge about the material class now showing itself to be the major limiting factor in this regard.

Thus, research is being made into every facet of SMC composite technology; manufacturing, testing, modelling, and analysis. Focusing on modelling, and following the trend of modern design techniques, we first characterise the material as suitably as possible so that we may be able to predict its response under any loading condition without the cost and inconvenience of a full-scale testing programme. Once this has been achieved, one may then move along to manufacturing with markedly more confidence in the resultant components' capabilities.

SMC composite modelling is at face value a relatively simple task since the nature of these materials, random reinforcement with fairly even distribution through the matrix media, results in a material that is fairly isotropic when considered globally. However, results show that modelling the material by reflecting its 'overall' isotropy alone may not be truly representative of its composite nature, and thus will yield inadequacies in the response of components modelled as such.

Possible areas which may lead to this discrepancy are identifiable. Firstly, and most importantly, modelling by using a simple isotropic material alone does not take into account the very specific progressive fracturing nature of composite materials, or the multiple failure modes inherent to these. Tensile failure, shear failure, and fibre-matrix debonding all bring about very different effects on the load-bearing capabilities and characteristics of the composite material in question, and it is by both verifying the areas of effect and quantifying them that we may begin to simulate the overall failure pattern of the material. It has been shown that some degree of accuracy is possible by applying a simple damage factor to the bulk moduli of the material, and that alternative methods of quantifying damage are also capable of some measure of exactness, including statistically based models similar to the newly proposed model discussed in the previous chapter. However, it is fairly evident that even though the general failure of a composite material, and specifically here, an SMC composite, may be approximated by such 'overall' solutions, it is probably only in the distinct incorporation of the multiple failure modes of the material into the model that true representative results may be achieved. This would also eventually result in the more efficient use of SMC composites, allowing the designer to incorporate the material's strengths, and work around the most prone failure modes for the material in question.

It is also evident that study into the modelling of composite materials must be narrowed to very specific material groupings. 'Composite materials' and even 'SMC composite materials' are perhaps too general descriptions, and it might be more useful to tackle this ever-growing family of materials in highly specific materials, for example '20-30% cylindrical glass-fibre reinforced SMC composite with fibres of length less than 6mm'. It is only under such specialisation that meaningful conclusions can be drawn, or when the effect of each of the definitive characteristics-fibre volume percentage, reinforcement geometry, reinforcement material, manufacturing technique and reinforcement size (to name only those mentioned in the above description)-have been confidently assessed and quantified.

Statistical formulations, such as that explored and implemented in Chapter Four of this work, certainly seem an appropriate technique for the modelling of randomly reinforced composites. Such analysis is justifiable when the defined random nature of these materials is considered. However, care has to be taken that the application of statistical techniques are conscientiously thought out and validated. Unfortunately, as random as one may consider such composites, there exist factors which in fact dictate the behaviour of the material, not necessarily describable by simple statistical analysis. For statistics to truly be useful, precise repeatability of results must be ensured, which, as is quite evident, is not always possible, and additionally, extensive experimentation must be performed to suitably characterise each parameter of the material.

A synopsis of what has been achieved may be presented as follows. Firstly, a survey of applicable modelling methodologies that have been traditionally used in the field of short

fibre composites in general has been made. Of these identified methods, a number have been incorporated into existing material and damage models, and these models have been analysed and explored in terms of their practicality and viability. These include both material constitutive models, the basis for modelling of the undamaged material, as well as progressive damage models which account for the composite phenomenon of multiple failure modes and points, and the associated implementation and experimentation process required to characterise these. This analysis, which will possibly be revealed to be the key aspect of this work due to the apparent lack of similar studies being made, coupled with numerical simulation and experimentation, though providing an insight into the implementation requirements of theoretically proposed models, also revealed a degree of impracticality and lack of specificity to SMC composites. Thus, a new model formulation is proposed, incorporating both a material model and progressive damage criteria that has been readied for adoption into the finite element analysis environment. In parallel to an analysis of the implementation requirements, trial numerical simulation was also performed, which also necessitated experimental characterisation and validation. The simulation served to first validate those models already present and available for SMC analysis, and also to provide a comparison with experimentally obtained data. Three separate test cases were explored: a tensile simulation for first stage validation of results, a three-point bending simulation to incorporate the combined tensile and compressive effects and tensile and compressive failure that is evident in a crash situation, and finally an added weight impact simulation, which is directly reflective of the simulations generally used to model crash situations. These all showed promising results, and thus the simulation process can be deemed to have been successful, but improvement and further consideration and study is evident, adding further weight to the need for more modelling options to be readily available and implementable. The associated manufacturing and testing regime also contributed to a build-up of the knowledge base regarding practical implementation, and highlighted areas where this may be improved, or more easily facilitated.

The results of this study have been incorporated in a series of six conference proceedings and journal publications (Morozov et al., 2003), which track the progress of the work performed here. Proposals for future work have already been intimated to, but significantly, it may be mentioned that meaningful next steps would be experimental quantification of the strain rate sensitivity of SMC composite materials, as discussed in Chapter Three, so that this may be incorporated into the strain rate models discussed in Chapter Two. Naturally, the proposed new model presented in Chapter Five may be incorporated into a finite element code so that a similar validation process as performed here may be repeated for this model. Finally, it is suggested that a study into ensuring maximum manufacturing repeatability for SMC composites, and incorporating a detailed study into sample manufacture and scaling theories (for more complicated shaped prototypes) may be made, in essence a refining of the initial processes defined in Chapter Three. Some of these are already being performed under the auspices of the industrial project which provided the platform for this work

It is the task of the modeller to be able to prepare a formulation that either accounts for every conceivable anomaly, an impossible task, or provide a solution that is suitable for the application being investigated. Even this solution may only be realistically obtained once the problem at hand has been meticulously described. It might be argued that over-specific formulations defeat the purpose of the modelling. However, with the build-up of such a knowledge base, and expertise of modellers, solutions which are relevant and beneficial will present themselves, and this will provide a valid basis for further development.

All this said, there exist many applications which may not require anything above the general isotropic models that exist today for the modelling of SMC composite materials. In the case of vehicle crashworthiness specifically, the application of SMC composites is being built up slowly and purposefully, and it has been shown that a fair level of compatibility is possible

between numerical simulation and experimental testing, fair enough, at any rate, for those components considered to be of less-than-critical nature in the automobile's crashworthiness set-up. As long as the response may be approximated reasonably enough that an over-design of the structure still yields the significant weight and strength benefits necessary to justify the inclusion of these materials in the manufacture of the components, along with their sometimes complicated manufacturing requirements, and a definite variation (however slight) in material parameters, then success can be claimed, and the path to further progress paved.

References

Bay, R. S. & Tucker III, C. L. (1992), *Stereological measurement and error estimates for three-dimensional fibre orientation*, Polymer Engineering and Science, Vol. 32, No. 4, pp. 240-253

Benveniste, Y., Dvorak, G. J. & Chen, T. (1991), *On diagonal and elastic symmetry of the approximate effective stiffness tensor of heterogenous media*, Journal of the Mechanics and Physics of Solids, Vol. 39, pp. 927-946

Budiansky, B. (1965), *On the elastic moduli of some heterogenous materials*, Journal of the Mechanics and Physics of Solids, Vol. 13, pp. 223-227

Bury, K. V. (1975), *Statistical Models in Applied Science*, John Wiley & Sons

Bylund, N., Bystrom, J. & Persson, L. (2001), *Reiterated Homogenization with Applications to Autopart Construction*, Proceedings of ICCE/8, Spain, pp. B31-B34

Carpick, R. W., Agraït, N., Ogletree, D. F., Salmeron, M., (1996), *Variation of the Interfacial Shear Strength and Adhesion of a Nanometer-Sized Contact*, Langmuir, 12 [13], pp. 3334-3340.

Chen, T. (1994), *Micromechanical estimates of the overall thermoelectroelastic moduli of multiphase fibrous composites*, International Journal of Solids and Structures, Vol. 31, pp 3099-3111

Chen, T. (1996), *Effective properties of platelet reinforced piezocomposites*, Composites: Part B, Vol. 27B, pp. 467-474

Chen T., Dvorak G. J. and Benveniste Y. (1992), *Mori-Tanaka Estimates of the Overall Elastic Moduli of Certain Composite Materials*, Journal of Applied Mechanics, Vol. 59, pp. 539-546

Christensen, R. M., Schantz, H. & Shapiro, J. (1992), *On the range of validity of the Mori-Tanaka Method*, Journal of the Mechanics and Physics of Solids, Vol. 40, pp. 69-73

Derrien, K., Fitoussi, J., Guo, G. and Baptiste, D. (2000), *Prediction of the effective damage properties and failure properties of nonlinear anisotropic discontinuous reinforced composites*, Computer Methods in Applied Mechanics and Engineering, 185, pp. 93-107

Desrumaux, F., Meraghni, F. & Benzeggagh, M.L. (1995), *Micromechanical modelling of damage mechanisms in randomly orientated discontinuous fibre composite*, Proceedings of ICCM-10, Canada, Volume I: Fracture and Fatigue, pp. 487-494

Edlund, A. (1993), *Finite Element Modeling of Low Velocity impact damage in composite Laminates*, Proceedings of ICCM-9, Madrid, Volume V: Composites Behaviour

Engineering Information Systems Incorporated (1983), *EISI Reference Manual, Program Execution*

Fischer, G. & Eyerer, P. (1988), *Measuring spatial orientation of short fibre reinforced thermoplastics by image analysis*, Polymer Composites, Vol. 9, No. 4, pp. 297-304

Ferrari, M (1991), *Asymmetry and the high concentration limit of the Mori-Tanaka effective medium theory*, Mechanics of Materials, Vol. 11, pp. 251-256

Gavazzi A.C. and Lagoudas D.C., (1990), *On the evaluation of Eshelby's tensor and it's application to elasto-plastic fibrous composites*, Computational Mechanics, Vol. 7, pp. 13-19.

Geers, M. G. D., Peijs, R., de Borst, R. & Brekelmans, W. A. M. (1995), *Experimental Dynamic Analysis of Damage Evolution in Short Fibre-Reinforced Composite Materials*, Proceedings of ICCM-10, Canada, Volume I: Fracture and Fatigue, pp. 755 to 762

Hahn, H.T. & Tsai, S.W. (1973), *Nonlinear elastic behaviour of unidirectional composite laminates*, Journal of Composite Materials, Vol. 7, pp. 102-118

Hashin, Z. (1979), *Analysis of the properties of Fibre Composites with Anisotropic Constituents*, Journal of Applied Mechanics, Vol. 46, p.543

Haug, E. & De Rouvray, A. (1993), *Structural Crashworthiness and Failure: Chapter 7*, Wierzbicki, T. & Jones, N. (eds.), Elsevier Applied Science

Haug, E., Clinckemaillie, J., Ni, X., Pickett, A.K., & Queckborner, T. (1996), *Recent Trends and Advances in Crash Simulation and Design of Vehicles*, ESI Group.

Hershey, A. V. (1954), *The elasticity of an isotropic aggregate of anisotropic cubic crystals*, Journal of Applied Mechanics, Vol. 21, p. 236-240

Hill, R. (1964), *Theory of Mechanical Properties of Fibre-Strengthened Materials: I. Elastic Behaviour,* Journal of the Mechanics and Physics of Solids, Vol.12, pp.199-212

Hill, R. (1965), *A self-consistent mechanics of composite materials*, Journal of the Mechanics and Physics of Solids, Vol. 13, pp. 213-222

Hine, P. J., Duckett, R. A., Davidson, N. & Clarke, A. R. (1993), *Modelling of the elastic properties of fibre/reinforced composites I: Orientation Measurement*, Composites Science and Technology, Vol. 47, p.65-73

Hoffmann, L. (1995), *Damage Process Modelling on SMC*, Proceedings of ICCM-10, Canada, Volume I: Fatigue & Fracture, pp. 335-342

Johnson, W & Mamalis, A. G. (1978), *Crashworthiness of Vehicles*, Mechanical Engineering Publications Ltd.

Kabelka, J. & Ehrenstein, G. W. (1992), *Structure and Thermo-elastic Properties of SMC*, 47th Annual Conference, CI SPI, Cincinnati, Sess. 1-E

Kalamkarov, A. L. & Liu, H. Q. (1998), *A new model for the multiphase fiber-matrix composite materials*, Composites Part B, Vol. 29B, pp. 643-653

Lardeur, P. (1990), *Developpement et Evaluation de Deux Nouveaux Elements Finis de Plaques et Coques Composites avec Influence du Cisaillement Transversal*, Doctoral dissertation, Universite de Technologie de Compiegne

Laws, N. (1974), *The overall thermoelastic moduli of transversely isotropic composites according to the self-consistent method*, International Journal of Engineering Science, Vol. 12, pp. 79-87

Liang, N. G., Liu, H. Q. & Wang, Z. C. (1995), *A meso elasto-plastic constitutive model for polycrystalline metal based on equivalent slip system with latent hardening*, Science in China, Vol A25, pp. 858-867

LS-DYNA Key-Words Manual (2001), Vol. 2, Livermore Software Technology Corporation

LS-DYNA Theory Manual (1998), Livermore Software Technology Corporation

Lukkassen, D., Persson, L. & Wall, P. (1995), *Some Engineering and Mathematical Aspects on the Homogenisation Method*, Composites Engineering, Vol. 5, No. 5, pp. 519-531

Mori, T., and Tanaka, K., (1973), *Average Stress in Matrix and Average Elastic Energy of Materials with Misfitting Inclusions*, Acta Metal., Vol. 21, pp. 571-574.

Meraghni, F. & Benzeggagh, M.L. (1995), *Micromechanical modelling of damage mechanisms in randomly orientated discontinuous fibre composite*, Proceedings of ICCM-10, Canada, Volume I: Fracture and Fatigue, pp. 487-494

Morozov, E. V., Kaczmarczyk, S., Morozov, K. E. & Selvarajalu, V. (2003), *Numerical simulation of the progressive failure of SMC composite materials*, Proceedings of ICCM-14, San Diego, U. S. A. (CD-ROM)

Morozov, E. V., Kaczmarczyk, S., Morozov, K. E. & Selvarajalu, V. (2003), *Numerical simulation of the progressive failure of SMC composite materials*, Technical Paper EM03-308 of the Society of Manufacturing Engineers (SME), 8pp.

Morozov, E. V., Morozov, K. E. & Selvarajalu, V. (2003), *Damage model development for SMC composites*, Proceedings of ICCST/4: The Fourth International Conference on Composite Science and Technology, South Africa, pp. 205-210

Morozov, E. V., Morozov, K. E. & Selvarajalu, V. (2003), *Progressive damage modelling of SMC composite materials*, Proceedings of ICCST/4: The Fourth International Conference on Composite Science and Technology, South Africa, pp. 531-537

Morozov, E. V., Morozov, K. E. & Selvarajalu, V. (2003), *Damage model development for SMC composites*, Composite Structures, Vol. 62, No. 3-4, pp. 373-378

Morozov, E. V., Morozov, K. E. & Selvarajalu, V. (2003), *Progressive damage modelling of SMC composite materials*, Composite Structures, Vol. 62, No. 3-4, pp. 361-366

Norris, A. N. (1989), *An examination of the Mori-Tanaka effective medium approximation for multiphase composites*, Journal of Applied Mechanics, Vol. 56, pp. 83-88

PAM-CRASH Solver Notes (2000), ESI Group

Parthasarathy, T. A., Folsom, C. A., Zawada, L. P. (1998), *Combined effects of exposure to salt water and oxidation on the strength of Uncoated and BN-Coated Nicalon™ Fibres.* Journal of the American Ceramics Society, Vol. 81, No. 7, pp. 1812-1818.

Tohgo, K., Cho, Y. & Ishii, H. (1997), *Damage mechanics of reinforcement cracking in particle or short-fibre reinforced composites,* Proceedings of ICCM-11, Australia, Vol. II: Fatigue, Fracture and Ceramic Matrix Composites, pp. 364-373

Toll, S. (1992), *Interpolative Aggregate Model for Short-Fibre Composites,* Journal of Composite Materials, Vol. 26, No. 12

Vasiliev, V.V. and Morozov, E. V. (2001), *Mechanics and Analysis of Composite Materials*, Elsevier

Voigt, W. (1889), *Ueber die Beziehung zwischen den Elasticitatsconstanten isotroper Korper.*Annalen der Physik und Chemie, pp. 573-587.

Walpole, L. J. (1969), *The overall elastic moduli of composite materials*, Journal of the Mechanics and Physics of Solids, Vol. 17, pp. 235-251

Zhu, Y. T., Blumenthal, W. R. and Lowe, T. C. (1997), *Determination of non-symmetric 3-D fibre-orientation distribution and average fibre length in short-fibre composites*, Journal of Composite Materials, Vol. 31, No. 13, pp. 1287-1301

Appendix A

Sample Mathematica™ Code for the Evaluation of the Eshelby Tensor

(Michael Hoarau, 2000)

```
(* Definition of the shape of the inclusions *)
a1=1; a2=1; a3=1;

(* Definition of the reduced vector variable of the inner
integral. x stands here for ζ3 *)
ζ = {Cos[ω]/a1*Sqrt[1-x^2], Sin[ω]/a2*Sqrt[1-x^2], x/a3}

(* Construction of a fourth-order matrix to represent the
stiffness tensor. One can then define each Cijkl to take a
particular expression of C into account (isotropic,
orthotropic,…) *)
C0 = Table[ToExpression["C" <> ToString[i] <> ToString[j] <>
ToString[k] <> ToString[l]], {i,1,3}, {j,1,3}, {k,1,3},
{l,1,3}];

(* Definition of [K] *)
MatK[i_,k_] := Sum[ C0[[i,j,k,l]] * ζ[[j]] * ζ[[l]], {j,1,3},
{l,1,3}]

(* Definition of [N] *)
MatN[i_,j_] := 0.5 * Sum[
epsilon[i,k,l] * epsilon[j,m,n] * MatK[k,m] * MatK[l,n],
{k,1,3}, {l,1,3}, {m,1,3}, {n,1,3}]

(* Definition od [D] *)
MatD[l_] := Sum[ MatK[m,1] * MatK[n,2] * MatK[l,3], {m,1,3},
{n,1,3}]

(* Expression of Gijkl *)
G[i_,j_,k_,l_] := ζ[[k]] * ζ[[l]] * MatN[i,j]/MatD[l]

(* Computation of the abscissas and weights needed for the Gauss-Legendre
integration *)
LegPol = Legendre[4,t];
Abscissas = Evaluate[t /. NSolve[LegPol == 0, t]];
DerLegPol = D[LegPol,t];
Weight = 2/((1-Abscissas^2)*(DerLegPol /. t -> Abscissas)^2);

(* Integrated value of G1111 = G[1,1,1,1] *)
ω = π*Ω+π
IntG1111 = Sum[Weight[[i]] * (G[1,1,1,1] /. Ω -> (Abscissas/π-
1)), {i,1,4}];
```